Resistance of closed-ended piles in a layered soil

A comparison of existing base and shaft capacity methods based on the measured jacking force

Rosa Hersbach

Technical University of Delft
Civil Engineering - Geo-Engineering
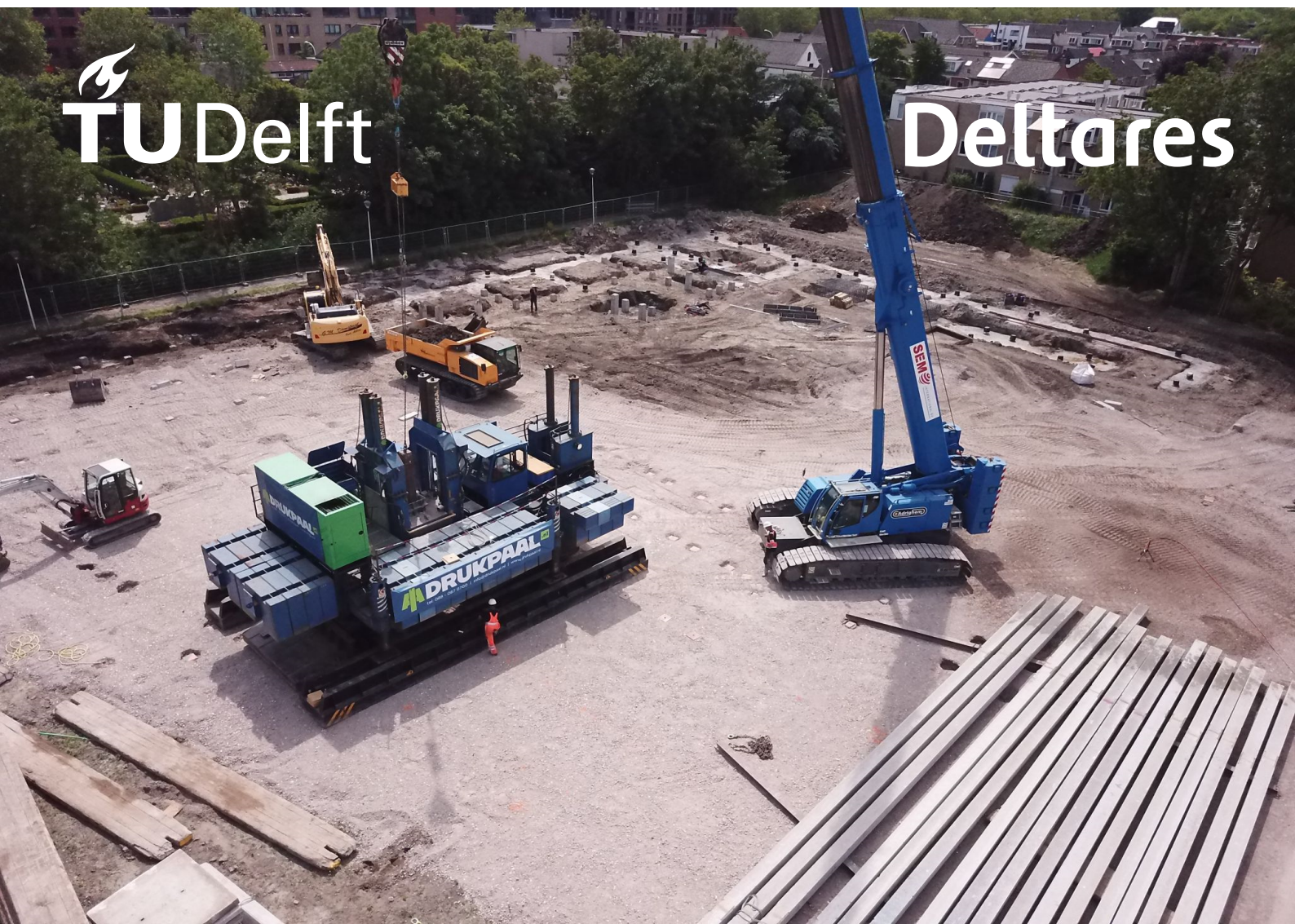
Resistance of closed-ended piles in a layered soil

A comparison of existing base and shaft capacity methods based on the measured jacking force

by

Rosa Hersbach

to obtain the degree of Master of Science
at the Delft University of Technology,
to be defended publicly on Monday April 8, 2024 at 13:45

Student number: 4757963
Project duration: June, 2023 – April, 2024
Thesis committee: Dr. ir. Mandy Korff,   TU Delft, Geo-Engineering (chair)
                    Ir. Dirk de Lange,   Deltares
                    Menrik Doornbos,   Drukpaal
                    Dr. ir. Roel Schipper   TU Delft, Structural Engineering

TUDelft

List of Symbols

Symbol	Description	Unit
α_p	Correction factor base capacity	-
α_s	Correction factor shaft capacity	-
β	Pile tip shape factor	-
ΔL	Length segment over which a value of q_c acts	m
$\Delta\sigma'_{rd}$	Increase in radial effective stress that occurs during pile loading	MPa
σ'_{rc}	Radial effective stress (stationary)	MPa
σ'_v	Vertical effective stress (estimated with $\frac{10\cdot z}{1000}$, 10 is estimated effective unit weight of the soil)	MPa
τ_f	Shear stress	MPa
A	Surface area of pile base	m^2
A_{re}	Effective area ratio (=1 for closed-ended piles)	-
C	A constant which determines the zone of influence (=6.5 above pile base and 10.5 below pile base) (de Boorder, de Lange, & Gavin, 2022)	-
C_1	Parameter equal to unity for points below cone tip, and linearly reduces to a values of 0.5 for points located more than 4 cone diameters above the cone tip	-
C_2	Parameter equal to unity for points below cone tip, and 0.8 for points above cone tip	-
f	Damping factor (=13.5) (de Boorder et al., 2022)	-
k_c	Correction factor for installation method and soil type	-
O	Circumference of pile	m
Q_b	Pile base capacity	kN
$q_{b,filt}$	Pile tip capacity with filter method	MPa
$q_{b,kop}$	Pile tip capacity with Koppejan method	MPa
$q_{b,LCPC}$	Pile tip capcity with LCPC method	MPa
$q_{b,munt}$	Pile tip capacity with Munta de Boorder method	MPa
$q_{c,avg}$	Average of q_c values determined using averaging techniques	MPa
$q_{c,I,avg}$	The arithmetic average of q_c values below pile tip over a depth which may vary between 0.7D to 4D as shown in Figures 2.22.	MPa
$q_{c,II,avg}$	The arithmetic average of the q_c values following a minimum pah rule recorded below the pile tip over the same depth of 0.7D to 4D	MPa
$q_{c,III,avg}$	The arithmetic average of the minimum q_c values following a minimum path rule recorded above the pile tip over a height of 8D.	MPa
$q_{c,tip}$	The cone resistance at the pile tip level	MPa
$q_c(z)$	Measured tip resistance from CPT at depth z	MPa
$q_{s,NEN}$	Shaft capacity as calculated by the NEN method	MPa
Q_s	Pile shaft capacity	kN
Q_T	Total pile capacity	kN
s	Pile shape (cross-section) factor	-
s_{munt}	A fit parameter (0.56 above the pile tip and 0.79 below pile tip) (de Boorder et al., 2022)	-
$w_c(z)$	Filter function for depth z	-
w_1	Filter function that takes into account relative influence of any soil decreasing with increasing distance from cone tip	-
w_2	Filter function that adjusts relative influence based on if soils away from cone tip are weaker or stronger than soil soil immediately at cone tip. Increasing soil influence if soil is weaker and decreasing if soil is stronger	-
z'	Depth relative to cone tip normalized by cone diameter (d_c)	-
z'_{50}	Normalized depth at which $w_1 = 0.5C_1$	-
z_{tip}	Depth of cone tip	m

Preface

This thesis is written to fulfil the final part of my master's in Civil Engineering at the TU Delft, with a focus on Geo-Engineering. I am grateful for the opportunity to complete my thesis at Deltares, where I was able to conduct a data analysis of data provided by Drukpaal, to gain an insight in the existing pile bearing capacity methods.

I would like to thank my committee who helped me throughout this process. Starting with Dirk de Lange, my daily supervisor at Deltares, who always helped me with enthusiasm and optimism, whether my questions were about the results of my analysis, an error in my code or the structure of my thesis. Secondly I would like to thank Mandy Korff, chair of my thesis committee, and Roel Schipper, my second supervisor, for all the feedback I recieved on every single version of my thesis and the constructive criticism of my presentations at progress meetings, which helped me move forward. I would also like to thank Menrik Doornbos who was kind enough to give me all the data I wanted from Drukpaal for this thesis and taking the time to answer the questions I had regarding said data.

Overall I feel very lucky with the graduation committee I had throughout this process.

I would also like to thank all the people who supported me in this thesis and listened to my rants about my various struggles during this process and gave me pep-talks when needed. Special acknowledgements to Alba Rodríguez, Astha Sharma, Rik Hoedemaker and Jorrit van Assen.

A special thanks goes out to my boyfriend, Matthijs Verdaasdonk, who is always there when I need him.

I am grateful for my years at the TU Delft, for all the friends I made here and opportunities to broaden my horizons on both personal and academic levels. From getting my teaching license in Mathematics, to doing various committees and boards and spending almost all my student years as part of a band. I am excited for what the future holds!

Rosa Hersbach
Delft, April 2024

Abstract

Foundations of buildings ensure the safety and serviceability are upheld. A common type of foundations used in the Netherlands is pile foundations which are typically founded on a thick sand layer in the subsurface. These pile foundations are the focus of this thesis and more specifically the methods used to design such foundations. This thesis aims to give a better understanding of the resistance of closed-ended piles in a layered soil by comparing existing pile design methods to the measured forces from the Drukpaal jacking machine. Drukpaal jacks precast concrete piles into the soil and the records collected give a valuable insight in the pile resistance in various locations and soil profiles with layered soil in the Netherlands.

The design of a pile foundations consists of the combination of two different types of methods. One will predict the base capacity of the pile foundations and the other will predict the shaft capacity. These two capacities together give the predicted bearing capacity of the pile. However, multiple base capacity and shaft capacity methods exist with varying influence zones and with that varying degrees of accuracy. In this thesis the different base and shaft capacity methods used are all based on the tip resistance as measured by a CPT. The following base capacity methods are included: Koppejan, LCPC, Filter method and the Filter method as adapted by Munta de Boorder (in this thesis referred to as the Munta de Boorder method). And for shaft capacity the NEN method and the ISO method are used.

This thesis aims to answer the following research question: *What combination of capacity prediction methods for shaft and tip resistance works best to estimate the total force over depth as measured by Drukpaal?*. This question will be answered by a series of simulations of different projects completed by Drukpaal, which is a company which jacks piles into the ground and records the required force over depth.

The measurements and simulations for the various sites were compared both visually and statistically.The Filter method with ISO gives the best visual fit.
For the statistical analysis the coefficient of variance (COV) is taken as well as the root mean squared error (RMSE) of the ratio line of the simulation (simulation divided by the measurement). Here the COV will account for the shape and the RMSE will account for the overall error. The sum of these two values is used to determine the best fit, since both of these values should be as small as possible. From this analysis it is found that Filter method in combination with ISO is overall the best combination, followed by Munta de Boorder with ISO and Filter method together with NEN.

The last aspect to be looked at is the location dependency of the combination of methods. From this it was found that the base capacity methods in combination with NEN vary a lot over the measured locations and these combinations are thus location dependent. For the base capacity, the LCPC method was also found to be location dependent in combination with ISO. So even though this combination worked really well for one of the projects (Gorinchem) it is not dependable to use because of the varying degrees of accuracy. The other three combinations; Koppejan, Filter method and Munta de Boorder together with ISO, were all found to be location independent. However, Koppejan with ISO garnered quite high values for RMSE and COV, meaning that this combination is not very accurate.

Overall, Filter method with ISO was found to give the best fit which was location independent. Munta de Boorder with ISO followed and Koppejan with ISO was found third best fit. The other combinations were found to be location dependent and thus are, based on the work in this thesis, less suitable for application in The Netherlands.

List of Figures

List of Tables

Contents

1

Introduction

One of the most important parts of any civil structure is the foundation. Whether its a building, a bridge or a tunnel, it is important that the structure is as safe as needed. The foundations of these structures ensure that little to no deformation will occur due to loads. Foundations come in different types and sizes, and these differ in the way the weight of the structure and live loads are distributed and passed to the subsurface. These are mostly referred to as shallow or deep foundations, which refers to the depth of the soil at which they are placed. Shallow foundations can be identified by the width of its footing. This width will help distribute the weight of the structure more evenly to the shallow subsurface. Deep foundations are identified as more slender elements which will convey the weight to deeper layers. In this thesis the focus will be on the latter, and specifically closed-ended pile foundations.

Because foundations have such a crucial role in civil structures, it is very important to know how to install the foundation (in this case piles) to the right depth to ensure enough bearing capacity. Various methods exist to predict the load-bearing capacity and displacement behaviour of deep foundations with sufficient reliability. Many of these methods are based on results of site investigation, often CPTs. These methods will be the focus of this thesis, including Koppejan, LCPC, Filter method and Munta de Boorder for base capacity and NEN and ISO for shaft capacity. A CPT is a pile with a small diameter (often $3.57\,\mathrm{cm}$) which is fitted with different sensors to measure the tip resistance and sleeve friction. These values can be used to characterize the subsurface, i.e. a higher tip resistance relative to the sleeve friction indicates a sandy soil and a lower tip resistance relative to the sleeve friction indicates a clayey soil. However, these different prediction methods all give different outputs with varying degrees of accuracy. Using a slightly conservative method can lead to having to use larger piles to get the bearing capacity needed for the project, which is more expensive. At this moment it is unclear which of these methods is the most accurate and thus the most economical. An accurate prediction method is preferred since it will be more economical.

Since a couple of years a company called 'Drukpaal' (literal translation: push pile) has started in the Netherlands. This company, as the name suggests, uses a hydraulic jacking mechanism to press piles into the ground as an alternative for drilling or hammering. During these installations the force needed to push the pile into the ground is recorded as well as the depth of the pile. This gives a continuous measurement of force over depth, which can be used to look deeper into the bearing capacity methods. Since the method of Drukpaal is very similar to a traditional CPT (which data is used in most prediction methods), this seems like a good opportunity to test these methods against the data from Drukpaal.

This research will focus on the capacity prediction methods based on CPT and their accuracy based on the measured jacking force as measured by Drukpaal. This is done to gain a better understanding of the factors that influence the pile bearing capacity. Before this can be done these different as methods will be explained, as well as the different aspects that influence the installation process and if and how these aspects are incorporated in these different methods.

2

Literature study

In this chapter background information on the topic will be given, which includes a section on pile soil interaction, a section on the sensing and development depth and a section on bearing capacity.

2.1 Bearing capacity

The bearing capacity of a pile foundation can be determined through data from pile load tests (PLT). These tests are performed on installed piles where the piles are loaded and the settlement of the pile in response to this load is recorded. From these tests load-settlement diagrams (or curves) can be determined, an example of one is shown in Figure 2.1. The load is plotted on the x-axis and the settlement is plotted on the y-axis. Initially during the pile load tests, the settlement will be elastic, which means that the pile will rebound when the load is removed. As the load continues to increase, the pile eventually reaches a point where the settlement becomes plastic, and will not fully rebound when the load is removed. This point is often considered the 'ultimate load' or 'ultimate bearing capacity'. This point is shown in the figure below as $q_{b,ult}$ as a dashed vertical line, showing where the curve has reached it's maximum.

The curve shown in the figure is an example of a typical load-settlement curve. The shape and values will differ depending on the type of pile used, installation method and soil profile in which the pile is installed.
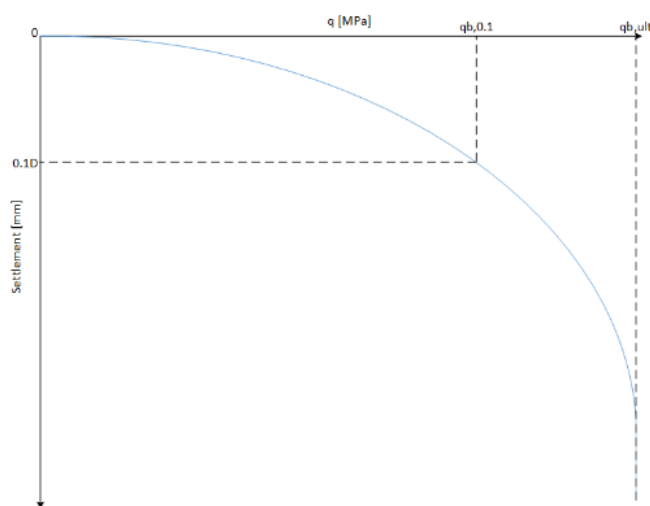
Figure 2.1: Example of a load-settlement curve (load is on the x-axis and settlement is on the y-axis) (de Boorder, 2019)
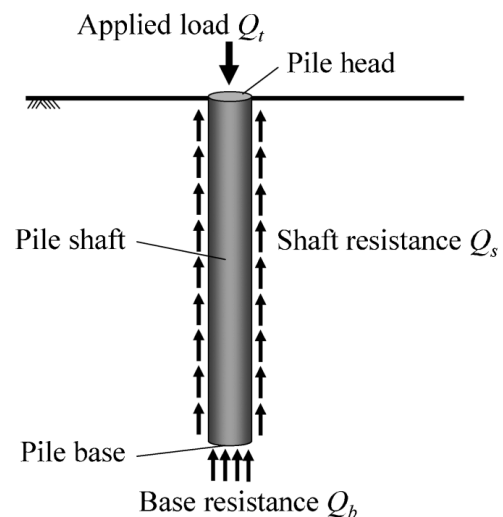
Figure 2.2: Illustration of base and shaft resistance mobilised at a given load (Salgado et al., 2011)

The ultimate bearing capacity can also be described as the total resistance the pile can offer. This total resistance can be divided into two parts: base resistance (the force of the soil acting on the pile base) and shaft resistance (force of the soil acting on the shaft). However, this value is a theoretical value that is

not used in practice, because if the pile is loaded to this point the pile foundation will fail (because no additional resistance from the soil is given and the pile will settle an excessive amount).

In practice a rule of thumb is used to design safe pile foundation, where no failure will happen. This rule is included in the Eurocodes (developed by Normcommissie 351 006 'Geotechniek' (2017)), guidelines to make sure all European construction projects follow the same rules and use the same safety factors. In the Netherlands these design rules are gathered in the NEN 9997-1 for 'Geotechnical Design and Structures'. In these guidelines the resistance is a function of settlement of the pile tip. The ultimate shaft capacity is reached when the pile tip has settled around 10 mm and the ultimate base capacity is reached when the pile tip has settled 0.1 times the diameter. In these cases only part of the total resistance is mobilised, meaning that the soil has more resistance to give that hasn't been mobilised yet.

To estimate these capacities different methods have been developed. The shaft capacity and base capacity are calculated separately and later added up to determine the total capacity. In early methods this calculation was based on effective stress and earth pressure design methods. For example, the API-69 method based on effective stress and relative density is still used today, with no significant changes to the formulation of the method since 1969 (Digre & Zwerneman, 2012). However, the most commonly used methods are CPT based (cone penetration test).

2.1.1 CPT-based methods

A CPT is typically done to gather more information on the subsurface in a specific location, i.e. the soil stratigraphy and soil properties. This information is gathered from the measurements from a CPT, which measures the tip resistance, sleeve friction and (sometimes) the water pressure. During a CPT a probe with a metal cone tip is pushed into the ground, this probe has multiple sensors to measure the before mentioned parameters. In the CPT-based methods for total capacity the measured q_c (tip resistance) is used. It is believed that these measurements can be used because of a CPT cone behaves similarly to a pile being pushed into the soil and they will experience the same soil failure mechanisms (which will be explained further in section 2.2). In section 2.4 the different methods used in the simulation in this thesis will be further elaborated, but the general form of these methods is shown below (van Tol, 2003).

$$Q_T = Q_b + Q_s \tag{2.1}$$

$$Q_b = q_{c,avg} \cdot \alpha_p \cdot A \tag{2.2}$$

$$Q_s = \sum q_c \cdot \alpha_s \cdot O \cdot \Delta L \tag{2.3}$$

Where:
Q_T	Total pile capacity	[kN]
Q_b	Pile base capacity	[kN]
Q_s	Pile shaft capacity	[kN]
α_p	Correction factor base capacity	[-]
α_s	Correction factor shaft capacity	[-]
$q_{c,avg}$	Average of q_c values determined using a specific averaging technique	[MPa]
A	Surface area of pile base	[m^2]
O	Circumference of pile	[m]
ΔL	Length segment over which a value of q_c acts	[m]

The total capacity is calculated in this equation for a specific depth, which is the bearing capacity. To be able to find for which depth a pile will reach the needed bearing capacity, the total capacity is calculated for entire length of a CPT. This will lead to a total capacity profile, from which the needed depth of a foundation pile can be found.

There are two correction factors in the equation above, one for the base capacity and one for the shaft capacity. These are to account for the differences that are still present between a CPT and a foundation pile. These can account for differences in installation technique, geometry of the pile (circular cone versus a (often) square pile) and material (metal cone versus a concrete pile). There is one other aspect that should be taken into account and that is the size of the foundation pile against the size of the CPT cone,

where the foundation pile is often 10 times bigger than the CPT. This means that the foundation pile will mobilise more soil than the cone penetrometer, this is also known as the influence zone (White & Bolton, 2005). This aspect is taken into account in the calculation of the base capacity, where instead of q_c, an average $q_{c,avg}$ is used. The extent of this influence zone and how this average is taken is different for the different methods, but are dependent on the diameter of the foundation pile. The geometrical effects will be further discussed in section 2.3.

2.2   Installation effects

When a pile is installed the soil state surrounding the pile will change. It is important to know how the soil reacts to the pile and how this relates to how the soil reacts to a CPT. First the soil displacement will be looked at including cavity expansion and pile grouping (do piles influence each other), friction fatigue will also be discussed and lastly the rate effects will also be mentioned.

2.2.1   Soil displacement

When a pile is installed it will pass through three stages, which can be seen in Figure 2.3. The first phase is the installation phase, where the pile enters the soil until it has reached the desired depth. During this phase, the soil around the pile will undergo severe distortion, compaction or dilation depending on the relative density and confining stress (Bolton, 1987). In the second phase the stresses that are built up during the installation phase will equalize/dissipate. At the end of the pile installation, the pile will be loaded and the soil will be mobilised, with a force acting upward on the pile tip and shear forces acting on the pile shaft.
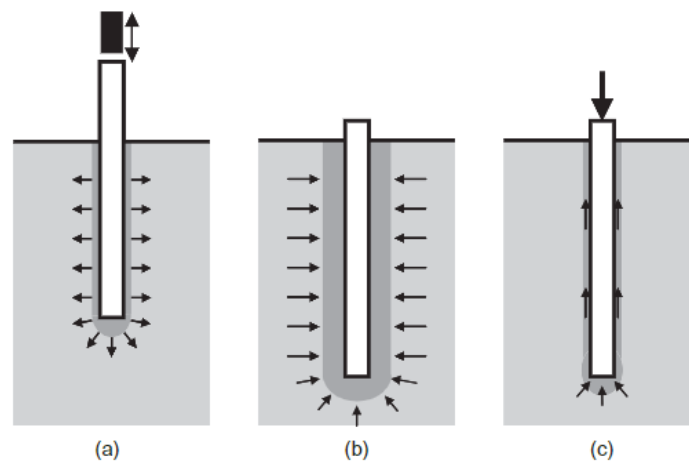
Figure 2.3: The three main phases of pile installation: (a) installation; (b) equalisation, (c) loading (Randolph, 2003)

Cavity expansion

The first phase of Figure 2.3 depicts the process called cavity expansion. During installation the soil surrounding the pile will be displaced, creating a cavity. The displaced (or mobilised) soil (compaction or dilation) will resist the piles installation, generating forces acting against the pile (either at the base or at the shaft) (Randolph, 2003). These are the forces contributing to the bearing capacity. These size of these forces are dependent on installation technique, soil strength and with that the soil stratification. Softer soils will give less resistance to the installation of a pile than stronger/stiffer soils. These forces will also be bigger if the size of the to be installed pile is bigger, since more soil will have to mobilised to fit the bigger pile. A foundation pile will thus generate more resisting forces than a cone penetrometer.

In Figure 2.4 the contours of cavity expansion from top view are given. Here a distinction is made between different zones and how the soils react in those zones (Salgado et al., 1997). In the first circle around the pile, the first zone, the stresses become so large that plastic deformation (failure) occurs. In the second zone the stresses are large enough to move into the nonlinear elastic zone, but failure does not occur. In the outer zone the stresses are so small that the soil behaves as a linear elastic material. This

horizontal influence zone might influence the resistance felt by piles if they are installed relatively close to each other. This will be further discussed at the end of this section. This zone is again dependent on the diameter of the pile.
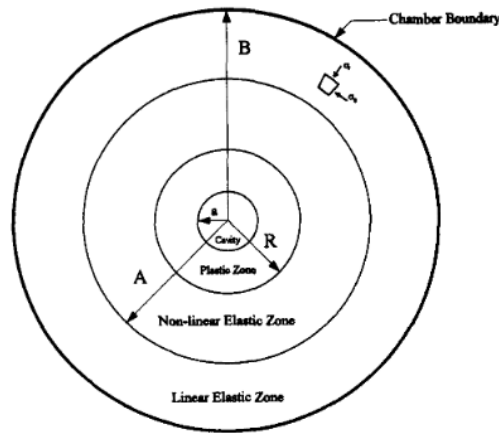
Figure 2.4: Cavity expansion contours top view. Cavity expansion generates plastic, nonlinear plastic elastic and elastic zone (Salgado et al., 1997)

This influence zone will be constant during installation in a uniform soil. However, soils are rarely uniform and will have different layers the pile will pass through. This will affect the influence zone as well as the cavity expansion. This is shown in Figure 2.5. Important to note here is that influence zone extends for a bit under the pile tip. This means that the pile will already 'feel' a different layer some time before it is actually in this different layer, which is shown the right figure. This will influence the resistance felt, which will be further elaborated in section 2.3.
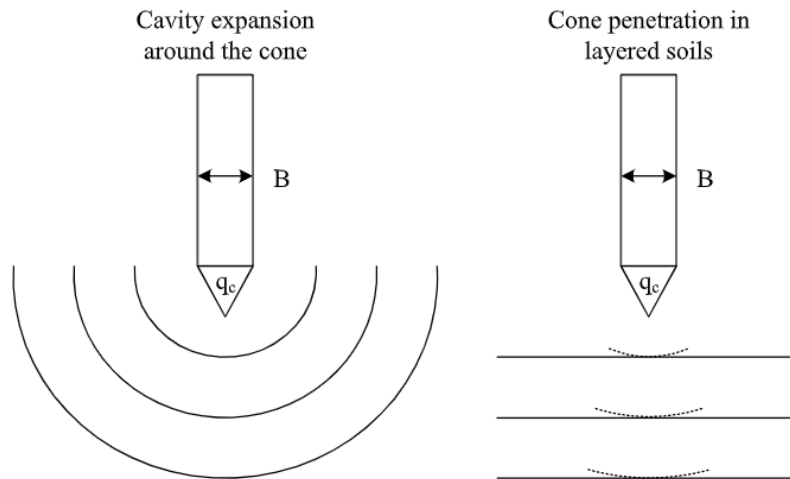
Figure 2.5: Schematic of cone penetration and cavity expansion in horizontal layers (Mo et al., 2017)

Pile grouping

Due to the horizontal influence zone, shown in figure 2.4, it is possible that piles installed close together might 'feel' each other. If these piles are in each others influence zones they might feel more resistance during the installation.

In Figure 2.6 five load curves are shown of 5 piles in one pile group, in this case the piles are micropiles (Le Kouby et al., 2016). These piles are arranged in a plus formation with the fifth one being in the middle. What can be seen is the more piles that are installed, the higher the load needed to install the pile. The biggest jump is seen between the fourth and the fifth pile. This is caused by the densification of the soil around the already installed piles, which are close enough to be in each others influence zones.
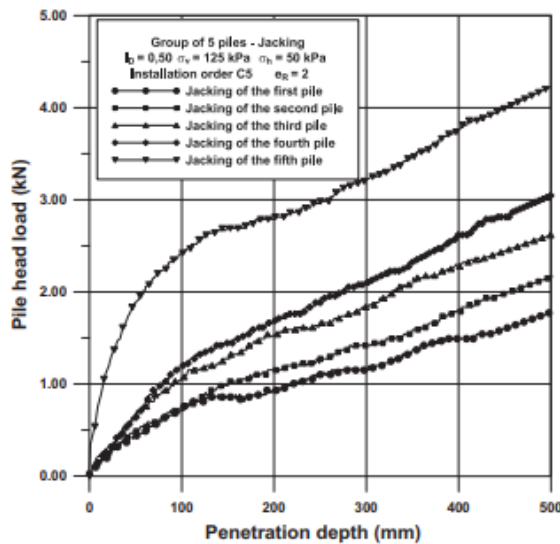
Figure 2.6: Load vs penetration depth for 5 installed piles, with the fifth pile being in the middle (Le Kouby et al., 2016)
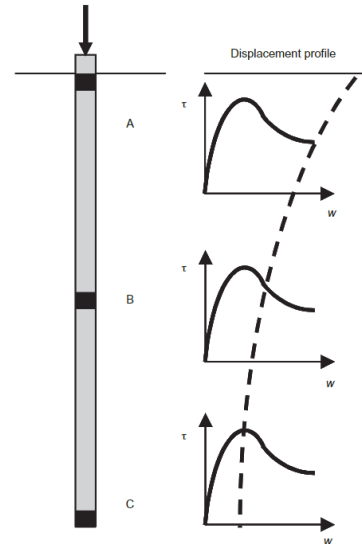
Figure 2.7: Progressive failure of pile in strain-softening soil (Randolph, 2003)

When designing pile groups, this effect is taken into account in the order and the distances. A minimum of 3 diameters distance is used between piles, which is also found by Freitas, Danziger, Pacheco, and Gerscovich (2015). And it is avoided to install a middle pile of a group last, since this one would feel the group effect the most.

Compaction and higher needed installation force is not the only negative consequence from placing piles too close to each other. Another effect that can happen is the occurrence of negative skin friction which in turn can drag a pile close-by down (Fellenius, 1999). This is dependent on the soil stratigraphy and soil properties through which the piles are installed. Here again the spacing is very important (as well as the order of placement), in a research done by Basile (2020) it is found that with a spacing of 3 diameters this effect is still very noticeable, but when this spacing is increased to 6 diameters this effect becomes negligible. In chapter 4 this will be further discussed and how this should be taken into account when selecting the data to be used.

2.2.2 Friction fatigue

As mentioned above, the soil directly next to the pile (tip) will experience severe deformation (Randolph, 2003). Soil elements that the pile tip has already passed will be more disturbed than soil elements closer to the pile tip, since these elements have had contact with a larger length of pile shaft during installation. This will not impact the horizontal stresses (shaft friction) for monotonic installations (continuous installation without interruptions) according to B. Lehane and White (2004). However, the methods most looked into in this thesis are not monotonic (hammering and hydraulic jacking) and will create cyclic shear cycles. These shear cycles are created along the shaft of the pile and this happens when the load on top of the pile is removed and (depending on what soil the pile is in) the pile will rebound. Soil elements near the surface level have endured more shear cycles due to installation of the pile, which then leads to strain-softening behaviour, which is shown in Figure 2.7. This process is also called 'friction fatigue'.

In a study done by Costa D'Aguiar et al. (2011) a numerical model was used to get a better understanding of the process of friction fatigue of cyclically loaded piles. This is done by performing multiple simulations with different axial loads. In Figures 2.8 and 2.9 the shaft resistance and base resistance in these different tests is shown. All these simulations are done in medium dense sand.
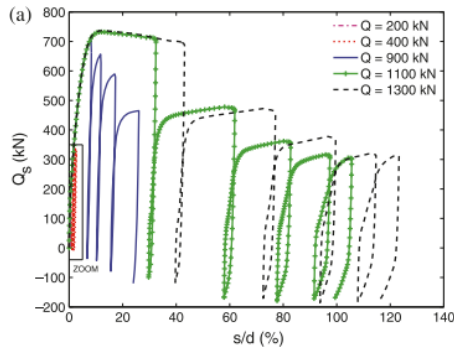
Figure 2.8: Shaft resistance for cyclic load tests for different load levels (Costa D'Aguiar et al., 2011)
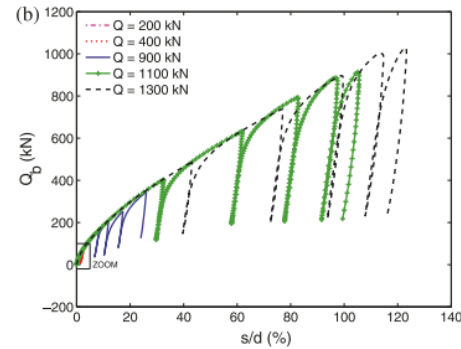
Figure 2.9: Base resistance for cyclic load tests for different load levels (Costa D'Aguiar et al., 2011)

In the left figure the shaft resistance is shown, and it can be clearly seen that the peak friction resistance reduces with an increase of cycles. In the right figure the base resistance is shown, and apart from the dips of unloading and reloading, no big influence from the cyclic loading can be seen. This has also been found by studies done by B. Lehane and White (2004) and DeJong, White, and Randolph (2006).
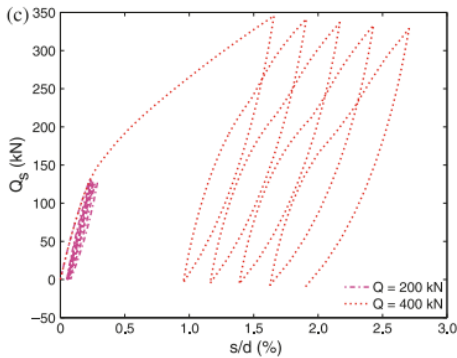
Figure 2.10: Magnification of shaft resistance for cyclic load tests for different load levels (Costa D'Aguiar et al., 2011)
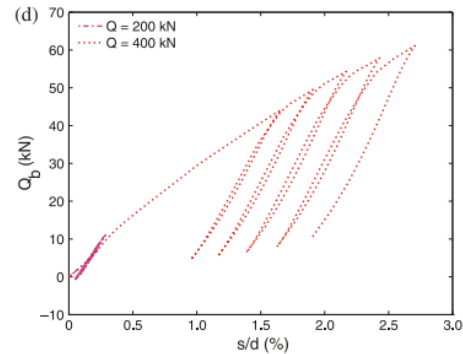
Figure 2.11: Magnification of base resistance for cyclic load tests for different load levels (Costa D'Aguiar et al., 2011)

In Figures 2.10 and 2.11 the results of the same tests are shown, but zoomed into the results of the lower loads (200 and $400\,\mathrm{kN}$). These graphs show that the lower loads yield little to now degradation in shaft resistance reduction. From this it can be concluded that the friction fatigue (reduction in shaft resistance) will increase with an increasing axial load (and shear cycles). Even though the installation method used here is pile driving instead of hydraulic jacking used by Drukpaal, this process is similar in both. In chapter 4 the mechanism of Drukpaal installation will be explained further.

The shaft capacity of the pile is thus dependent on the embedment length, shear cycles and installation load, but also the type of soil the pile passes through. However, friction fatigue is a process that is found in clay as well as in sand (Kraft Jr, Focht Jr, & Amerasinghe, 1981). To be able to predict the shaft capacity correctly, the factor α_s is used. In section 2.4 this will be elaborated further.

2.2.3 Rate effects

Rate effects in soil refer to the changes in soil behaviour that occurs due to the rate or speed of a certain process, for example shear rate effects, strain rate effects, penetration rate effects and loading rate effects. Here some of these rate effects will be looked into Quinn (2013) and Robinson and Brown (2013).

The data to be analyzed for this thesis has varying speed setting dependent on the type of soil the pile is installed in (the ammount of resistance felt). It is therefore important to see if this could influence the tip resistance felt by the pile. In Figure 2.12 the tip resistance is shown from a discrete element method model from different penetration velocities (Esposito et al., 2018).
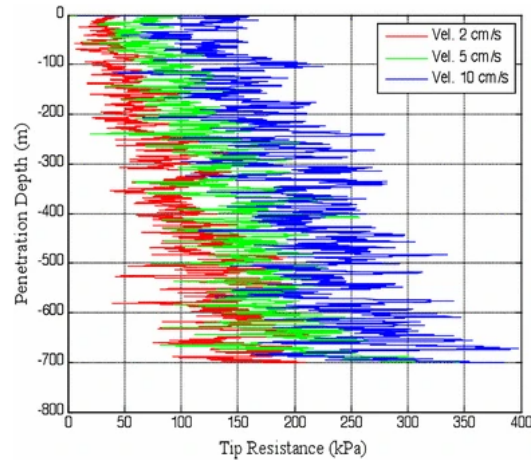
Figure 2.12: Tip resistance results from a discrete element method model from different penetration velocities (Esposito et al., 2018)

In this figure it can clearly be seen that if the installation velocity increases, the measured tip resistance also increases. However, these numerical tests were performed in a homogeneous soil and no pore pressures were accounted for. This was done to only get the correlation between installation velocity and tip resistance. However, in the data from Drukpaal, the soil is not homogeneous and pore pressures are certainly present in the soil.

In a research done by Chow et al. (2018) the influence of different drainage paths on the measured tip resistance was studied. In this research, in a centrifuge test, a model piezocone was jacked into saturated loose and dense silica sand at varying penetration rates. In Figures 2.13 and 2.14 backbone curves are shown for the net cone resistance normalised by the drained net cone resistance and the excess pore pressure normalised by the vertical effective stress.
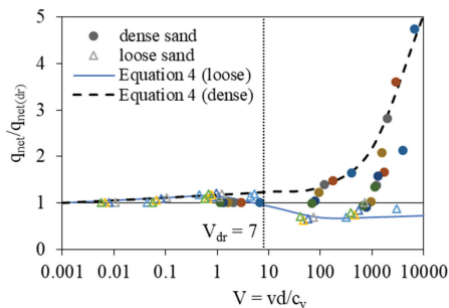
Figure 2.13: Net cone resistance normalised by the drained net cone resistance plotted against the range of non dimensional velocity V (Chow et al., 2018)
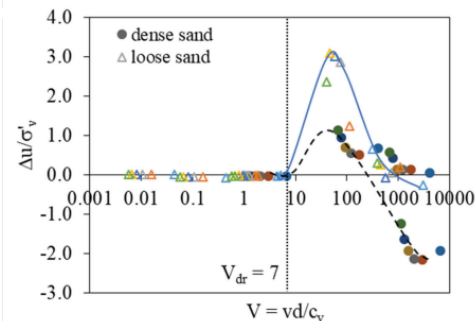
Figure 2.14: Excess pore pressure normalised by the vertical effective stress plotted against the range of non dimensional velocity V (Chow et al., 2018)

From these figures it can be seen that if the velocity increases in loose sand that the net cone resistance decreases and the pore pressures increase, this soil is exhibiting contractive behaviour. While the dense sand exhibits dilative behaviour, with an increase in velocity the net cone resistance increases and the pore pressures (with regards to vertical effective stress) decreases.

This shows that the penetration rate effects are dependent on various factors which can cause different soil behaviour. It is possible that in the analysis the difference in installation speed can influence the needed installation force, but it will be very hard to conclude.

Another research done by Al-Mhaidib (2005) the shearing rate effect on the interfacial friction angle between sand and steel was found. Here it was found that the interface friction angle between sand and steel with different surface roughness increases as the shearing rate increases. And an increase in friction angle in sands was found with in increase in shearing rate. To tie this back to the installation of piles, with a higher installation speed the sand along the pile shaft will experience more shearing which could

lead to a higher friction angle which in turn could lead to higher friction along the shaft.

And lastly, in a research done by Al-Mhaidib (2001) it was found that the loading rate significantly influences the compressive capacity of a model pile. Increasing the loading rate resulted in an increase in pile capacity, which is an interesting find when the loading rate in the to be analysed data is not constant.

2.3 Geometrical effects

In this section the concept of sensing and development depth will be explained and how these influence the total capacity of a pile. After this the influence of the geometry of the pile tip on the sensing and development depth will be discussed.

2.3.1 Diameter

Sensing and Development depth

In Figure 2.15 a schematic is shown of the so called sensing and development depth, this is also the influence of the diameter on the felt resistance. This was already shortly mentioned in section 2.2 and shown in Figure 2.5.

The thick black line (in Figure 2.15 shows the q_c profile of a uniform strong layer and the dashed line shown the q_c profile of a uniform weak layer. However, the q_c profile of the layered soil (weak layer overlying a strong layer) doesn't follow strictly these two paths. From a certain distance from the interface the overlying soil will feel the underlying soil, this distance is called the sensing depth. After the interface the q_c also hasn't reached the q_c values from the strong profile yet, this distance is called the development depth, which is the distance over which the overlying layer still influences the underlying layer. These two distances can be very hard to predict and can have a big impact on the development of the bearing capacity, especially in layered soils.

These distances are determined by the influence zone, which has already been discussed in section 2.2. The shape and size of this influence zone is determined by the shape of the pile tip and the diameter of the pile itself. A bigger diameter pile will feel underlying layers earlier, because of how much soil is displaced (mobilised) around it.
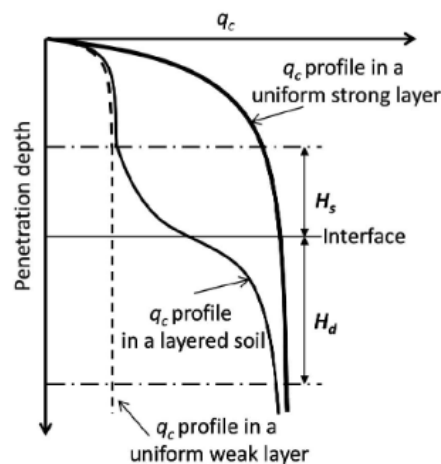
Figure 2.15: Sensing and development distance (Tehrani et al., 2018)

In Figure 2.16 different cases are shown of an embedded sand layer in clay. In the graph the tip resistance is shown for these different cases. As can be seen in the graph, the peak resistance decreases when the height of the sand layer decreases. This is because the sand layer is getting smaller than the development depth and sensing depth combined. The sand doesn't reach its true resistance. The true resistance of a soil is the resistance that is expected of said soil if there was no influence from overlying/underlying stronger/weaker soils (if there is no gradual transition necessary).
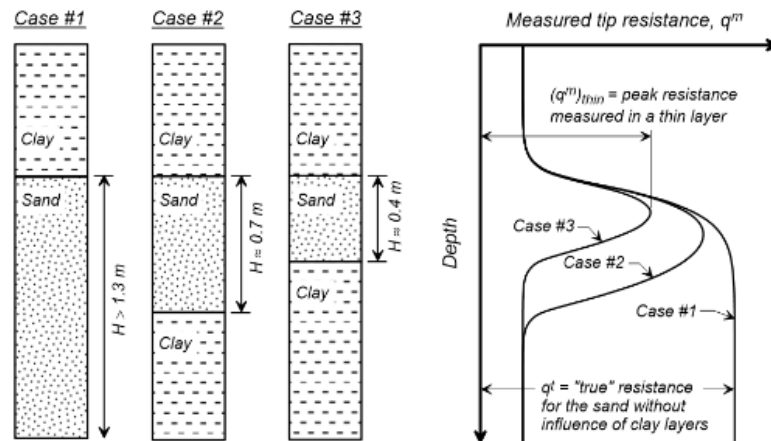
Figure 2.16: Schematic of thin layer effect of a sand layer embedded in a clay layer (Boulanger & DeJong, 2018)

In section 2.4 the current methods will be shown. Here it will be explained how all of these methods take the influence zone into account.

Punch through

When a strong soil layer is situated on top of a relatively big weak soil layer there is a chance that punch-through happens during the installation of a pile. When this happens the strong soil fails and the bearing capacity of the soil will rapidly decrease when the pile is still in the strong soil. In Figure 2.17 a typical load-penetration response is shown, where at a certain point in the sand the weaker underlying clay layer is felt and the pile will only feel the resistance from that layer.
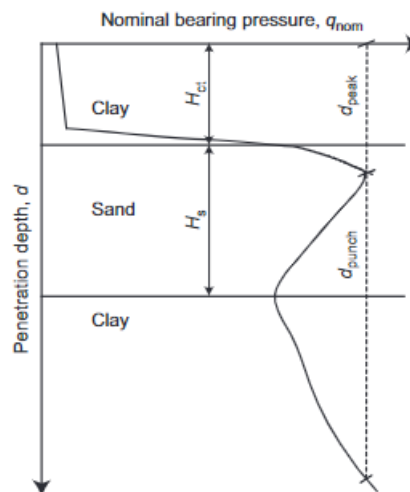
Figure 2.17: Typical load-penetration response in clay-sand-clay stratigraphy where punch through is shown (Ullah et al., 2017a)

This is a different phenomena than the sensing depth earlier mentioned. It was found that this phenoman is a function of distance to the clay layer, the diameter of the penetrating object and the ratio of strength between the clay and sand layers (Ullah et al., 2017a) (Ullah, Stanier, Hu, & White, 2017b). Punch-through is more likely to happen if the underlying clay layer is very weak with regards to the overlying sand layer. This situation might also occur when a strong embedded soil layer is encountered which is surrounded by a weaker soil. In this case the sand layer might be felt only minimally depending on how big the layer is with regards to the diameter of the pile. This will be further discussed in chapter 4.

2.3.2   Shape of pile tip

It is important to note that there is a difference in pile tip between a CPT, which has a conical tip, and a foundation pile, which has flat base. This difference might influence the way both of these experience resistance of soil. In Figure 2.18 the idealized slip mechanism for a conical base is shown. In zone 1 of the figure there is mainly vertical displacement, in zone 2 radial displacement is built-up and in zone 3 this radial displacement is prevalent. When the pile has a flat base the movements in zones 2 and 3 decrease significantly. A conical based penetrometer might thus feel less of the soil resistance underneath the tip, but will feel more resistance from zones 2 and 3 of the soil surrouding the pile tip, while for a flat based pile this is the other way around (Tovar-Valencia et al., 2021).
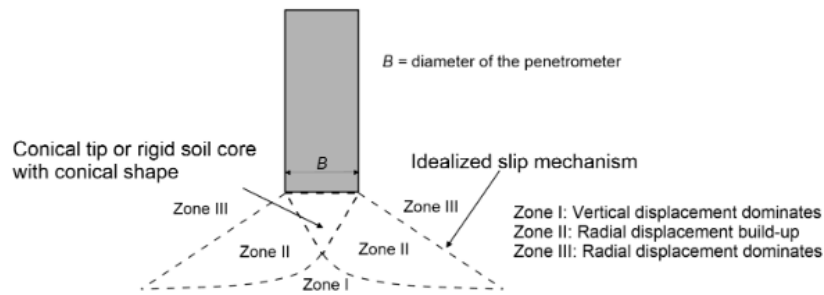
Figure 2.18: Idealized slip mechanism of a conical tip (Tovar-Valencia et al., 2021)

This can also be seen in Figure 2.19, which are the results from a numerical model performed by Hunt et al. (2023). In these figures the absolute particle displacement is shown in the top row and the incremental particle displacement vectors is shown in the bottom row. These figures show the movement of the particles surrounding the pile tip for varying angles of conical tip with the last one being a flat base. Here it is shown that in the first image there is most movement at the sides of the cone outward, while in the last figure the most movement is underneath the flat base directly down.
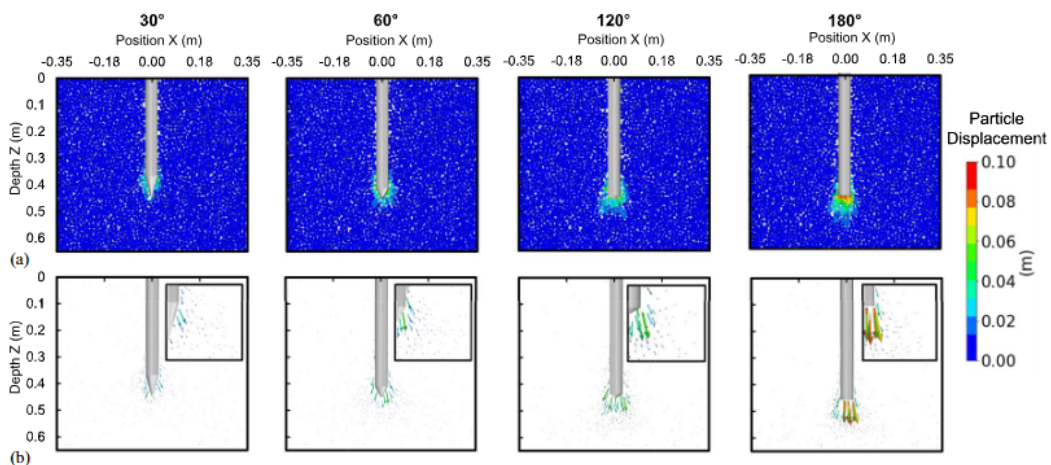
Figure 2.19: Particle displacement form confined discrete element model simulations with tips of varying apex angles: (a) absolute particle displacement; and (b) incremental particle displacement vectors (Hunt et al., 2023)

In Figure 2.19 the results of tests performed on model piles in sand are shown. Model piles with a flat base and conical base are installed in dense sand (shown with the square markers, top two lines) and medium-dense sand (shown with circular markers, bottom two lines), performed by Tovar-Valencia et al. (2021). From these test a significant effect can be seen from the different pile tip. A flat base, according to this study, will feel significantly more resistance than a conical base.
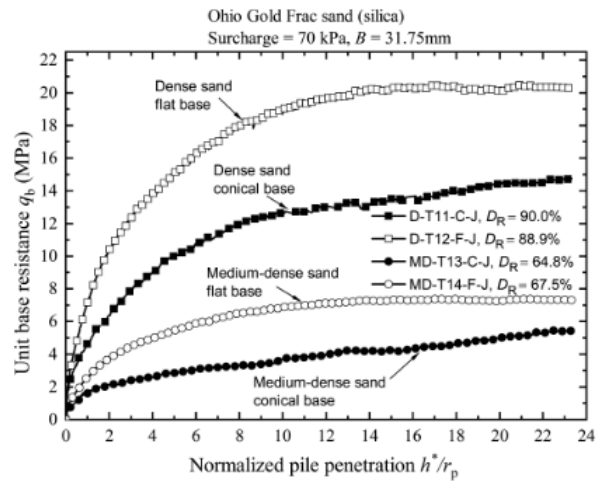
Figure 2.20: Tip resistance of model piles with conical and flat bases jacked in dense and medium-dense sand (Tovar-Valencia et al., 2021)

A CPT cone might thus feel less resistance than a typical flat based pile will. This effect, however, is already accounted for in the CPT-based prediction methods, just like the diameter difference between the CPT and pile have also been accounted for in these methods.

2.4 Current methods

2.4.1 Base capacity methods

Mierlo and Koppejan - Dutch method

This method was developed by ir. W. C. van Mierlo and ir. A. W. Koppejan and is the most commonly used method in the Netherlands (van Mierlo & Koppejan, 1952). This method is also known as the 4D-8D method. In Figure 2.21 the influence zone from Koppejan is shown. Underneath the tip, the influence zone varies from 0.7D to 4D, dependent on the layer underneath. Above the tip the influence zone is always 8D.
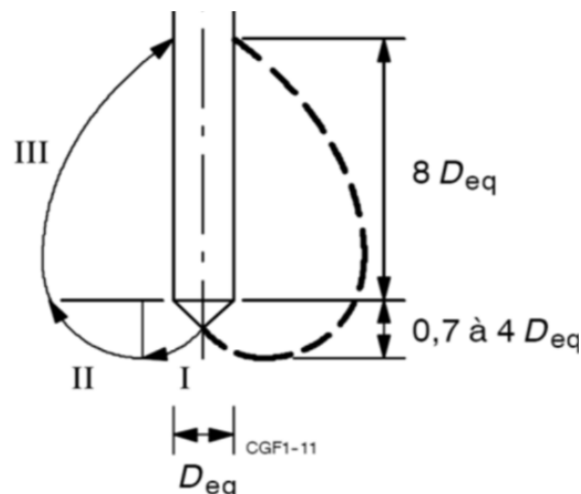
Figure 2.21: Influence zone Koppejan method (van Mierlo & Koppejan, 1952)

In Figure 2.22 a schematization is shown of how the value for $q_{c,avg}$ is found. The different average parts (I, II and III) are the same as in the influence zone figure.
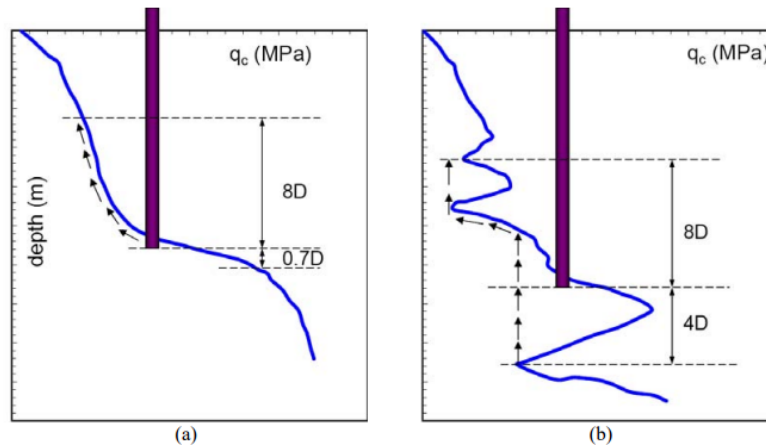
Figure 2.22: Calculation of the average cone tip resistance $q_{c,avg}$ in the Koppejan method (Xu, 2007)

$$Q_b = A \cdot q_{b,kop} \tag{2.4}$$

$$q_{b,kop} = \frac{1}{2} \cdot \left(\frac{q_{c,I,avg} + q_{c,II,avg}}{2} \cdot q_{c,III,avg} \right) \tag{2.5}$$

Where:

$q_{b,kop}$	Maximum pile tip capacity	[MPa]
$q_{c,I,avg}$	The arithmetic average of q_c values below pile tip over a depth which may vary between 0.7D to 4D as shown in Figures 2.22.	[MPa]
$q_{c,II,avg}$	The arithmetic average of the q_c values following a minimum path rule recorded below the pile tip over the same depth of 0.7D to 4D	[MPa]
$q_{c,III,avg}$	The arithmetic average of the minimum q_c values following a minimum path rule recorded above the pile tip over a height of 8D.	[MPa]

LCPC

The Laboratoire Central des Ponts et Chaussees (LCPC) method uses instead of the 4D/8D influence zone from the Dutch method a constant influence zone of 1.5D above and below pile tip level. These dimensions for the influence zone were found by analyzing the results of 197 result tests (Bustamante & Gianeselli, 1982). This method, as well as the Dutch method, is an empirically based method. The averaging technique is shown in Figure 2.23.
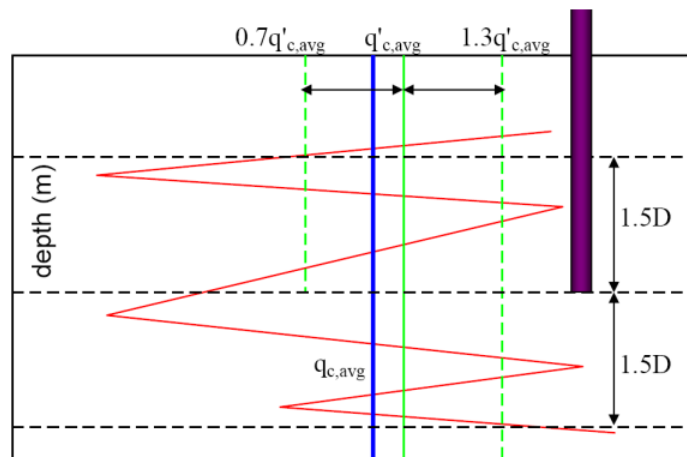
Figure 2.23: Calculation of $q_{c,avg}$ in the LCPC method (Xu, 2007)

The calculations steps are as follows:

- Calculate the average of all q_c measurements 1.5D above and below the tip of the pile, $q'_{c,avg}$ in Figure 2.23.
- Eliminate all values below $0.7 \cdot q'_{c,avg}$ and above $1.3 \cdot q'_{c,avg}$.
- Calculate the average again with the remaining values of q_c. This average is denoted as $q_{c,avg}$ in the figure.

The tip capacity of the pile is then calculated using the following equation.

$$q_{b,LCPC} = k_c \cdot q_{c,avg} \tag{2.6}$$

The correction factor k_c in equation 2.6 is used to take into account the installation method and soil type. This correction factor will not be used in this thesis.

Boulanger and DeJong

This method is also known as the filtering method. This method wasn't originally not meant to be used for piles. It was however adopted for piles in a Unified method (Bittar, Lehane, Boulanger, & Dejong, 2020). The original method was meant to be used to estimate the true resistance (q_c^t) of the soil from the measured tip resistance (q_c^m) from a CPT (Boulanger & DeJong, 2018). However, in the method adopted for piles the resistance measured by CPT is thought to be the true resistance, since the diameter of a CPT is so much smaller than that of a pile.

In Figure 2.24 a schematic is shown on how this method works. To get from the true resistance to the measured resistance, the true resistance is multiplied with a filter (w_c). This filter is a normalized product from two different filter functions (w_1 and w_2), as can be seen in equation 2.8. The function of w_1 is used to account for the relative influence of any soil decreasing with increasing distance from the cone tip, see equation 2.9. The function of w_2 is used to adjust the relative influence based on whether the soils away from the cone tip are stronger or weaker than the soil at the cone tip, see equation 2.10. Here weaker soils will get a bigger influence and stronger soils will get a smaller influence.
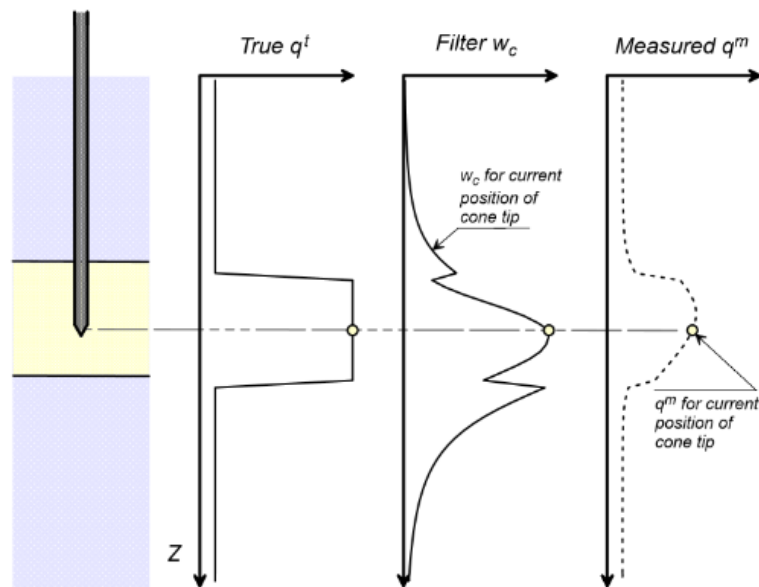
Figure 2.24: Schematization of the filtering method (Boulanger & DeJong, 2018)

Here all the needed equations for finding the $q_{b,filt}$ can be found. In the equations q_c^m and q_c^t have been replaced by $q_{b,filt}$ and q_c respectively.

$$q_{b,filt}(z) = \sum q_c \cdot w_c(z) \tag{2.7}$$

$$w_c = \frac{w_1 w_2}{\sum w_1 w_2} \tag{2.8}$$

$$w_1 = \frac{C_1}{1 + \left(\dfrac{z'}{z'_{50}}\right)^{m_z}} \tag{2.9} \qquad\qquad w_2 = \sqrt{\frac{2}{1 + \left(\dfrac{q_c(z)}{q_{c,tip}}\right)^{m_q}}} \tag{2.10}$$

$$z' = \frac{z - z_{tip}}{d_c} \tag{2.11}$$

$$z'_{50} = 1 + 2\left(C_2 \cdot z'_{50,ref} - 1\right)\left(1 - \frac{1}{1 + \left(\dfrac{q_{c,tip}}{q_c(z)}\right)^{m_{50}}}\right) \tag{2.12}$$

Where:

$q_{b,filt}(z)$	Base capacity using the filter method at depth z	[MPa]
$q_c(z)$	Measured tip resistance from CPT at depth z	[MPa]
$w_c(z)$	Filter function for depth z	[-]
w_1	Function that takes into account relative influence of any soil decreasing with increasing distance from cone tip	[-]
w_2	Function that adjusts relative influence based on if soils away from cone tip are weaker or stronger than soil immediately at cone tip. Increasing influence if soil is weaker and decreasing if soil is stronger	[-]
z'	Depth relative to cone tip normalized by cone diameter (d_c)	[-]
z_{tip}	Depth of cone tip	[m]
z'_{50}	Normalized depth at which $w_1 = 0.5C_1$	[-]
z'	Depth relative to cone tip normalized by cone diameter	[-]
C_1	Parameter equal to unity for points below cone tip, and linearly reduces to a value of 0.5 for points located more than 4 cone diameters above the cone tip	[-]
C_2	Parameter equal to unity for points below cone tip, and 0.8 for points above cone tip	[-]

The following parameters are constants and their values have been taken from Boulanger and DeJong (2018); $z'_{50,ref} = 4.0$, $m_z = 3.0$, $m_{50} = 0.5$ and $m_q = 2$.

Munta de Boorder

This method was made by adjusting the filter method by Boulanger and DeJong to better fit for thin layers. The measured resistance from the CPT is again multiplied by a filter w_c and this is again a normalized product of w_1 and w_2. The equations for the latter two are however different than in the original filter method. Here, as can be seen in equation 2.14, w_1 is determined by a cosine function. How this function works can be seen in Figure 2.25. It basically shows the influence zone around the pile tip, which extends 7D below the pile tip and 3.7D above pile tip. At the pile tip the influence is equal to 1.
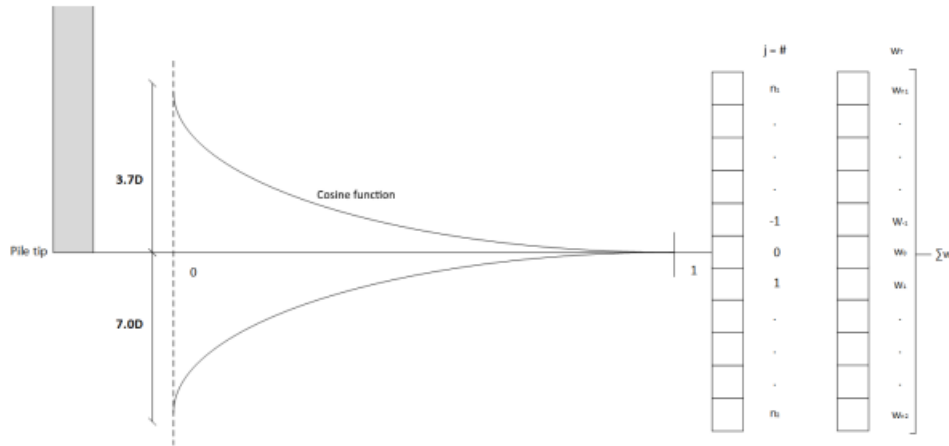
Figure 2.25: An overview of the influence zone and weights used in the method from Munta de Boorder (de Boorder, 2019)

$$q_{b,munt} = \sum q_c \frac{w_1 w_2}{\sum(w_1 w_2)} \tag{2.13}$$

$$w_1 = e^{-f \cdot |z'|} \cos\left(0.5 \cdot \pi |z'|\right) \tag{2.14} \qquad\qquad w_2 = \left(\frac{q_{c,tip}}{q_c(z)}\right)^s \tag{2.15}$$

$$z' = \frac{z - t_{tip}}{C \cdot D} \tag{2.16}$$

Where:

f	Damping factor (=13.5) (de Boorder et al., 2022)	[-]
z'	The normalized distance to pile base	[-]
$z - z_{tip}$	The distance to the pile base	[-]
C	A constant which determines the zone of influence (=6.5 above pile base and 10.5 below pile base)(de Boorder et al., 2022)	[-]
$q_{c,tip}$	The cone resistance at the pile tip level	[MPa]
$q_c(z)$	The cone resistance at level z	[MPa]
s	A fit parameter (0.56 above the pile base and 0.79 below pile base)(de Boorder et al., 2022)	[-]

2.4.2 Shaft capacity methods

NEN

The first shaft capacity method is the NEN method as stated in the NEN (Normcommissie 351 006 'Geotechniek', 2017). This method is fairly straight forward. The tip resistance is multiplied by a factor α_s, which is dependent on the soil and pile type. This factor will be 0.01 for sandy soils and 0.025 for clayey soils for precast concrete piles, which is the type of piles used by Drukpaal. Here it can be seen that clayey soils count more in the shaft resistance. The whole function is also summed up for how deep the pile is already in the soil. The deeper the pile, the more shaft friction there will be. Normally the type of soil is determined by calculating the friction ratio (Robertson, 2010), which is calculated by dividing the shaft friction (as measured by the CPT) by the tip resistance. However, not all CPT's measure the shaft friction. To mitigate this problem an arbitrary boundary has been set to determine whether the soil is sand or clay. If the tip resistance is smaller than $2\,\mathrm{MPa}$ than the soil is set to be clay, if it is higher, the soil is thought to be sand. This will make it possible to apply the right correction factor. This boundary has also been used in the ISO shaft capacity method.

$$q_{s,NEN}(z) = \sum_0^z \alpha_s \cdot q_c(z) \tag{2.17}$$

Where:

$q_{s,NEN}$	Shaft capacity as calculated by the NEN method	[MPa]
α_s	Correction factor shaft capacity (0.025 for clay and 0.01 for sand)	[-]
q_c	Cone resistance	[MPa]

ISO Unified method

This method was developed to get a better estimation of the axial capacity of piles in sand (B. M. Lehane et al., 2020) and clay (B. M. Lehane et al., 2022) separately. These different methods work quite similarly, but there are some differences that should be mentioned. In equations 2.19 and 2.22 the equations for τ_f can be found. For the equation for clay the tip resistance is included. In the method as described by B. M. Lehane et al. (2022) this should actually be the true resistance. This value can be found by correcting the tip resistance with the measured pore pressures. However, these pore pressures aren't always measured so to simplify this equation the tip resistance is used instead of the true resistance.

$$Q_s = \pi D \int_0^L \tau_f \, dz \tag{2.18}$$

$$\text{Sand: } \tau_f = \left(\frac{f_t}{f_c}\right) \cdot (\sigma'_{rc} + \Delta\sigma'_{rd}) \cdot \tan 29° \tag{2.19}$$

$$\sigma'_{rc} = \left(\frac{q_c}{44}\right) \cdot A_{re}^{0.3} \cdot (max[1, (h/D)])^{-0.4} \tag{2.20}$$

$$\Delta\sigma'_{rd} = \left(\frac{q_c}{10}\right) \cdot \left(\frac{q_c}{\sigma'_v}\right)^{-0.33} \cdot \left(\frac{d_{CPT}}{D}\right) \tag{2.21}$$

$$\text{Clay: } \tau_f = 0.07 \cdot q_c \cdot (max[1, (h/D)])^{-0.25} \tag{2.22}$$

Where:

τ_f	Shear stress	[MPa]
f_t/f_c	Coefficient for pile loaded in compression or tension (= 1 or 0.75 respectively)	[-]
σ'_{rc}	Radial effective stress (stationary)	[MPa]
$\Delta\sigma'_{rd}$	Increase in radial effective stress that occurs during pile loading	[MPa]
A_{re}	Effective area ratio (=1 for closed ended piles)	[m^2]
σ'_v	Vertical effective stress (estimated with $\frac{10 \cdot z}{1000}$, 10 is estimated effective unit weight soil)	[MPa]

2.5   Previous research

In this section previous research done on the main topics in this thesis will be discussed and how these relate to this research done.

2.5.1   Plantema (1948)

In a research done by Plantema (1948) a connection was found between the cone resistance of a pile-sounding (which is similar to a CPT now) and the tip resistance of a foundation pile, since the two behave similarly but have different base areas. In Figure 2.26 the stress distribution under a circular plate is shown, which is dependent on size. From this figure it can already be seen that the bigger the circular plate, the bigger the influence zone is going to be.
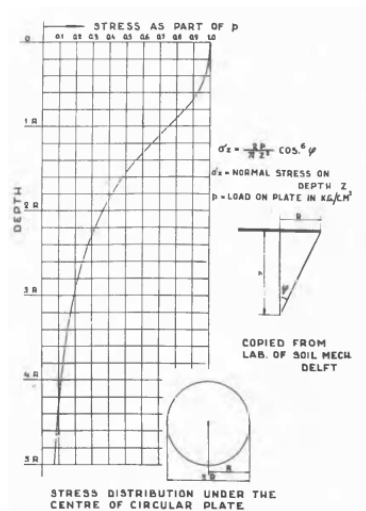
Figure 2.26: Stress distribution under the centre of a circular plate (Plantema, 1948)
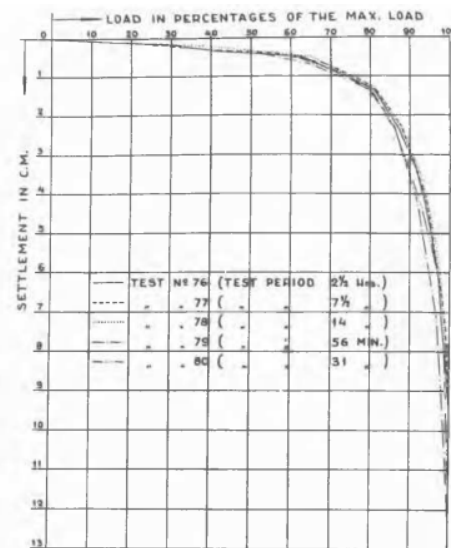
Figure 2.27: Load-settlement curve found by Plantema (1948)

From this figure an influence zone under the pile of around 4R can be found, which is 2 diameters, which is a lot smaller than the influence zones found in the current base capacity methods except for LCPC. However, these tests were only done in sand so a weak underlying layer is not included in this influence zone.

In this research the load-settlement curve was found as well as the safety factor to keep settlement under a foundation within a certain limit. This curve is seen in Figure 2.27.

2.5.2   White and Bolton (2005)

In a research done by White and Bolton (2005) the base resistance of a pile was compared to that of a CPT. In this research it was found that the the tip resistance as measured by a CPT can be easily linked to the base resistance of a foundation pile, almost one to one. However, certain mechanisms occur during installation which would recommend using a reduction factor on the tip resistance. These mechanisms include partial embedment into the bearing stratum and therefore only partially mobilising the base resistance. This is accounted for in this study by weighing the tip resistance of the CPT with the overlying weak layers in the soil profile.

Taking into account of overlying weak layers is found in multiple of the current methods to be used in this thesis and is thus a very important part in equating the CPT tip resistance to base capacity of a foundation pile.

2.5.3   Xu and Lehane (2005)

In this research an evaluation was done by B. Lehane et al. (2005) on the relative reliability of certain design methods (Fugro-04, ICP-05 and NGI-99) for assessment of the end-bearing capcity of closed

ended piles as well as an evaluation on various averaging techniques for the tip resistance including the Dutch method (Koppejan) and LCPC.

These latter evaluation was done by performing a CPT and (continuously) jacking a pile into the same soil and recording the resistance felt by both. The different averaging techniques are used on the CPT data plotted in the same figures with the CPT tip resistance and pile tip resistance. What was noticed was that the Dutch method worked quite well to predict the tip resistance of the continuously jacked foundation pile, see Figure 2.28. There is some disagreement between the prediction of the Dutch method and the tip resistance of the jacked pile, see Figure 2.29, however, from the different averaging techniques compared to each other the Dutch method seemed the most accurate.
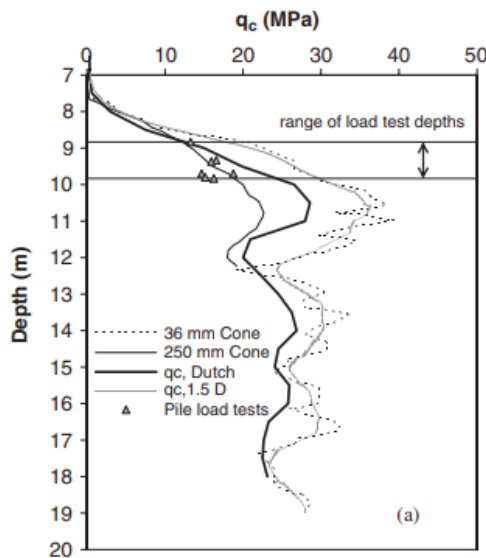
Figure 2.28: Tip resistance profile of a continuously jacked 250 mm cone (B. Lehane et al., 2005)
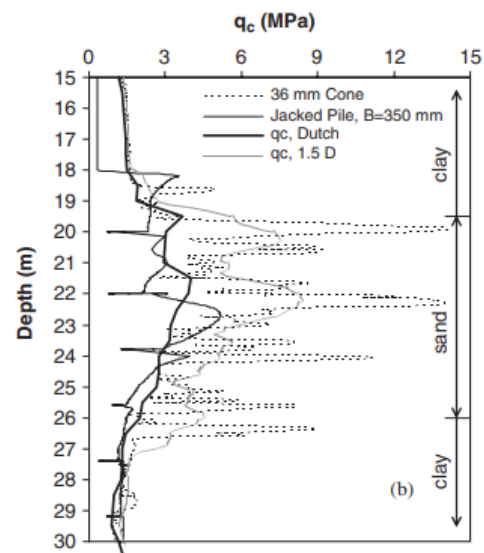
Figure 2.29: Tip resistance profile of jacked 350 mm square pile (B. Lehane et al., 2005)

In this thesis both of these averaging techniques will be compared. From this research it is now expected that the Dutch method will work better than the LCPC method.

2.5.4 CRUX (2018)

Lastly a research was done on the data that will be used in this thesis by Dieteren, Katerberg, Meindhardt, and Tekofsky (2018). Here the emphasis was on creating a program that could be used to design the foundation piles. This program predicts the needed input force as well as calculate the needed foundation depth on basis of CPT profile.

Within this program the Dutch method for base and shaft capacity was used (Koppejan and NEN). However, for the base capacity a choice can be made between two influence zone sizes, either 4D/8D or 2D/4D. The former is a safer approach than the latter. No other methods were compared to the force measured by Drukpaal.

This thesis is similar to this paper, however it is more extensive. More methods will be compared as well as why certain methods work better than others.

3

Research approach

3.1 Research objectives

The aim of this research is to get a better understanding of the existing capacity prediction by comparing them to the jacking force measurements from Drukpaal. The main question for this research is as follows:

What combination of capacity prediction methods for shaft and tip resistance works best to estimate the total force over depth as measured by Drukpaal?

To help answer this research question and structure this report the following sub-questions are formulated:

- What is the best statistical method to compare the simulations to the measurements?

- Are the combinations of capacity prediction methods independent on location (i.e. the subsurface profile)?

3.2 Methodology

Here it is explained how the above mentioned questioned will answered:

- In the preliminary data analysis the Drukpaal measurement will be closely looked at. Here it will be determined how these measurements should be used in the further analysis. There are multiple aspects that influence the measurements, think of installation speed and order, as well as limitations in the recordings of the data of Drukpaal. Here the measurements to be used in the further analysis will be selected and it will be explained how the different aspects are accounted for.

- In the subsurface analysis the CPT profiles of the chosen CPTs per project are shown as well as how variable they are. In combination with an overview of the base capacity methods on theoretical profiles a hypothesis will be made on which method will work well for which projects.

- Two different analysis will be done, one visual and one statistical. In the visual analysis the results of the simulations will be shown in plots where the simulations and measurements are plotted against depth. It will be discussed if the results are expected or not and why certain methods behave the way they do. If the simulations do not align it will be discussed what factors influenced this.

- After the visual analysis a statistical analysis will be done to (numerically) show how similar the simulations are to the measurements. First comparison methods are shown and a choice is made for which of these methods to use to gain the best statistical outcome. With this a value can be given to each combination of methods for each project, which will be used to find the overall best method (combination, base or shaft). Here it will also be discussed whether the methods are location dependent and what subsurface profiles fit best with which method.

In Figure 3.1 a flowchart is shown of the order in which this research is done and what parts influence each other.

3.3   Outline

This research will have the following structure. The main literature study with background information on the topic is given in chapter 2, here the used capacity prediction methods are also explained. In chapter 4 a preliminary data analysis is done to show the available data and how the appropriate data for the analyses are chosen. The subsurface analysis will be done in chapter 5 where the subsurface profiles of the projects are shown as well as an overview of how the different base capacity methods work on different theoretical subsurface profiles. From this a small conclusion and hypothesis will be given on the outcome of the simulations. In chapters 6 and 7 the visual analysis and statistical analysis of the results are shown. In the discussion and conclusion (chapters 8 and 9) the results will be highlighted as well as the limitations of this research. In these chapter recommendations will be made on what possible follow-up research should focus on.
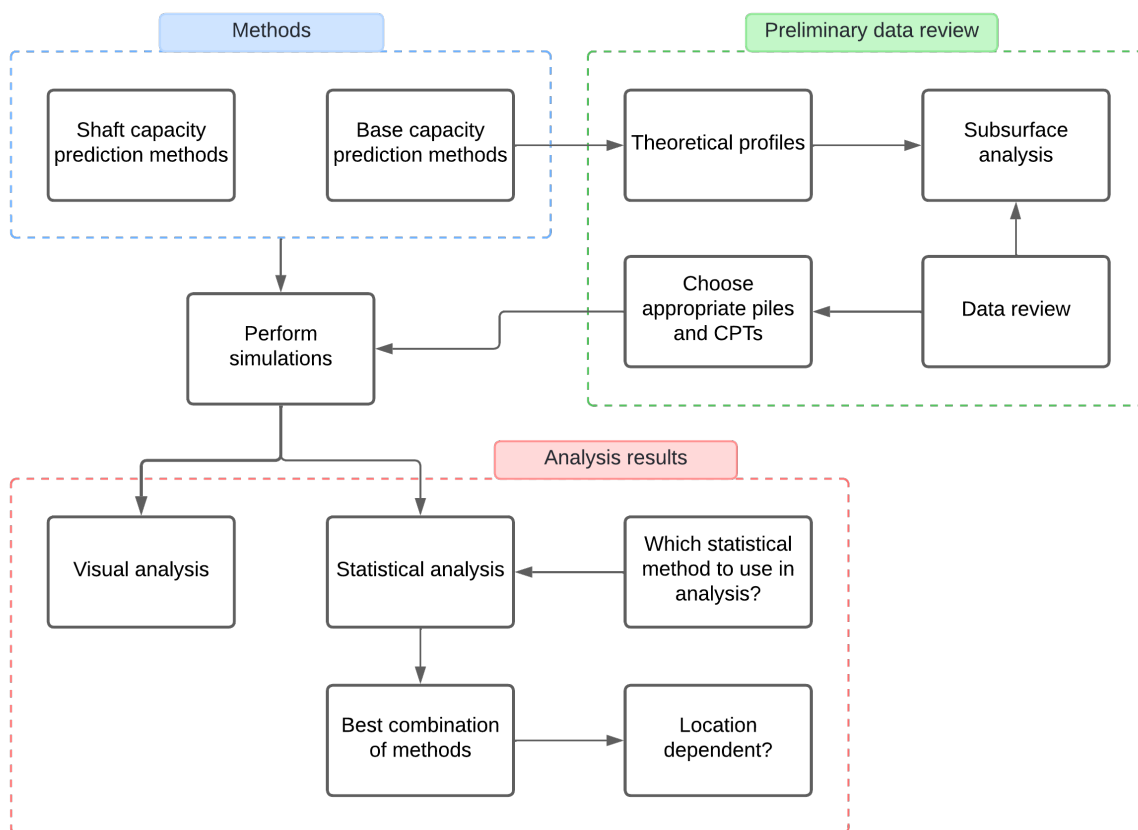
Figure 3.1: Flowchart thesis

Part I

Preliminary data analysis

4

Preliminary analysis of Drukpaal datasets

In this chapter the datasets from Drukpaal will be analysed shortly. First the installation technique of Drukpaal itself will be explained after which the measurements are shown. Here the effects of installation speed and installation order will be looked into and how these effects will be taken into account in the simulations or selection of the data. After this the limitations of the data will be mentioned. In the last part of this chapter an overview of the locations of the projects will be given as well as an explanation of the chosen piles and CPT for the simulations.

Figure 4.1: Overview of Drukpaal set-up at Pijnacker (Doornbos, 2023)

4.1   Installation technique

In Figure 4.1 an overview of the set-up of Drukpaal machinery is given. The left machine is the machine that is used to press the piles into the ground while the right machine is a crane used to hoist the piles into the air to get the base of the pile at ground level. The machine on the left employs hydraulic jacks that utilize counterweights to generate a reaction force. This is not a continuous process however. The machine will jack the pile into the ground in strokes of $2\,\mathrm{m}$ after which the machine has to regrip the pile. This process will continue until the entire length of the pile is installed except for the last $2\,\mathrm{m}$, since the clamping mechanism can not install closer to the ground level. A steel attachment is used to install the pile to the wanted depth. The machine can reach a maximum installation force of $3100\,\mathrm{kN}$, but the machine also has a minimum installation force equal to the weight of the clamping mechanism and pile together. This force is not included in the total force measurements and needs to be manually added. These two weights together produce a downward force of around $120\,\mathrm{kN}$.

During installation the installation force is recorded over depth, which is the measurement to be used in the simulations because of the similarities to a cone penetration test. In the next section the format of the data will be looked at closer as well as how this data will be used in the simulations.

4.2   Drukpaal measurements

Per project the available data consisted of: piling plans with locations of piles and CPT where these are numbered, the CPT measurements and installation records which numbers correspond to the piling plans.

Three different measurement are taken during the installation of a pile. The depth, the total installation force and the installation speed. In Figure 4.2 the recorded installation measurements from one pile in Harlingen have been plotted to get a better understanding of the data. Here the total force and installation speed have been plotted against penetration depth from ground level.

In the right figure there are prominent dips in the otherwise constant installation speed. These dips correspond to the regripping moments of the machine, which are highlighted by the yellow dashed lines. Since the measurements are taken per depth interval of $5\,\text{cm}$, the dips don't necessarily reach zero but rather a mean value from the interval surrounding that point.

The dips in speeds can sometimes also be seen in the left figure (total force against depth), but mostly when the pile tip has reached a stronger (probably more sandy) soil. In these soils it is possible that when the machine lets go of the pile to reprip (unloading of the pile), the pile will rebound. The mobilised soil surrounding the pile will try to go back to its original undisturbed state. With this the pile might be pushed back up. When the pile is reloaded (regripped) the force needed to overcome this rebound length is smaller until 'new' undisturbed soil is encountered. Here the original resistance path will be followed again, this is due to the elastic properties of these materials. This will cause the small dips in the left figure. These dips in total force will be ignored in the further analysis of the data and in the simulations, since they do not impact the bearing capacity.
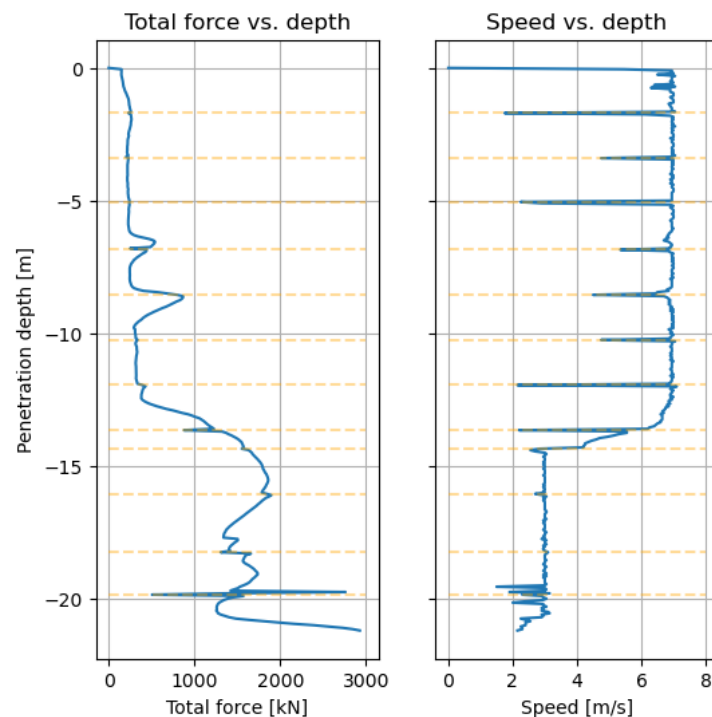
Figure 4.2: Example of data registration of installation of one pile in Harlingen. The yellow dashed lines show where the machine has regripped the pile. Both the total force and speed are plotted against the penetration depth from ground level.

Another thing to note from this figure is the constant speeds shown in the right figure. Apart from the regripping moments, the speed is fairly constant for the first $12\,\text{m}$ and for the $5\,\text{m}$ following. The installation speed of the pile is dependent on the resistance and thus the installation force. The machine has four different speed settings: $13, 7, 3$ and $1.5\,\text{cm/s}$. These speeds are used for increasing installation

forces and thus increasing soil strengths. In section 2.2 the effect of installation speed has been looked into. Here it is shown that a higher installation velocity can affect the resistance felt. However, other researches had found that it is possible that the tip resistance would be smaller, because the soil has less time to react to the pile. It is thus unclear how these installation velocities will influence the installation force. The influence of the installation velocity will not be taken into account in the further analysis and comparison between these measurements and the simulations of the capacity prediction methods.

4.3   Limitations

The available data also has its limitations which should be taken into account and considered if conclusions are taken solely on this data. The first limitation is in the precision of the depth registration together with the fact that sometimes the pile will rebound during unloading. This is not recorded in the depth registration and might cause a disconnect between the simulations and measurements. The order of magnitude of the distance the pile will rebound is estimated to be around 2 to $3\,\text{cm}$ per regrip moment. Something to note is that this same mechanism occurs during CPTs. It is therefore not possible to correct both of these measurements for this rebound distance. Correcting this could cause overfitting or over-correcting, which is an unwanted effect. The measurements are therefore kept as they are to avoid this.

Another limitation lies in the minimal installation force which is not recorded. The self weight of the clamping mechanism and pile also act upon the foundation pile before any other force is added. This force of $120\,\text{kN}$ is added manually to the total force of the Drukpaal measurements. This is not a big problem in stronger soils, but this could pose problems in very weak soils like clay or peat (which are very prevalent in the west of the Netherlands). The minimal installation force might be too big for the soil the pile passes through. The installation force and with that the resistance/strength of the soil might be overestimated by the machine in this process. But this is only likely to happen in very soft soils.

The last limitation of the measurements is the different installation speeds. Since it is not clear how the installation speed influences the required force this can not be taken into account in the further analysis, i.e. the total force measured can not be corrected for this. But this might cause discrepancies between the simulations of the methods and the measurements. Later on the possible effects of the installation speed will be discussed

4.4   Selection of data

Since there is a lot of available data it is important filter this data. The following things were looked at when making the selections.

- First the pile measurements were ordered from first installed to last installed. From this list the first piled within pile groups were selected. This was done to be able to ignore the pile grouping effect.

- From this list of 'first' piles around seven piles are selected that are located relatively close to each other and the available CPTs to minimize subsurface variance. This step is most important in bigger projects. Smaller project might have only a limited amount of CPTs which are all used in the simulations.

- With these selected measurements and CPTs a first round of simulations is done. Here the dips from the regripping moments in the total force measurements are filtered out using a rolling mean to make the comparison of the measurements and simulations easier. Outliers will be filtered out at this point. This includes removing measurements or simulations (CPTs) from the visual analysis if they differ too much from the majority of said analysis. Most of these differences are thought to be from local subsurface variability. The subsurface variability of the used CPTs is looked at closer in the next chapter.

In appendix A the pile plans for all the different projects are shown as well as the locations of the used piles and CPTs highlighted.

5

Subsurface analysis

In this chapter the subsurface profiles of the to be analysed projects will be looked into and a hypothesis will be made on which base capacity prediction method might work best for each of these subsurface profiles. To be able to make these hypotheses the base capacity methods are used on theoretical profiles with different transitions; strong to weak, weak to strong and embedded layers.

In Figure 5.1 the locations of the projects are shown

Figure 5.1: Location of projects

5.1 Comparison base capacity methods for different subsurface profiles

In this section an overview of the different methods will be given. Different theoretical profiles have been made to show how the different methods react to different transitions. The depth and tip resistance have been normalized. The depth has been divided by diameter so the influence zone can easily be seen with regards to diameter. The tip resistance has been divided by the maximum tip resistance.

5.1.1   Two layer profiles

The first profiles shown here are simple two-layer profiles; strong over weak and weak over strong, shown in Figures 5.2a and 5.2b.

First the Koppejan method will be looked at. In the left figure the influence zone below the pile tip can easily seen to be 4D, because the layer below is weaker and thus has a lower resistance, so the influence distance below the pile tip is as big as it can be. In this configuration the influence zone above the pile tip is not visible, because when it has reached the weaker layer it will follow the minimum path rule. On the right side the underlying layer is stronger and thus the influence distance above the transition is 0.7D. Below the transition the influence distance of 8D can be seen.

For the LCPC method the transition zones in either figure is almost identical, with the intersection point with the 'CPT' located at around 0.8, which is about 0.7 of the interval shown (0.3 - 1 q_c). This is because of the way values outside of the range of $0.7q_{c,avg}$ and $1.3q_{c,avg}$ are eliminated. This transition zone will not change depending on the stiffness of the soils and this method is therefore the most straightforward.

The filter method has smoother transitions than the previously mentioned methods. Interesting is that in the left figure, the filter method doesn't even start on the cone resistance of the CPT, because of the underlying weak layer that is already taken into account at a distance larger than 10D. After the transition the filter method has reached the cone resistance from the CPT in around 4D. In the right figure the filter method does start at $q_{c,true}$ and increases more slowly than it decreased in the left figure. After the transition zone it takes almost 15D to reach the maximum tip resistance, because it is still feeling the weaker layer above. This method has quite large transition zones, so it will have quite some overlap between the sensing and development depth when layers are introduced.

The method from Munta de Boorder has a smaller influence zone as can be seen in both figures and it is also more sensitive for weak layers as can be seen above the transition in the left figure. This method gives the smoothest transition out of all the methods shown.

(a) Strong over weak   **(b)** Weak over strong
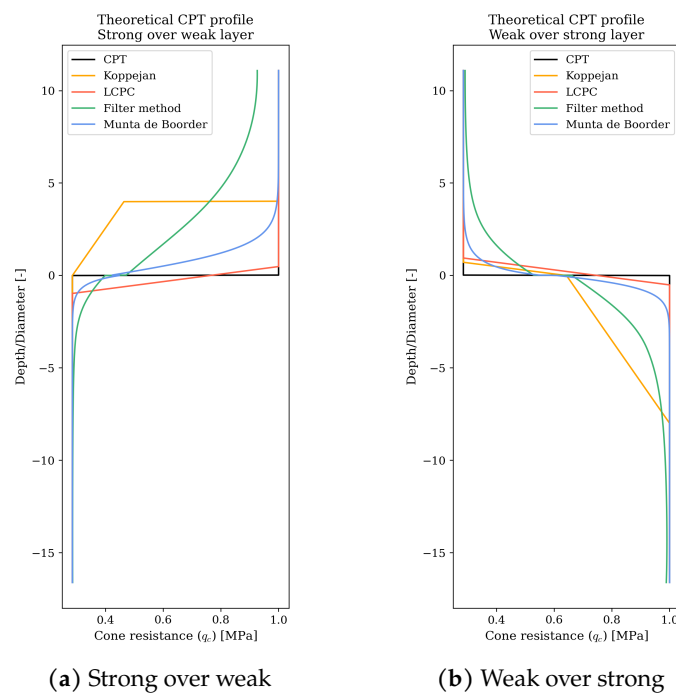
Figure 5.2: Theoretical profiles which show a strong layer over a weak layer (left) and a weak layer over a strong layer (right)

5.1.2   Embedded strong layer

In the next three figures a profile is shown with an embedded strong layer with increasing thickness (3D, 7D and 11D), figure 5.3a, 5.3b and 5.3c.

Koppejan has the same first transition as in Figure 5.2b, however the transition zone in the embedded layer is a combination of the 8D development depth to reach the maximum cone resistance and the 4D sensing depth to reach the minimum cone resistance. Here the layer would have to be 12D thick for this method to reach the maximum cone resistance. The Koppejan method averages out the resistance of the thin embedded strong layer because of the presence of the underlying weak layer.

LCPC has the same transition zones as discussed in the two-layer profiles. These transition zones are constant and are not affected by the thickness of the embedded layer. This method therefore works well to approach true resistance of the embedded layer in these theoretical profiles, even if they are very thin.

The filter method has a large influence zone, as already discussed in the previous section, and here that becomes more clear. The embedded strong layer is too thin (in all three profile) for the line to reach the true resistance. Just like the Koppejan method, this method is very sensitive to weaker underlying soil layers. As can be seen in the theoretical profiles, it averages out thin embedded strong layers because of this.

The method of Munta de Boorder doesn't reach true resistance in the left figure, but it does in the middle and right figures. This shows that this method has relatively small sensing and development distances, at around 3D. The sensing distance when transitioning from a strong soil to weak soil is slightly bigger, at around 5D. This method is thus also slightly more sensitive to weak underlying layers.

(a) Embedded strong layer (3D)

(b) Embedded strong layer (7D)

(c) Embedded strong layer (11D)
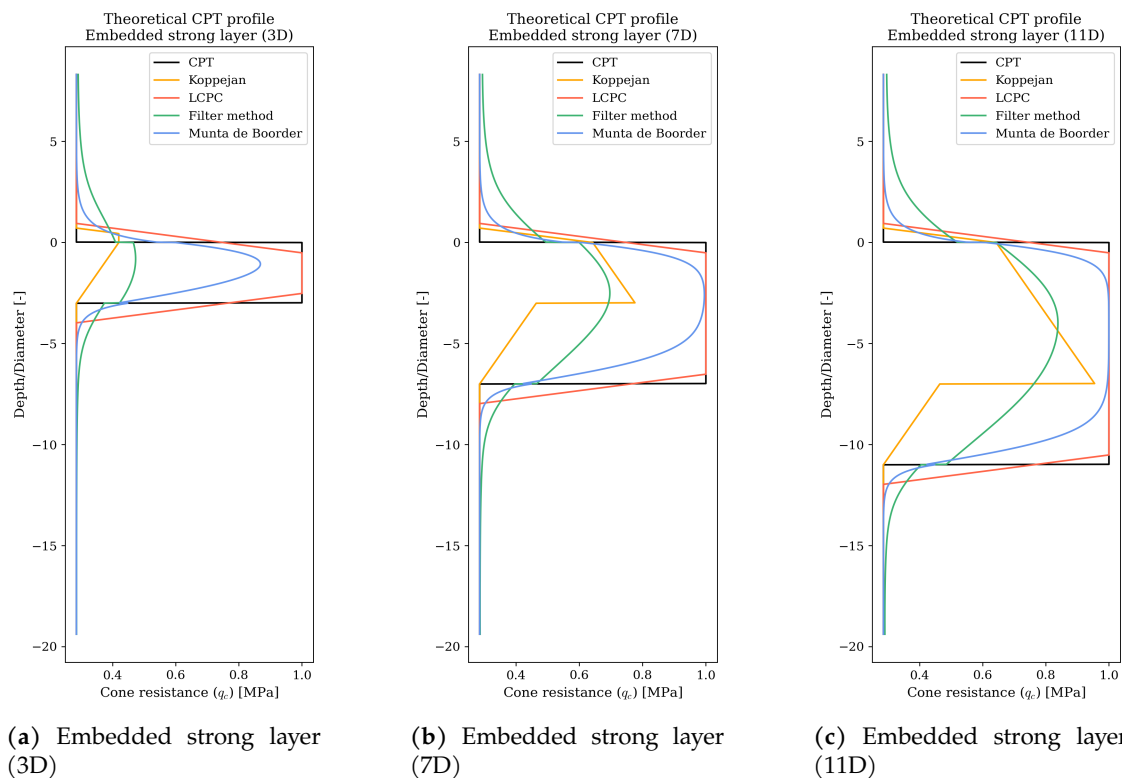
Figure 5.3: Theoritical profiles which show strong embedded layers with varying thickness; 3D, 7D and 11D.

5.1.3   Embedded weak layer

In the next three figures a profile is shown with an embedded weak layer with increasing thickness, similar to the embedded strong layer above, see Figures 5.4a, 5.4b and 5.4c.

Here it becomes clear that the Koppejan method is very sensitive to weak layers in the soil subsurface. This is because of the minimum path rule the Koppejan method follows. Here the method will feel the embedded weak layer from 4D above the layer until 8D below the layer. This is true for all the three profiles. Because of these sensing and development distances and the minimum path rule, the Koppejan method will make the embedded layer seem bigger than it in actuality is.

For LCPC there is no difference in transition zones between the now embedded weak layer compared to the earlier embedded strong layer or the two-layer profiles. This method will keep close to the true resistance profile.

For the filter method the same becomes clear as for the Koppejan method. It is more sensitive towards weak layers. Here the resistance is closer to reaching the true resistance in the embedded layer than in the embedded strong layer (for all cases). This method also senses the presence of the embedded weak layer very early, but it has a less drastic transition to the weak layer than the Koppejan method has.

The Munta de Boorder method is also more sensitive to weak layers, but less noticeably so. This is because of the smaller influence zones above and below the tip. These small influence zones are the reason that this method follows the true resistance (CPT) quite closely.

(a) Embedded weak layers (3D)   **(b)** Embedded weak layer (7D)   **(c)** Embedded weak layer (11D)
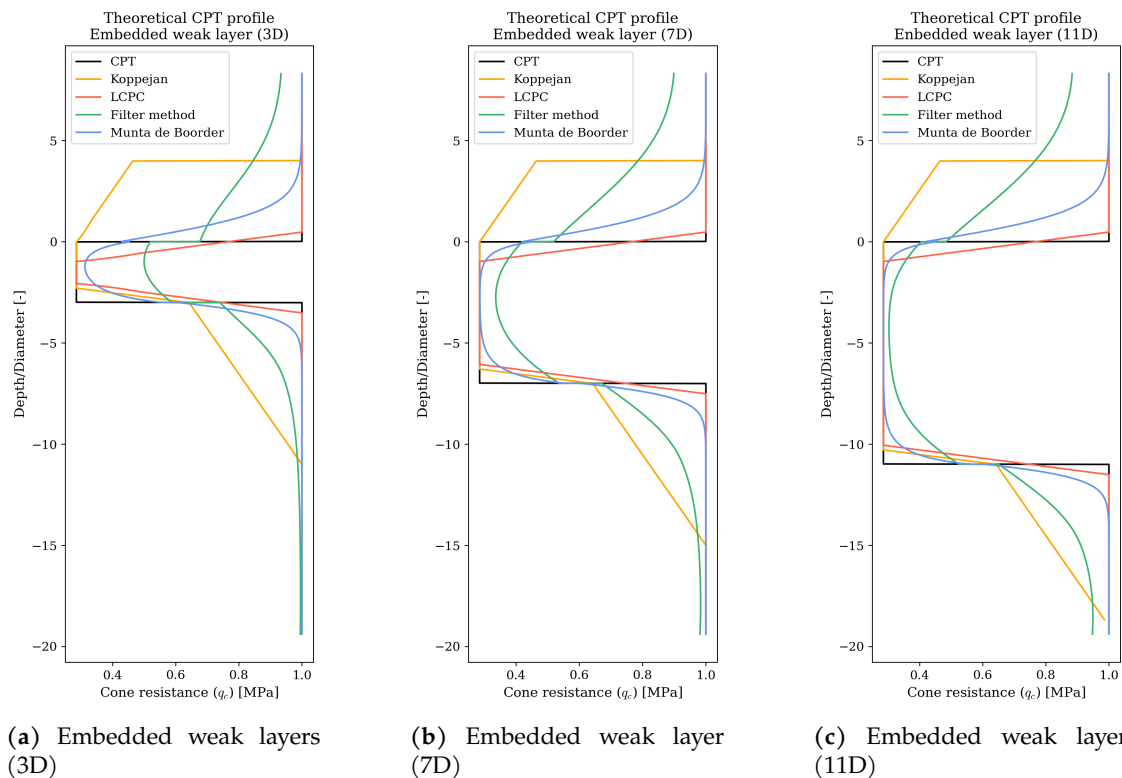
Figure 5.4: Theoritical profiles which show weak embedded layers with varying thickness; 3D, 7D and 11D.

5.1.4   Summary

The Koppejan method is very sensitive to underlying weak soil layers in the soil profile because of the minimum path rule. In a soil profile with multiple thin embedded strong layers, these will be averaged out. In a soil profile with multpile thin embedded weak layers, these will be felt very strongly and might appear bigger than they actually are.

The LCPC method is very consistent in its transition zones and these are also not influence by if the underlying soil is weak or strong. This method will give a fairly accurate depiction of the soil profile with its embedded weak and strong layers, since it has quite a small influence zone.

The Filter method is very similar to the Koppejan method, because they are both sensitive to weak layers. Different than the Koppejan, the Filter method doesn't apply the minimum path rule so its transition zone is more gradual, but both have quite big sensing distances when it comes to underlying weaker soils. The development distance from weak to strong soil is very similar to that of Koppejan, which is bigger than its development distance from strong to weak soil.

The Munta de Boorder method has smaller transition zones than Koppejan or Filter method and therefore reaches the true resistance fairly fast. This method does have some sensitivity to weak underlying soils, but this is less obvious than for the Filter method or Koppejan. The same as for LCPC, this method will give an accurate depiction of the subsurface, because of its small influence zones.

5.2   Subsurface profiles

Here the subsurface profiles are shown for each project used in this research. Note that only the CPT profiles used in the analyses are plotted in the figures. Also, not the entire CPT profile is shown, the profile is only plotted to where the Drukpaal piles are installed. The locations of the used CPTs can be seen in appendix A. Next to the subsurface profiles the coefficient of variation (which is standard deviation divided by mean) of these CPTs is plotted per project. This is done show the variability in the profile and which layers are more uniform than other. This can help with the visual analysis of the simulation in the next chapter. In Figure 5.1 the locations of the different projects is shown.

First the subsurface profiles of Gorinchem, Rotterdam and Ridderkerk will be looked into, see Figures 5.5, 5.6 and 5.7. These projects have very similar profiles, which is probably because of the proximity of the projects.

The Gorinchem profile consists of a small sandy soil layer on top followed by a weaker soil from -2 to -8 meters. After the weaker soil layer the profile starts to linearly increase. Looking at the coefficient of variation, it can be seen that the peaks are mostly around transition zones, at around -2 an ad -8. Which makes sense because of the heterogeneous nature of soil layers, which will not have the same transition at the same depth at every location. Other than these two peaks the profile seems to be fairly constant in COV values. Because of the structure of this profile (no small embedded layers or sudden transitions), it is thought that most of the base capacity profiles will fit reasonably and most of the differences will come in with the addition of shaft capacity methods.

The Rotterdam profile is very similar to the Gorinchem profile, but does have a few differences to be mentioned. The sandy layer on top is bigger in the Rotterdam profile and more variable. The profile is also longer (piles are installed to a larger depth). In this profile there is a small embedded weak layer around -20 meters depth. The COV is again the biggest around the transition zones. Because of the addition of the small embedded weak layer, it is thought that Koppejan might not be the best method for this profile. The other methods are thought to get a reasonable fit for this profile.

The Ridderkerk profile differs from the previous two profiles, because it doesn't have the top sandy layer the other two profiles have. There seems to be quite some variability in the soil layer from -12 to -18 meters. In this profile the peaks in the COV are more frequent and not only concentrated to the transition zones. This will probably cause the simulations also to have more variability. There is again a small embedded weak layer at 20 meters depth. Because of this it is thought that Koppejan might not be the best fit for this profile.

Something to note with these three profiles is that they all have a very weak layer in the top half of

the profile. This weak layer has a measured cone resistance value of lower than $0.5\,\text{MPa}$. This soil layer might be too soft for the minimal installation force of the Drukpaal machine. So here, the total force measured by Drukpaal might be too high compared to the values from the simulations. If this is the case, the top weak layer will be excluded in the analysis.
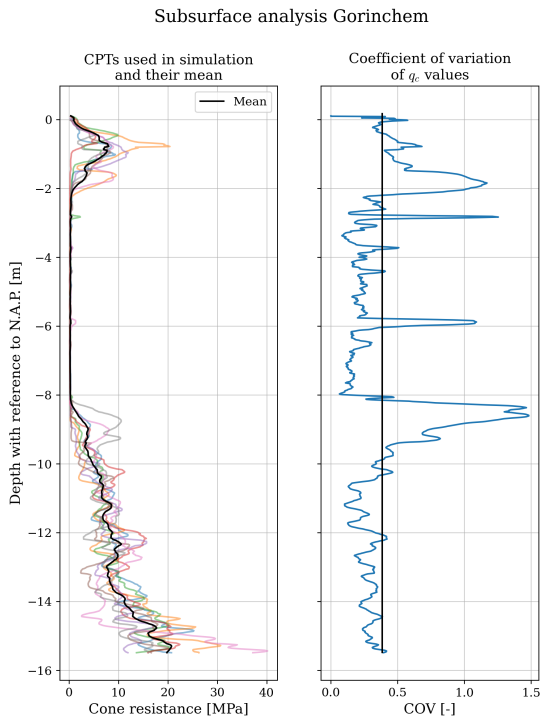
Figure 5.5: Subsurface analysis Gorinchem
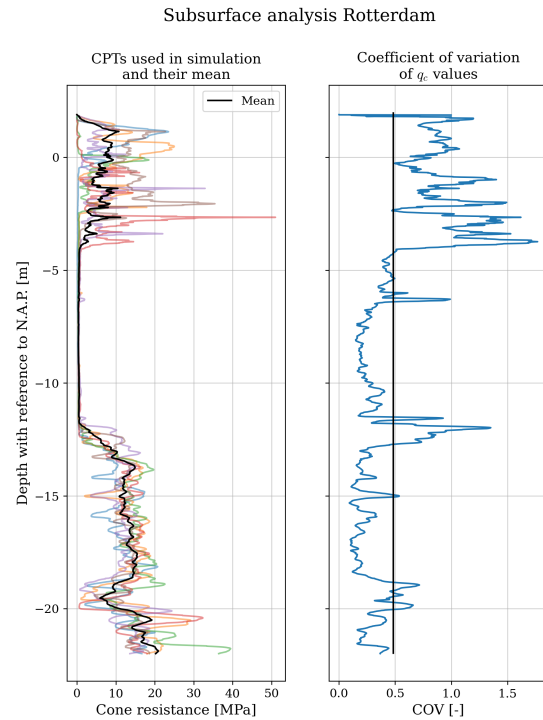
Figure 5.6: Subsurface analysis Rotterdam
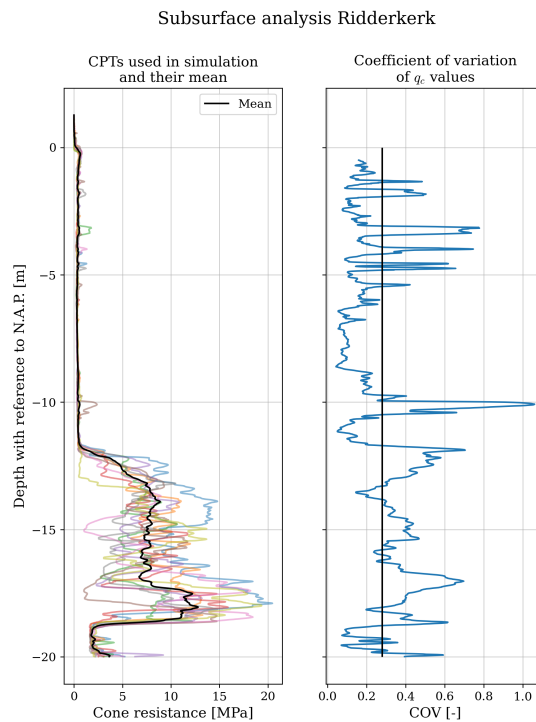
Figure 5.7: Subsurface analysis Ridderkerk

The next profile to be discussed is from Naaldwijk, see Figure 5.8. This profile has multiple embedded strong layers, before it reaches a strong enough layer to found the pile on. The biggest COV values are found at the top and at the layer at -10 meters. Because of the underlying weak layer of the three embedded strong layers, it is thought that both the Filter method and Koppejan might not fit well for this profile.

In Figure 5.9 the subsurface profile of Harlingen is shown. It has two small embedded strong layers around -6 meters depth and a strong layer at -12 meters. The peaks in the COV values are again just before transition zones. Because of the presence of embedded strong layers and transition zones from weak to strong (-11 meters) and strong to weak (-14 meters) it is thought that all the methods will fit for some parts of the profile, but they all will have discrepancies at different parts.
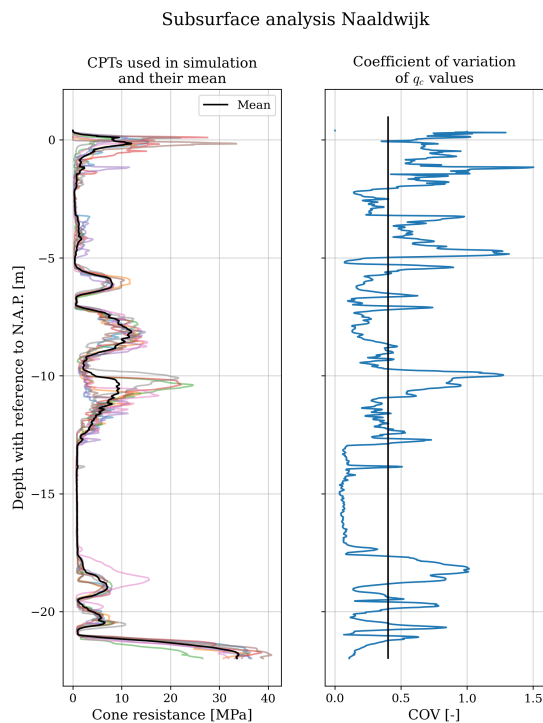
Figure 5.8: Subsurface analysis Naaldwijk
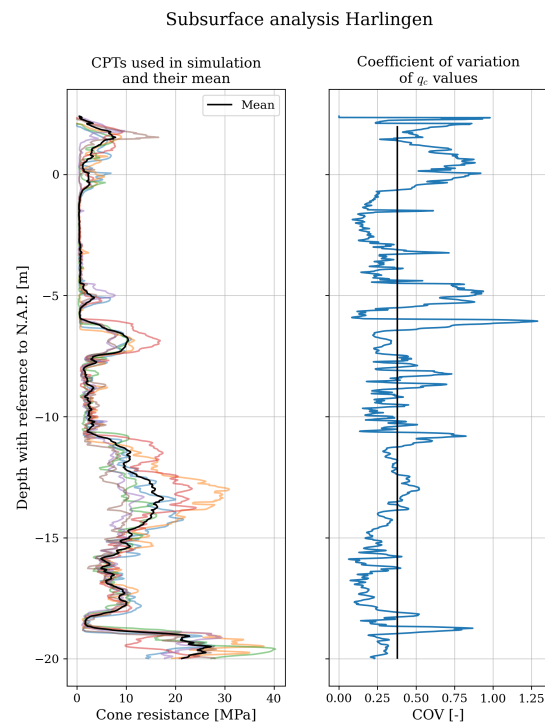
Figure 5.9: Subsurface analysis Harlingen

The subsurface profile of Hoogeveen is shown in Figure 5.10. This profile very subtle transition zones from weak to strong (at 2 meters and at -6 meters) but a very sudden transition from strong to weak at -2 meters. Because of the subtle transition zones most of the base capacity prediction methods will fit reasonably.

The subsurface profile of Nijmegen has the most constant variability, see Figure 5.11. However, this figure doesn't have many outstanding aspects. It has one strong layer at 8 meters with with a very subtly transition zone back to a weaker zone after which it again increases. The transition zone to the strong layer at 8 meters is probably best estimated by LCPC or Munta de Boorder, but for the rest of the profile all the methods will probably give a good fit.
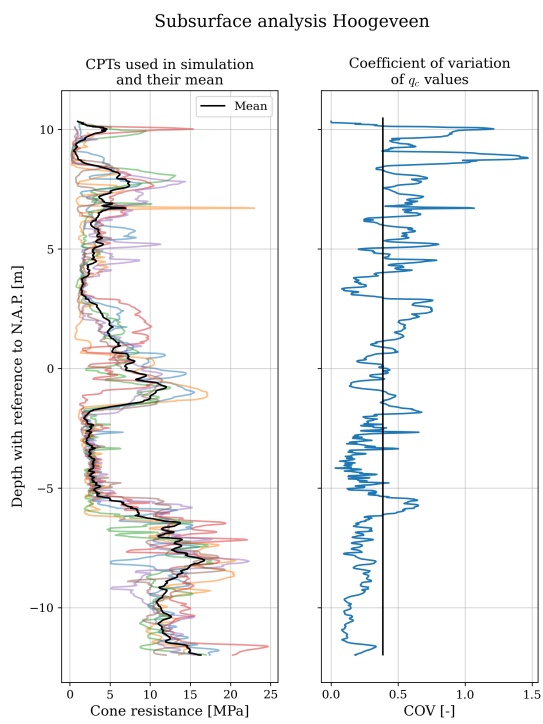
Figure 5.10: Subsurface analysis Hoogeveen
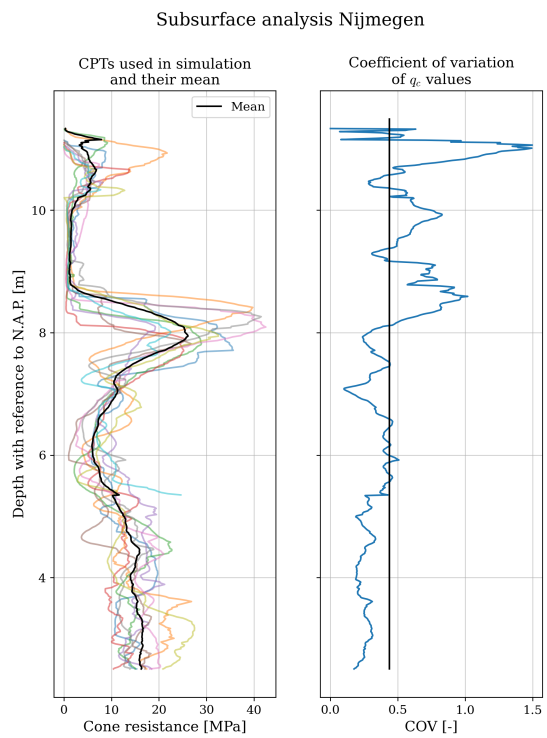
Figure 5.11: Subsurface analysis Nijmegen

Part II

Analysis of results

6

Visual analysis of results

In this chapter an overview of the results will be given per project. For all the simulations observations will be added to further explain why different methods work well for certain subsurface profiles. For each project the best three found matches will be ranked and given 3, 2 or 1 point respectively. At the end these scores will be all added up to get the overall best combination based solely on the visual analysis.

6.1   Rotterdam

In Figures 6.1 and 6.2 the different base capacity methods with either NEN or ISO as shaft capacity methods is shown. Here 6 different simulations (based on 6 different CPT's) and 6 different Drukpaal measurements are plotted. First thing to note is that there is a disconnect in the first 4 meters between the simulations and the measurements for all different simulations. The measurements feel something at the top, but not to the extent that the simulations (and thus the CPT's) do. This could be due to variability of the subsurface or the sensitivity of the CPT cone. In an earlier version of the simulations the simulations overestimated the resistance when compared to the measurements. With the difference at the top it was thought this difference was due to the accumulation of shaft capacity which included the top part of the CPT. Since it looks like the Drukpaal measurements don't feel this top layer, it is thought they also don't have the added shaft capacity that the simulation do. The shaft capacity for the simulations was recalculated with the first 4 meters of the CPT set to zero. The result of this is seen in the shown figures. The rest of the observations for Rotterdam will focus on the depth interval from -10 to -20 meters.

The rest of the profile doesn't have that much variety. From 12 meters depth pile enters a stronger soil, which is a relatively homogeneous sand. With the added shaft capacity the total force increases over depth until around 19 meters depth where there is a thin weaker embedded layer. After this the stronger soil continues on which the piles have been founded since the measurements stop here.

Most of the simulations follow the line and the shape pretty well. Overall the simulations with the added NEN method seem to have a better fit than with the ISO method. Filter method with NEN looks like a good fit where the simulations don't go to far over or under the measured force. However, the filter method does look like it averages the embedded weaker layer out, as was also seen in the theoretical profiles.

Munta de Boorder and LCPC with NEN also follow the measurement really well, but both these methods follow the embedded weaker layer better. But these methods also follow all other peaks in the used CPT profiles better, since their sensing and development depths are quite shallow. These methods go 'outside the lines' of the measurements more often. Koppejan and NEN seems to underestimate the needed force and thus the gained capacity. This is probably because of the embedded weaker layer, which the Koppejan method feels more strongly than other methods.

With the simulations with the added ISO shaft capacity method the biggest difference with the before made observations is that the simulations now all are lower at 20 meters depth. The deviation starts at around 14 meters depth. Due to this deviation these simulations fit less well over the measurements.

From observations alone it looks like the simulations with the added NEN shaft capacity method approximate the measurement better, with exception of the Koppejan method. Filter method works well, but evens out the embedded weak layer, while Munta de Boorder and LCPC follow the embedded layer more closely. All these things have also been observed in the theoretical profiles. In Table 6.1 the top three of the simulations for Rotterdam are shown. Here the first ranked simulation gets 3 points, the second ranked simulation 2 points and the third ranked simulation gets 1 point.

Table 6.1: Ranking of simulations of Rotterdam

Rank	Simulation
1	Filter method + NEN
2	LCPC + NEN
3	Munta de Boorder + NEN

Methods + NEN

(**a**) Filter method + NEN   (**b**) Munta de Boorder + NEN   (**c**) Koppejan + NEN   (**d**) LCPC + NEN
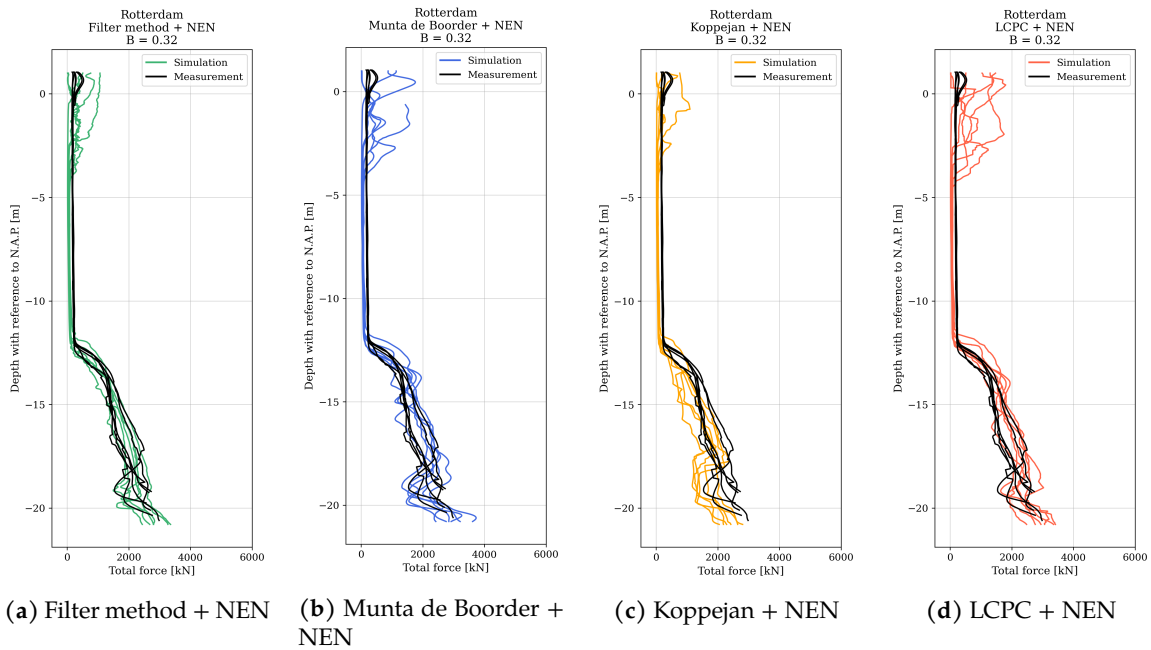
Figure 6.1: Simulations of the different base capacity methods together with NEN shaft capacity method for Rotterdam

Methods + ISO

(**a**) Filter method + ISO   (**b**) Munta de Boorder + ISO   (**c**) Koppejan + ISO   (**d**) LCPC + ISO
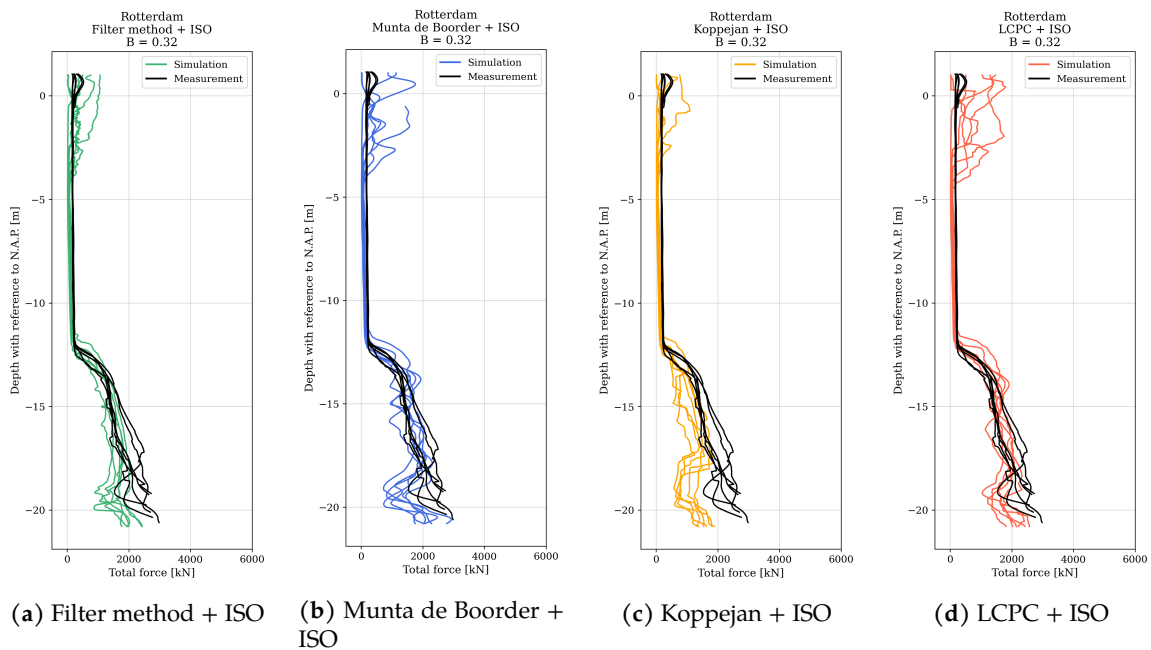
Figure 6.2: Simulations of the different base capacity methods together with ISO shaft capacity method for Rotterdam

6.2 Gorinchem

The next project is located in Gorinchem. In Figures 6.3 and 6.4 the simulations and measurements are shown. The profile is very similar to that of Rotterdam, but less deep. This profile is quite simple, it consists of a very uniform weak layer from 0 to -8 meters depth after which the cone resistance constantly increases. It was expected that most of the simulations will follow the measurements quite well, since the biggest deviations mostly come from embedded strong or weak layers. The biggest difference in this profile between simulations is because of the different shaft capacity methods. Something to note from the measurements is that there seems to be a little bit of a weaker zone which some of the measurements go through at around -14 meters. This indicates that the layer starting from -8 meters depth is quite variable.

The simulations with NEN can be seen in Figure 6.3. All these simulations match the measurement fairly well. There seems to be small disconnect between the simulations and measurements in the first 8 meters of the profile. This is probably the same issue that was mentioned in the part about Ridderkerk. These first 8 meters will thus not be taken into account in the observations. The Filter method with NEN looks like it matches the measurements quite closely. However, no simulation shows the weaker zone felt by the measurements at -14 meters. This could be due to the CPT's chosen for the simulations, that these don't pass through this weaker zone. Or this could be due to the averaging effect that the Filter method has. When looking at the other method simulations, both of these seem to be the case. There seems to be one CPT chosen that does feel this weaker zone, but not to the extent of the measurements. Munta de Boorder with NEN is also a good match, but as seen in other projects, it is more variable since this method averages out less than the Filter method. Koppejan with NEN is very similar to the Filter method, since it averages out the variability of the CPT more. And in this case it also feels the weaker zone more strongly. This seems to be a good fit. LCPC with NEN feels certain peaks 'too much' in comparison to Koppejan or the Filter method. This means that these simulations often overestimate the total force.

The observations for the simulations with ISO are very similar to the observations for the simulations with NEN. One of the biggest differences between them is that the total force at the end of the profile is smaller with the added ISO method. This makes the Filter method, Munta de Boorder and LCPC fit better over the measurements. Only the simulations with Koppejan and ISO fits less well than with the NEN method.

Overall most of these simulations fit well over the measurements. ISO seems to get better results for three of the four base capacity methods, but the difference is not that big with the NEN method. Further it is noticed that Koppejan tends to be on the lower limit of the simulations, which is to be expected from the theory behind the method. Filter method averages out all the little dips and peaks from the CPT, which is not always advantageous but works quite well for this profile. Munta de Boorder and LCPC feel these little dips and peaks more and are thus less uniform, but they will feel small weak zones that the Filter method overlooks (because of the averaging).

Table 6.2: Ranking of simulations of Gorinchem

Rank	Simulation
1	Filter method + NEN
2	Munta de Boorder + ISO
3	Koppejan + NEN

Methods + NEN

(**a**) Filter method + NEN   (**b**) Munta de Boorder + NEN   (**c**) Koppejan + NEN   (**d**) LCPC + NEN
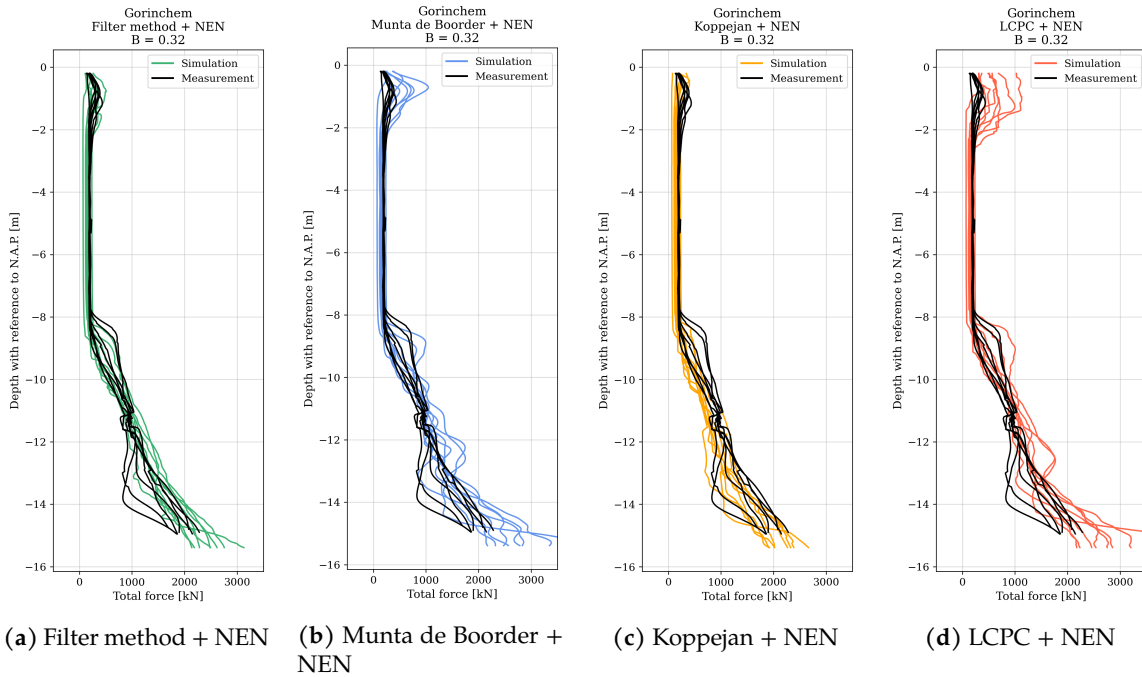
Figure 6.3: Simulations of the different base capacity methods together with NEN shaft capacity method for Gorinchem

Methods + ISO

(**a**) Filter method + ISO   (**b**) Munta de Boorder + ISO   (**c**) Koppejan + ISO   (**d**) LCPC + ISO
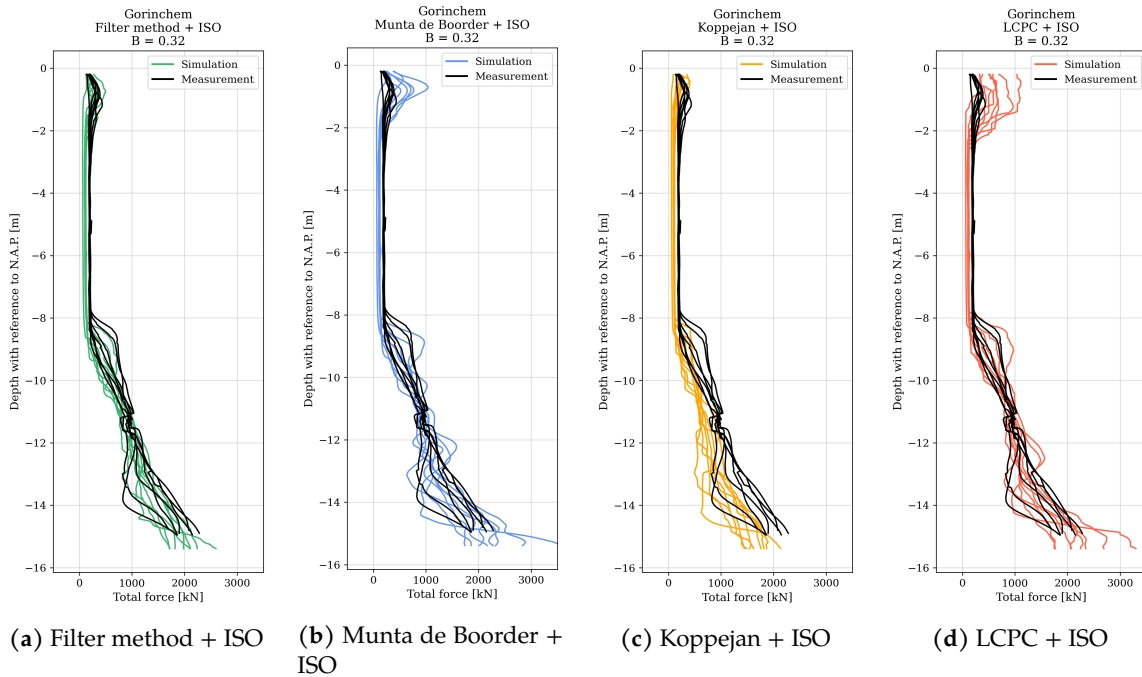
Figure 6.4: Simulations of the different base capacity methods together with ISO shaft capacity method for Gorinchem

6.3   Ridderkerk

The next project is located in Ridderkerk, which borders Rotterdam. It is therefore not a suprise that these profiles are very similar. The biggest differences in the profiles is that the sand layer starting at -12 meters is less strong and less uniform (a q_c value of around 8 where the sand layer in Rotterdam had a q_c value of around 14) and that the piles are founded slightly deeper.

In Figures 6.5 and 6.6 the simulations and measurements of the Ridderkerk project are plotted. In all the simulations something can be seen. In the first 12 meters depth the simulations all underestimate the total force. Or it is possible the total force is overestimated by the measurement. This second option seems feasible because of how constant this force is. It is possible that the force caused by the weight of the pile and hydraulic jacks (which is added to the measured force manually) is more than the resistance the soil can give. This would explain the difference between the simulations and the measurements and how constant the force is over the first 12 meters of installation. The rest of the observations will focus on the depth interval -12 to -22 meters.

The Filter method with NEN follows the measurement lines nicely, but doesn't decrease as much as the measurements at the embedded weak layer at -19/-20 meters. After that the simulation exceeds the line of the measurement. With Munta de Boorder and LCPC with NEN the same is happening as in Rotterdam. They follow the measurement line relatively well, but because of their sensing and development depth being quite small, these simulations will have more deviations. These simulations also follow the small embedded weak layer very nicely, but than overestimate the capacity of the layer underneath. Koppejan and NEN underestimates the capacity of the soil over the interval -12 to -17 meters after which it follows the measurement line quite well.

The Filter method with added ISO method seems to be a better fit than with the NEN method, because of how the simulations follow the embedded weak layer and the bottom layer. However, it underestimates the capacity in the middle layer. Munta de Boorder and LCPC with ISO have a better fit than both these base capacity methods with NEN. But these simulations still have a lot of variance in the middle layer, which adds a bigger error margin in these methods depending on the variances of the CPT's. Koppejan with the added ISO really underestimates the force, which is due to the weaker embedded layer at -20 meters and the variance of the CPT's since the Koppejan method will follow the minimum path.

Overall the simulation here with the ISO shaft capacity method seem to get a better fit except for Koppejan. Filter method, Munta de Boorder and LCPC all follow the measurement lines quite well. Filter method has less deviations since it averages out more. Munta de Boorder and LCPC have more deviations, but don't underestimate the force as much in the middle layer (-12 to -17 meters).

Table 6.3: Ranking of simulations of Ridderkerk

Rank	Simulation
1	Filter method + ISO
2	Munta de Boorder + ISO
3	LCPC + ISO

Methods + NEN

(**a**) Filter method + NEN   (**b**) Munta de Boorder + NEN   (**c**) Koppejan + NEN   (**d**) LCPC + NEN
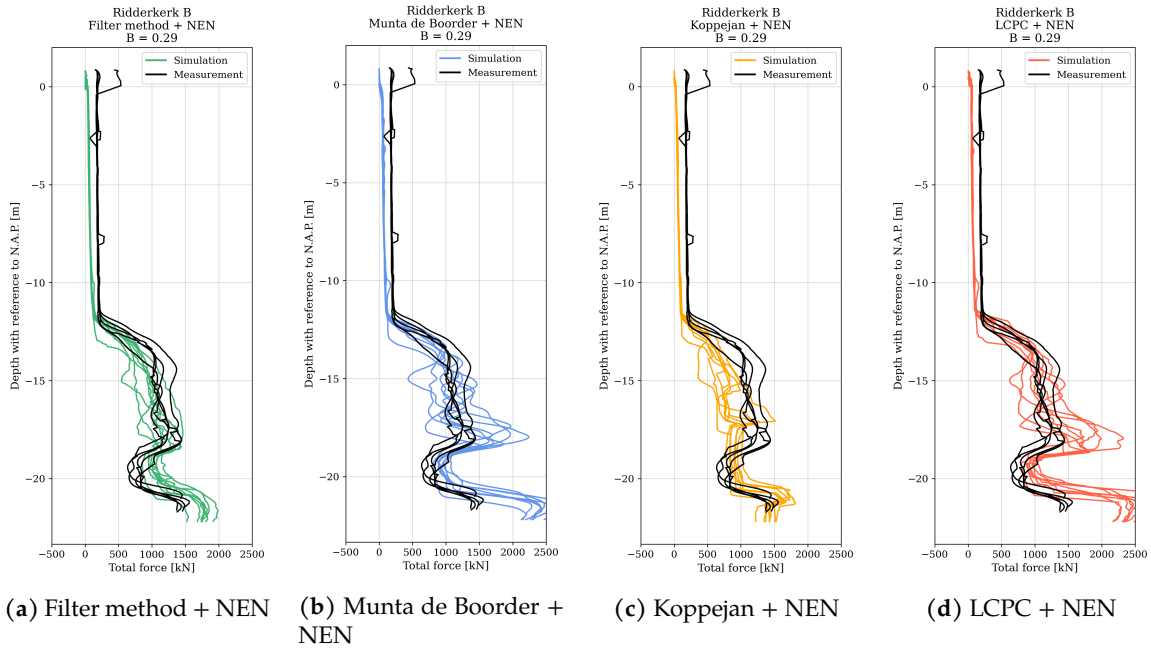
Figure 6.5: Simulations of the different base capacity methods together with NEN shaft capacity method for Ridderkerk

Methods + ISO

(**a**) Filter method + ISO   (**b**) Munta de Boorder + ISO   (**c**) Koppejan + ISO   (**d**) LCPC + ISO
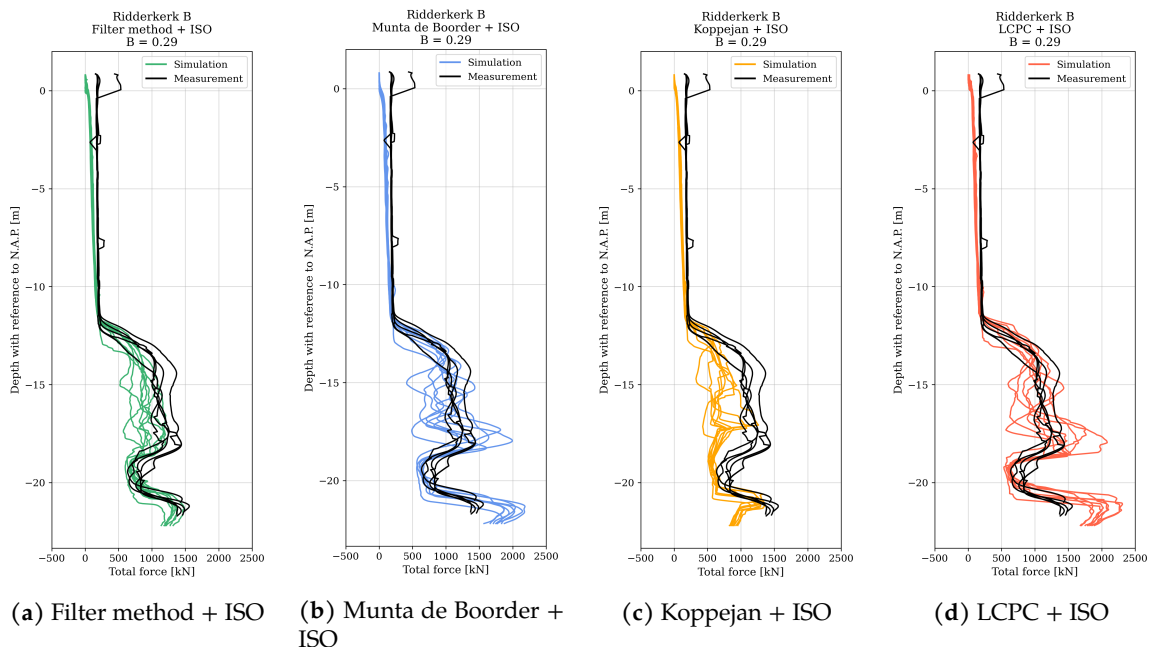
Figure 6.6: Simulations of the different base capacity methods together with ISO shaft capacity method for Ridderkerk

6.4   Naaldwijk

Naaldwijk is the next location to be discussed. Naaldwijk is located close to Rotterdam, but more towards the coast. This location has a very different subsurface profile than Rotterdam, Ridderkerk or Gorinchem, which were all very similar. The profiles, shown in Figures 6.7 and 6.8, show a very weak subsurface up until -22 meters where a strong sand layer is encountered where the piles are founded upon. The profiles also show that there are three embedded strong layers between -5 and -12 meters depth. These seem to be felt by almost all the measurements and simulations at the same depths, that they can be assumed to be quite uniform. There are 3 measurements that feel the last embedded layer a little differently, this one is thus a little more variable. This can also be seen from looking over all the different method simulations.

The simulations with NEN shaft capacity method (Figure 6.7) all consistently overestimate the force from -13 meters depth and on. For the Filter method with NEN the first embedded layer follows the measurement quite well. From the peak of the second embedded layer the disconnect between the simulation and the measurements start. From this point the simulation is consistently too high. For Munta de Boorder with NEN the embedded strong layers are overestimated also, but this simulation senses the weak layer between the embedded strong layers very well. The shape of this simulations is nice. Koppejan with NEN has a less nice shape, because the embedded layers are quite thin the simulation feels the weak underlying layer quite fast. LCPC with NEN is the worst fit of all the simulations with NEN. From -5 meters depth it overestimates the total force.

The simulations with ISO give better results than the ones with NEN. The Filter method especially matches the measurements very well. Munta de Boorder with ISO has again a nice shape, but this simulations significantly overestimates the total force of the embedded layers. Koppejan with ISO is also a nice fit, but this simulation (contrary to Munta de Boorder) consistently underestimates the total force of the embedded layers, the development depth is too big for the thickness of these embedded layers. LCPC with ISO is a better fit than LCPC with NEN, but around the embedded layers this simulation isn't as accurate as the other simulations and overestimates the total force.

Overall the ISO shaft capacity method gives the best results for this profile. Munta de Boorder has a nice shape for this profile, however it overestimates the total force because this method takes an underlying weaker layer less into account than the Filter method or Koppejan. The same is the problem with LCPC. Another problem with LCPC in this profile is that it doesn't follow the dip around -6 meters as well as the other simulations do. This could be due to the set sensing and development depth of 1.5 D, which in this case might still be too big. Koppejan follows these dips quite well, but the peaks don't reach the same force level that the measurement line does. This is because of the big sensing depth and how sensitive this method is to weak layers. Filter method follows the peaks and dips very well and is the best match for the measurements.

Table 6.4: Ranking of simulations of Naaldwijk

Rank	Simulation
1	Filter method + ISO
2	Koppejan + NEN
3	Munta de Boorder + ISO

Methods + NEN

(**a**) Filter method + NEN   (**b**) Munta de Boorder + NEN   (**c**) Koppejan + NEN   (**d**) LCPC + NEN
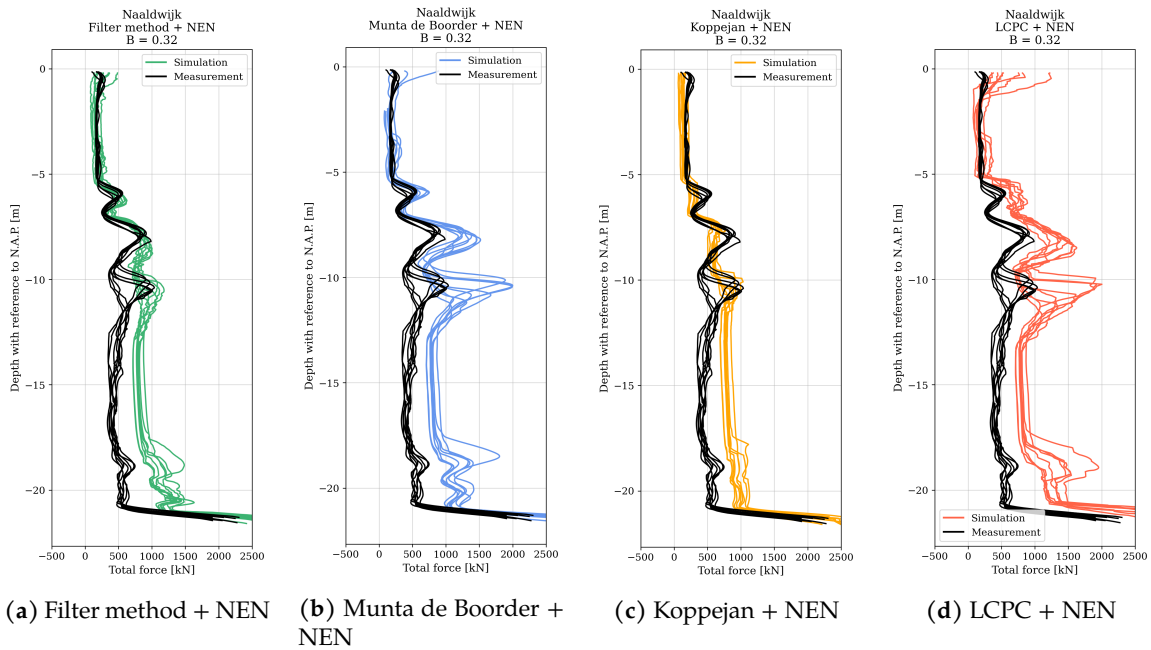
Figure 6.7: Simulations of the different base capacity methods together with NEN shaft capacity method for Naaldwijk

Methods + ISO

(**a**) Filter method + ISO   (**b**) Munta de Boorder + ISO   (**c**) Koppejan + ISO   (**d**) LCPC + ISO
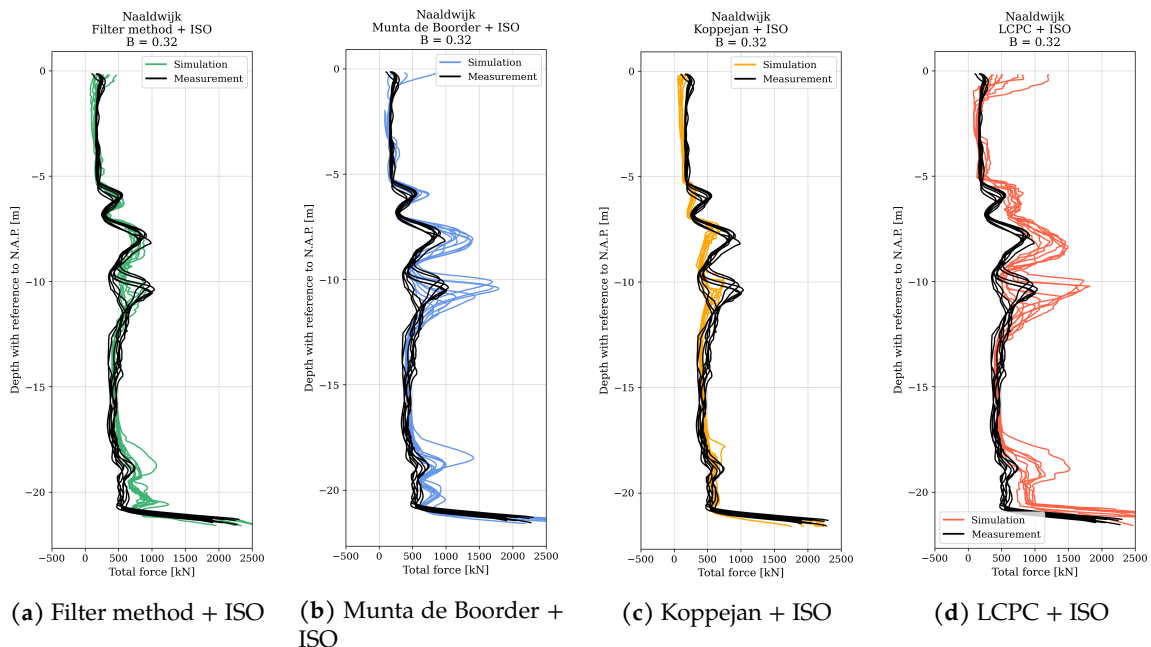
Figure 6.8: Simulations of the different base capacity methods together with ISO shaft capacity method for Naaldwijk

6.5   Harlingen

The next project to be discussed is located in Harlingen. Harlingen is located in the north of the Netherlands bordering the sea. The first 10 meters of the subsurface consists mainly of soft soils with some strong embedded layers. After this a stronger layer starts with an embedded small weak layer at around -18 meters after which the strong layer continues, on which the piles are founded. In Figures 6.9 and 6.10 the simulations are shown. Something that stands out for all these simulations is that there is a big spread in the peak force around -13 meters in the simulations. This shows that this layer is quite variable, while the measurements are fairly uniform. This is probably due to that the measurements used are from piles close to each other, while the CPT's are farther away from each other and thus covering a bigger area and with that capturing the variability in this layer.

The simulations with NEN all overestimate the total force from -8 meters and on. The Filter method follows the peak of the embedded layer at -6 meters very closely, but the layer after is overestimated significantly probably due to the shaft prediction. The shape of the simulation for the following layer is quite nice even if it is too high. The little embedded layers at the end are also shown quite nicely. Almost the same can be said for the Munta de Boorder simulation with NEN, but here the overestimation is even more, but again the shape of the simulation fit quite well with the measurements. Koppejan overestimates the measurements the least, but it also doesn't follow the peak at -6 as nicely as other methods do. Some of the simulation lines do follow the measurement lines from -10 and on quite well. LCPC with NEN also overestimates the total force, but also overestimates the thickness of the embedded layer at -6 meters. It also doesn't show the embedded layers (especially the last one) as well as the other methods do.

It is clear that the simulations with ISO overestimate the total force less, even though there is still a lot of spread in the layer from -11 to -16 meters, which is probably just due to the variability of this layer, which is not shown in the measurements. Filter method with ISO matches the measurements very well. However, the simulation overestimate the measurements between -7 to -10 meters. The spread of the middle layer (from -11 to -16 meters) is bigger for Munta de Boorder with ISO, because of the smaller sensing and development depths and less sensitivity for the layer below this stronger zone. This is also the case for the weak embedded layer at -18 meters. Koppejan with ISO starts to underestimate the total force from -15 meters, after which the simulations don't match anymore. The small embedded layer is also felt really early which causes this layer to show as way bigger than it really is. LCPC with ISO is a relatively good match even though it overestimates the force and thickness of the first embedded layer.

Overall ISO gives better results, except for the Koppejan method, which has a better result with NEN. The first embedded layer is best matched with either the Filter method and Munta de Boorder. The Filter method matches the profile the best from -11 meters and on. Munta de Boorder and LCPC are here just a little less of a good fit, because these methods take the underlying layers less into account, whether this layer is strong or weak. With this these methods either overestimate peaks or underestimate dips of the embedded layers. Koppejan with NEN works relatively well, even though the shape from other simulations is better, but the big downfall of Koppejan in this profile is that the small embedded layers, either strong or weak are not predicted accurately. Small strong embedded layers are underestimated (in force and thickness) while small weak embedded layers are overestimated in thickness and with that underestimates the strength of the layer before this embedded layer.

Table 6.5: Ranking of simulations of Harlingen

Rank	Simulation
1	Koppejan + ISO
2	Filter method + ISO
3	Koppejan + NEN

Methods + NEN

(**a**) Filter method + NEN   (**b**) Munta de Boorder + NEN   (**c**) Koppejan + NEN   (**d**) LCPC + NEN
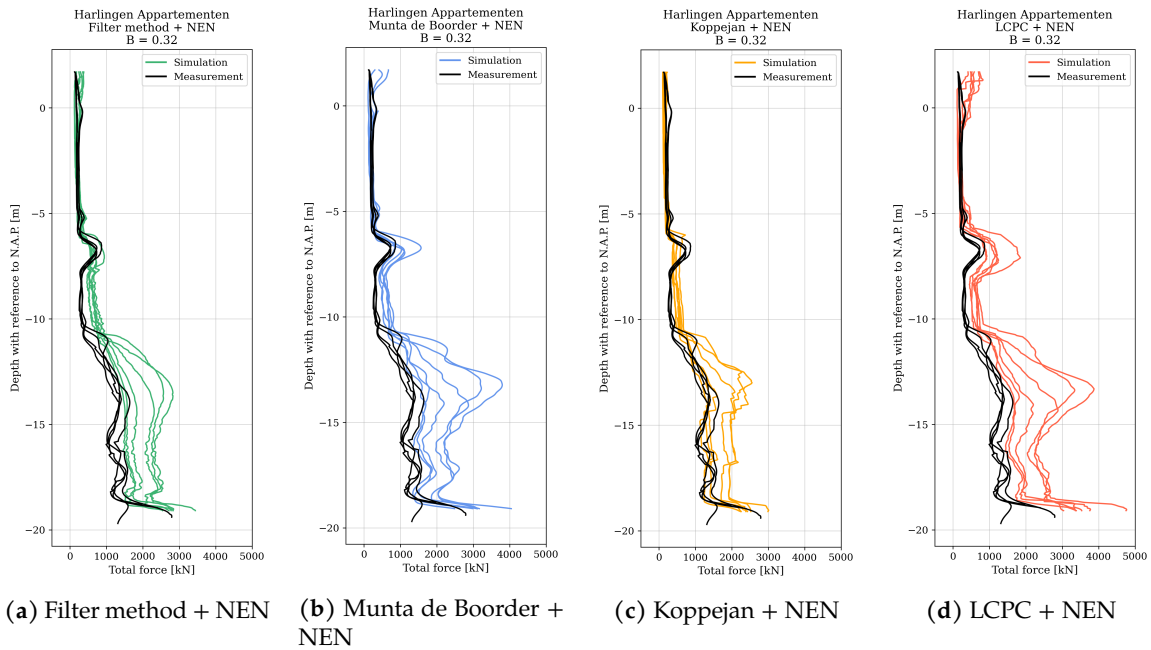
Figure 6.9: Simulations of the different base capacity methods together with NEN shaft capacity method for Harlingen

Methods + ISO

(**a**) Filter method + ISO   (**b**) Munta de Boorder + ISO   (**c**) Koppejan + ISO   (**d**) LCPC + ISO
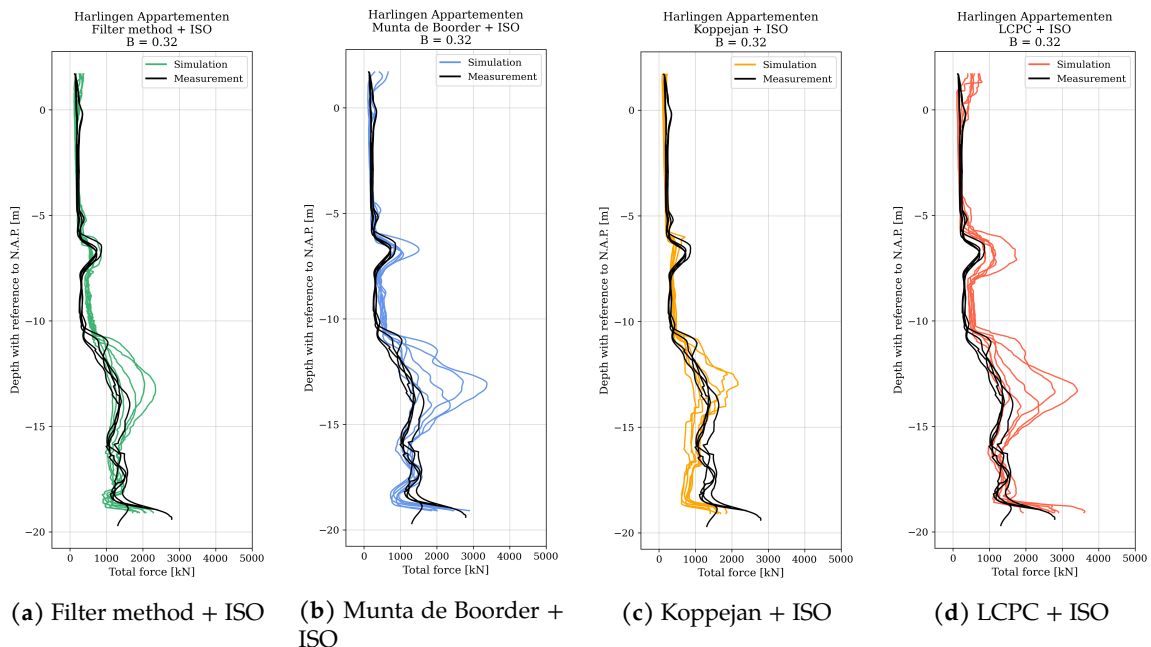
Figure 6.10: Simulations of the different base capacity methods together with ISO shaft capacity method for Harlingen

6.6   Hoogeveen

The next project to be discussed is in Hoogeveen, which is situated in the north-east of the Netherlands. Something that stands out is that the Drukpaal measurements aren't as close together as in the before mentioned projects, especially in the weak layer at -2 to -5 meters, as can be seen in Figure 6.11 and 6.12. This might indicate more variability in the subsurface. However, the small strong layer at -1 meters is clearly felt throughout the different measurements as well as the start of the strong layer at -5 meters depth. These are aspects the simulations should feel to be a close match to the measurements.

The Filter method with NEN follows the measurement lines really nicely and seem to be a good fit for this profile. For the simulations of Munta de Boorder with NEN almost the same can be said, but these simulations are less smooth than the Filter method ones. Also with these simulations the peaks are a bit higher than the measurements (around -1 meter and -6 meter). Koppejan with NEN seems to be a good fit as well. However, the simulations don't follow the peak around -1 very well. This is due to the minimum path rule that the Koppjan method follows, because of this the peak at this point is not fully taken into account. For all the other parts of the profile these simulations make a great fit. LCPC with NEN is very similar to Munta de Boorder with NEN in this profile. It overestimates the peaks a little, but overall matches the measurements very well.

Now on to the methods with ISO seen in Figure 6.12. The Filter method with ISO follows the measurements fairly well. However, the peak at -1 meters depth fits less well than with the NEN method added and the strong layer starting at -6 meters depth, the force needed is underestimated by the simulations. With Munta de Boorder with ISO the peak at -1 meter depth is followed quite nicely, but, just like with the Filter method with ISO, the force at the end of the profile is underestimated a bit with these simulations. Koppejan with ISO underestimates the force needed over almost the entire profile. The fit of LCPC with ISO looks quite nice. The peak at -1 meter depth is shown as a good match and even the interval from -5 to -8 meters is a good match. However, after that the simulation force drops a bit, as if a weaker layer sets in, which is not seen in the measurements.

Overall it seems that the simulations with NEN give the best fit. Munta de Boorder and LCPC seem to follow the thin strong embedded layer the best, while Koppejan and Filter method average this peak out a bit more. The simulations with ISO tend to underestimate the force of the bottom layer which is why the simulations with NEN are thought to be a better fit. Most of the simulations work quite well, except for Koppejan with ISO which differs too much from the measurements.

Table 6.6: Ranking of simulations of Hoogeveen

Rank	Simulation
1	Koppejan + NEN
2	Filter method + NEN
3	Filter method + ISO

Methods + NEN

(**a**) Filter method + NEN   (**b**) Munta de Boorder + NEN   (**c**) Koppejan + NEN   (**d**) LCPC + NEN
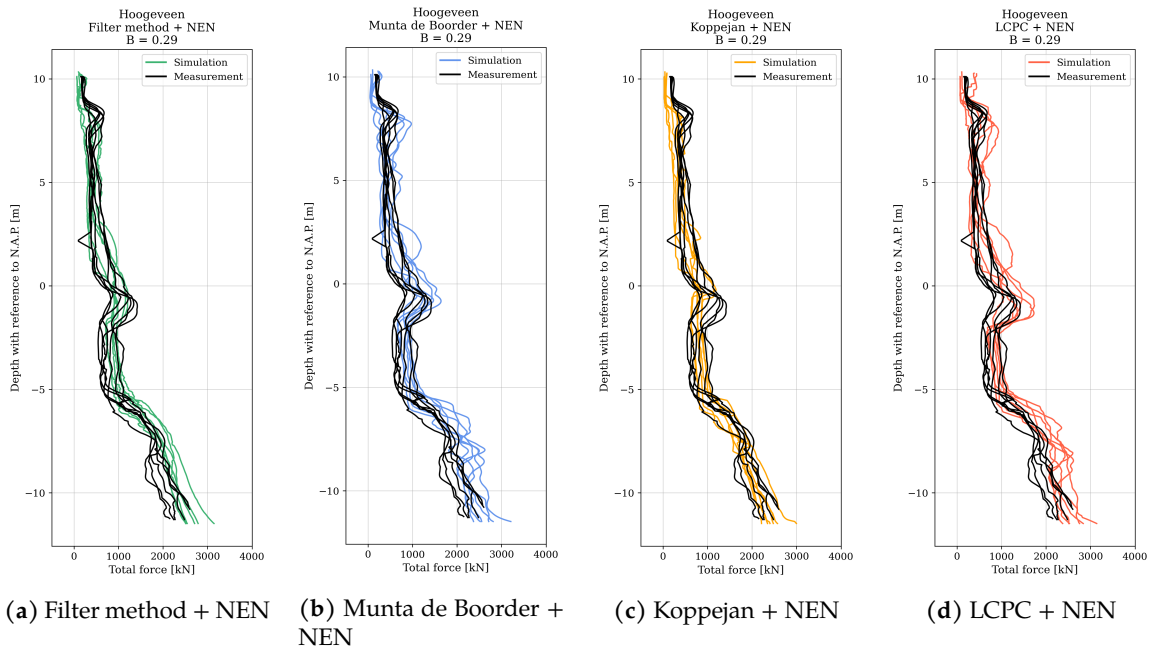
Figure 6.11: Simulations of the different base capacity methods together with NEN shaft capacity method for Hoogeveen

Methods + ISO

(**a**) Filter method + ISO   (**b**) Munta de Boorder + ISO   (**c**) Koppejan + ISO   (**d**) LCPC + ISO
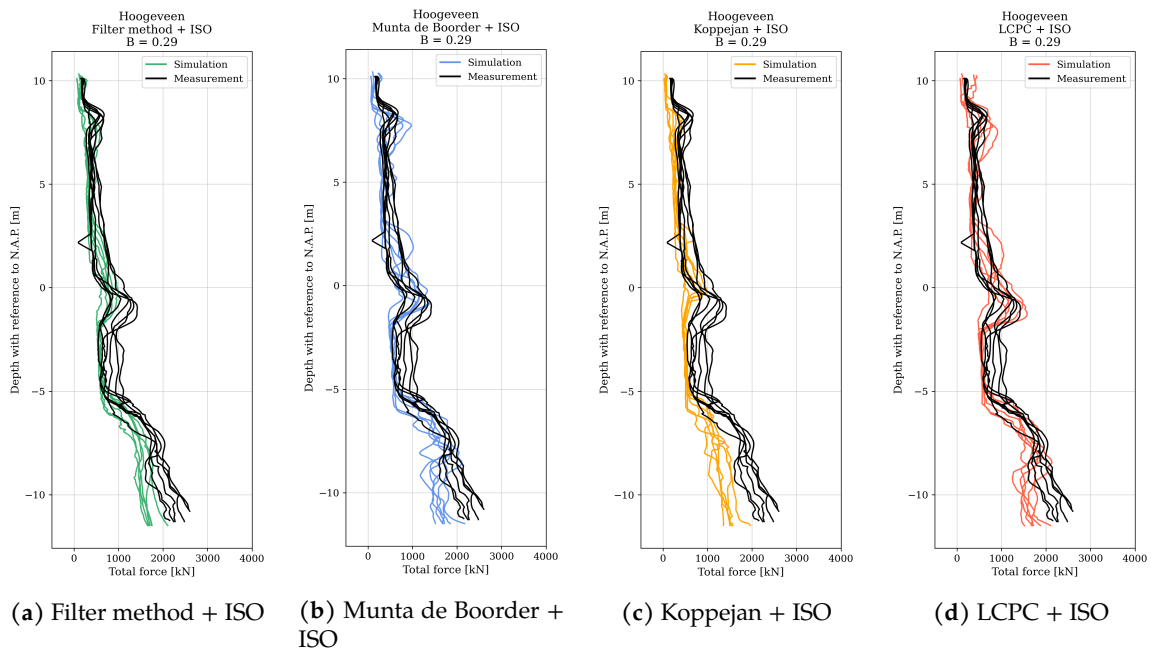
Figure 6.12: Simulations of the different base capacity methods together with ISO shaft capacity method for Hoogeveen

6.7 Nijmegen

The last project to be discussed is located in Nijmegen. From the simulations shown in Figures 6.13 and 6.14 it can be seen that the subsurface here consists mainly of sandy soils. The first 3 meters, until 9 meters, consists of a weaker soil after which an embedded stronger layer is felt. After this layer the total force linearly increases until 3 meters, where the pile is founded.

Filter method with NEN is a close match to the measurements even though the simulation overestimates the total force a bit from 7 meters and on. Munta de Boorder with NEN matches less well. The main problem is with the embedded layer being overestimated by this method, which has been a problem for all profiles with an embedded strong layer. After the embedded layer the simulation lines overestimate the force and are less constant than the Filter method. Koppejan with NEN follows the measurement lien quite well apart from the embedded layer which capacity has been underestimated. LCPC with NEN overestimates the total force consistently throughout the profile. This combination of methods is not a good match for this profile.

Filter method with ISO is an even closer match than Filter method with NEN because the simulations follow the measurments overall very well. For Munta de Boorder the combination with ISO fits better than the combination with NEN, because the overestimation for the profile after the embedded layer fits better. However, the embedded layer is still overestimated quite significantly. Koppejan with ISO is a worse fit than Koppejan with NEN and now underestimates the force over almost the entire profile. LCPC with ISO has the same story as Munta de Boorder with ISO. It is a better fit than the combination with NEN, but for the embedded layer it is still not a great fit.

Here Filter method seems to work the best with ISO, but with NEN the fit is also quite nice. After that Koppejan with NEN seems to match the measurements the best. Munta de Boorder and LCPC fit best when combined with ISO, but they both overestimate the embedded layer too much, which is because of small sensing and development distances both of these methods have.

Table 6.7: Ranking of simulations of Nijmegen

Rank	Simulation
1	Filter method + ISO
2	Koppejan + NEN
3	Filter method + NEN

Methods + NEN

(**a**) Filter method + NEN   (**b**) Munta de Boorder +   (**c**) Koppejan + NEN   (**d**) LCPC + NEN
                               NEN
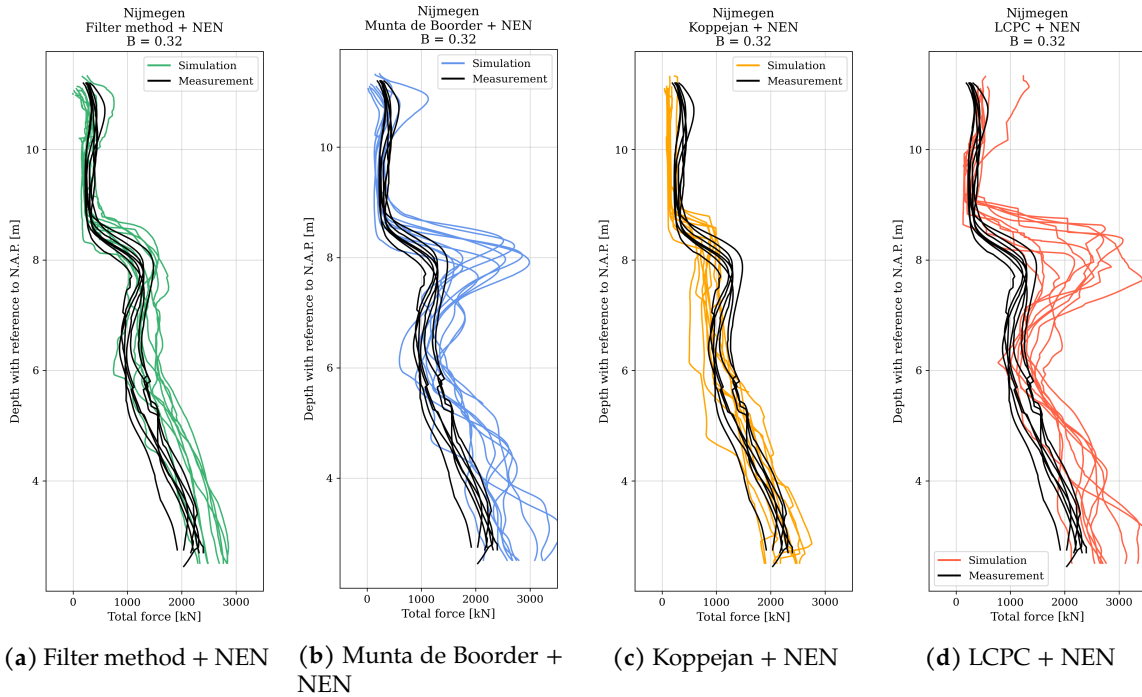
Figure 6.13: Simulations of the different base capacity methods together with NEN shaft capacity method for Nijmegen

Methods + ISO

(**a**) Filter method + ISO   (**b**) Munta de Boorder +   (**c**) Koppejan + ISO   (**d**) LCPC + ISO
                               ISO
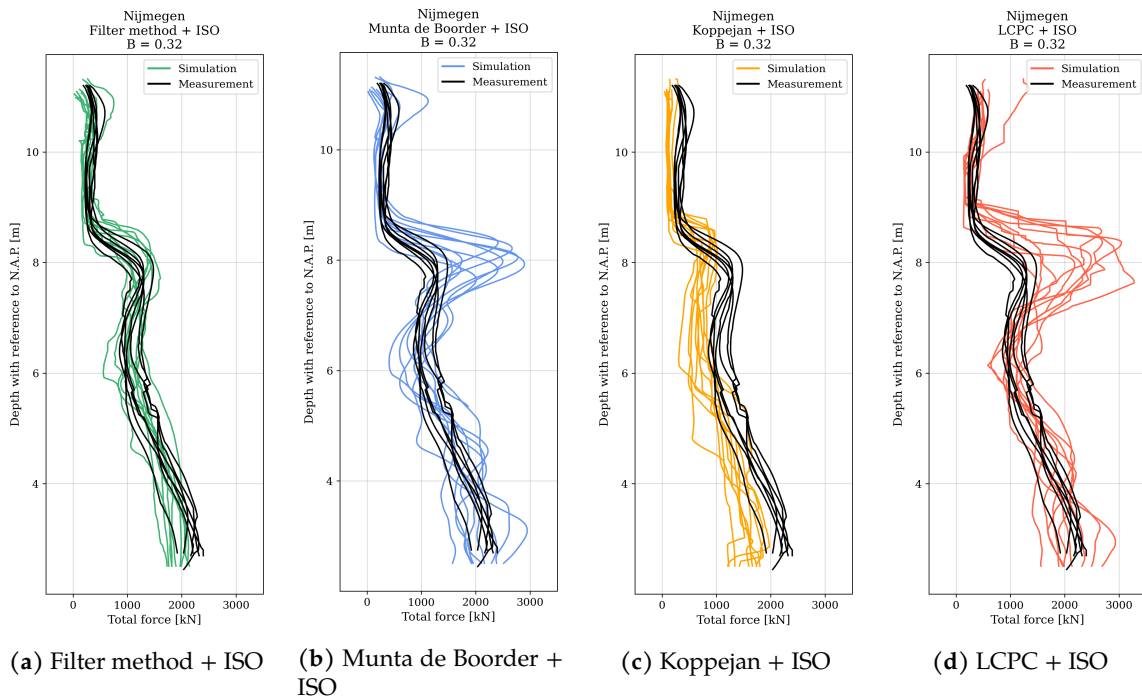
Figure 6.14: Simulations of the different base capacity methods together with ISO shaft capacity method for Nijmegen

6.8 Results and reflection

In Table 6.8 an overview of all the rankings is shown as well as the total per simulation. From this overview Filter method with ISO seems to get the overall best fit based on the visual analysis. This is followed by Filter method with NEN and Koppejan with NEN. Something else to note here is that LCPC has a quite low score for both the combination with NEN and ISO, suggesting that this method doesn't get a very good fit for any of the projects. It also seems that Filter method works quite well in combination with both of the shaft capacity methods, while Munta de Boorder and Koppejan seem to have a preference for one of them. Munta de Boorder scores better in combination with ISO and Koppejan scores better in combination with NEN.

Table 6.8: Overview of rankings with total score per simulation

	Rotterdam	Gorinchem	Ridderkerk	Naaldwijk	Harlingen	Hoogeveen	Nijmegen	Total
Filter method + NEN	3	3				2	1	9
Munta de Boorder + NEN	1							1
Koppejan + NEN		1		2	1	3	2	8
LCPC + NEN	2							2
Filter method + ISO			3	3	2	1	3	12
Munta de Boorder + ISO		2	2	1				5
Koppejan + ISO					3			3
LCPC + ISO			1					1

7

Statistical analysis of results

In this chapter the simulations shown in the previous chapter will be looked at with a statistical view. First the chosen statistical methods used in this analysis will be shortly discussed. These statistical methods are used to determine the goodness of fit of the simulation to the measurement. After this these statistical methods are applied to the simulations of the different projects to give a numerical value on the fit of each simulation.

7.1 Statistical methods

Firstly in this analysis an average is taken from the measurements per project and from each set of simulations. This will give one representative measurement line over depth and one representative simulation line per combination of methods over depth. From these representative datasets the ratio per simulation is calculated, see equation below.

$$ratio(z) = R(z) = \frac{F_{simulation}(z)}{F_{measurement}(z)} \tag{7.1}$$

This will give a ratio line over depth per simulation which values will vary around 1. A vertical straight line will denote the measurements which these simulations should match, since $F_{measurement}/F_{measurement} = 1$. The closer to 1 the ratio line of the simulations lie, the closer to the measurements. There are multiple methods to determine the goodness of fit of these simulations, but some are better for this situation than others. In the list below different statistical methods are discussed and what the ideal outcome of this method should be in this case.

Table 7.1: Statistical methods overview

Name	Abbreviation or symbol	Equation	Wanted outcome
Mean	μ	$\mu = \frac{1}{n}\sum_{i=1}^{n} R_i$	1
Standard Deviation	σ	$\sigma = \sqrt{\frac{1}{n}\sum_{i=1}^{n}(R_i - \mu)^2}$	0
Coefficient of Variation	COV	$COV = \frac{\sigma}{\mu}$	0
Area	A	$A = \sum_{i=1}^{n} \Delta z \cdot (R_i - 1)$	0
Mean Absolute Error	MAE	$MAE = \frac{1}{n}\sum_{i=1}^{n}|R_i - 1|$	0
Root Mean Squared Error	RMSE	$RMSE = \sqrt{\frac{1}{n}\sum_{i=1}^{n}(R_i - 1)^2}$	0

As shown in the table above, all of the outcomes of these methods, when applied to the ratio lines, should be close to zero or one to test fit of these simulation. The first three methods focus only on the simulation ratio line, these are independent from the measurement ratio line that these lines are supposed to match. The last three methods incorporate the measured ratio line and will give an outcome on how the two ratio lines differ.

The ratio lines of the simulations have two criteria to match the measurement ratio line. They should match the shape (in this case a straight vertical line) and they shouldn't differ too much from the measurement line. To test the first criteria the COV is used and to test the second criteria the RMSE is used, because this method will take bigger errors more into account.

Because both are important for different criteria, the simulation which has the lowest sum of the two values is deemed to have the best fit with the measurements per project.

7.2   Statistical analysis of simulations

For the actual statistical analysis of the simulation for each project the ratio lines are plotted with in the left figure the simulation with the NEN shaft capacity method and in the right figure the simulation with the ISO shaft capacity method. After these figures a bar plot will be shown with the values of the outcomes for RMSE and COV. The bar plots will give numbers instead of the names of the combination of methods following the legend in table 7.2. The actual values of the statistical methods can be found in tables in Appendix B.

Table 7.2: Legend for tables

Nr.	Simulation
1	Filter method + NEN
2	Munta de Boorder + NEN
3	Koppejan + NEN
4	LCPC + NEN
5	Filter method + ISO
6	Munta de Boorder + ISO
7	Koppejan + ISO
8	LCPC + ISO

Gorinchem

(a) Methods + NEN
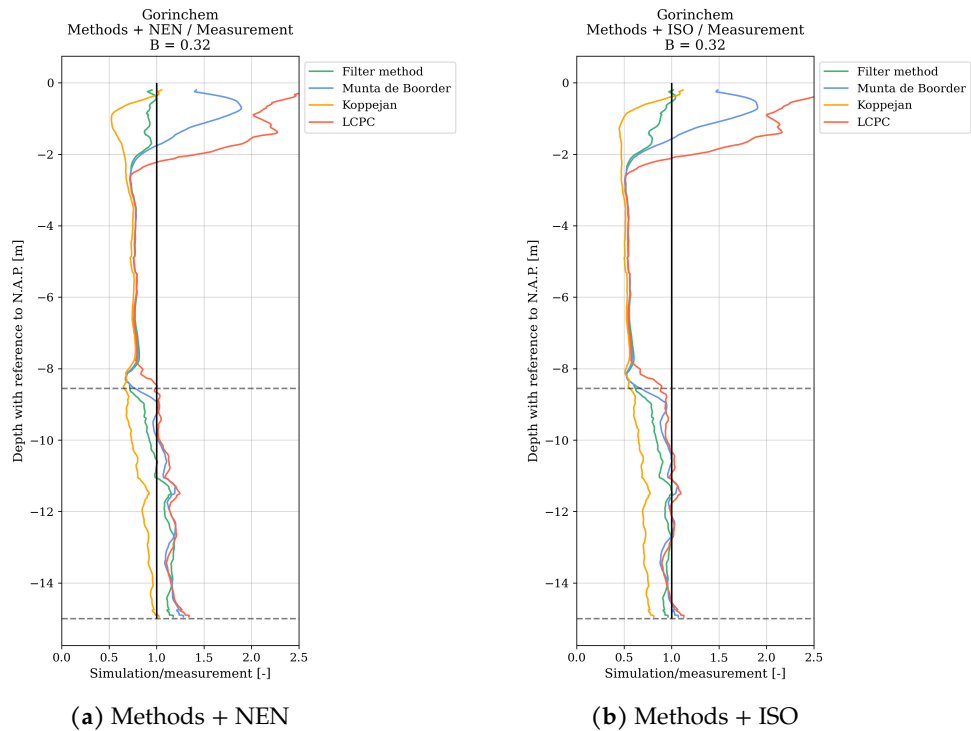
(b) Methods + ISO

Figure 7.1: Ratio between simulations with either NEN or ISO shaft prediction method and measurements for Gorinchem

In Figure 7.1 the ratio's of the simulations is plotted over depth for methods + NEN in the left figure and methods + ISO in the right figure. The measurement ratio line is plotted as a vertical straight line in black at value 1. The dashed lines show over which length the RMSE and COV have been taken. Since there is an error between the measured force and predicted force in the top half of the profile this part has been excluded in the statistical values. If they were taken into account the methods in combination with ISO will be 'punished' harder than in combination with NEN, while this error is probably not due to the accuracy of these simulations.

In Figure 7.2 the bar plot with the RMSE and COV values for all the simulations is shown as well as their sum. Overall the methods with the ISO shaft prediction methods score the best apart from Koppejan (5, 6 and 8) with 8 being the overall best fit for this profile, which is LCPC + ISO.

Something to not from this bar chart is the difference between the COV and RMSE in number 7 (Koppejan + ISO). This simulation has a good fit for the shape, it is fairly straight, giving it a low COV, but is quite far removed from the 1 which attributes to the high RMSE. This shows why both values are important to find a good fit.
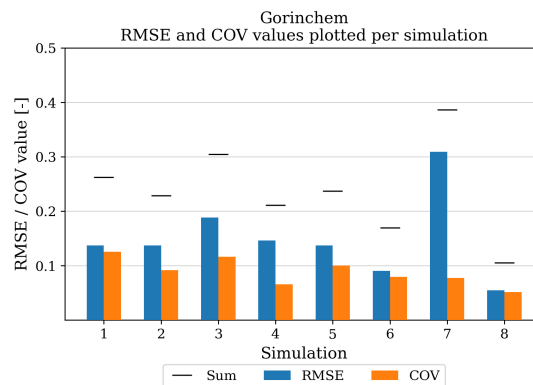
Figure 7.2: Bar chart with the RMSE and COV values and their sum plotted per simulation for Gorinchem

Rotterdam

(**a**) Methods + NEN

(**b**) Methods + ISO
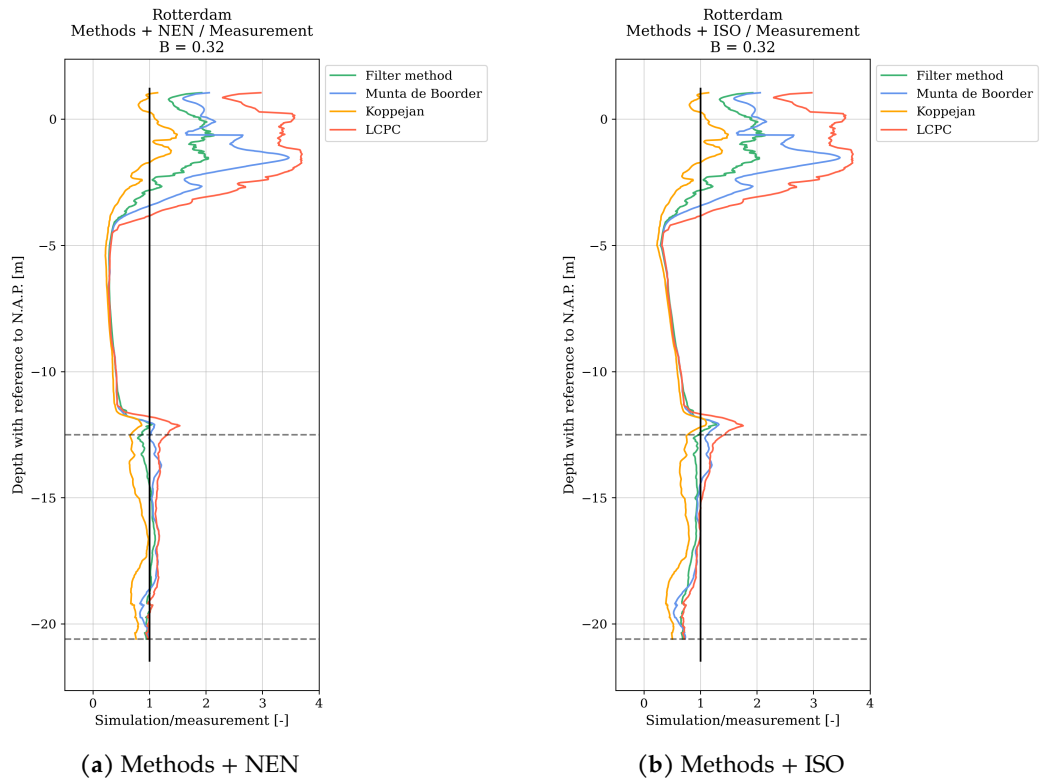
Figure 7.3: Ratio between simulations with either NEN or ISO shaft prediction method and measurements for Rotterdam

In Figure 7.3 the ratio lines for the simulations are shown. The statistical values for fit have again been taken only after the weak layer on top, for the same reason as in Gorinchem. Here the simulations with the NEN shaft prediction method seem to follow the straight line at 1 better than the simulations with the ISO shaft prediction method.

This is also found from the RMSE and COV values, shown in Figure 7.4, where 1 and 2 give the best fit (Filter method and Munta de Boorder with NEN), which was also found in the visual analysis.
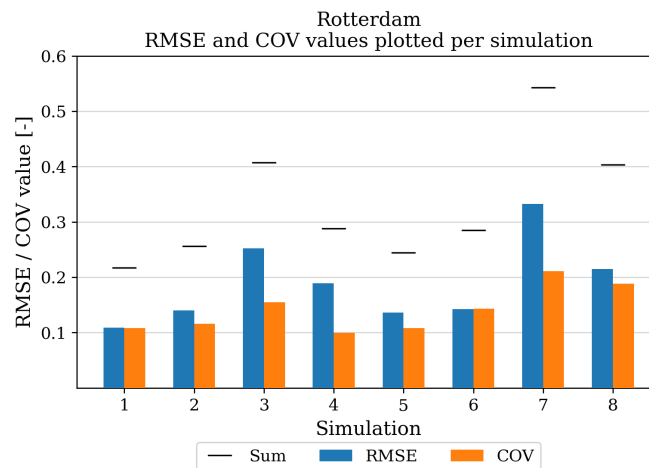
Figure 7.4: Bar chart with the RMSE and COV values and their sum plotted per simulation for Rotterdam

Ridderkerk

(**a**) Methods + NEN   (**b**) Methods + ISO
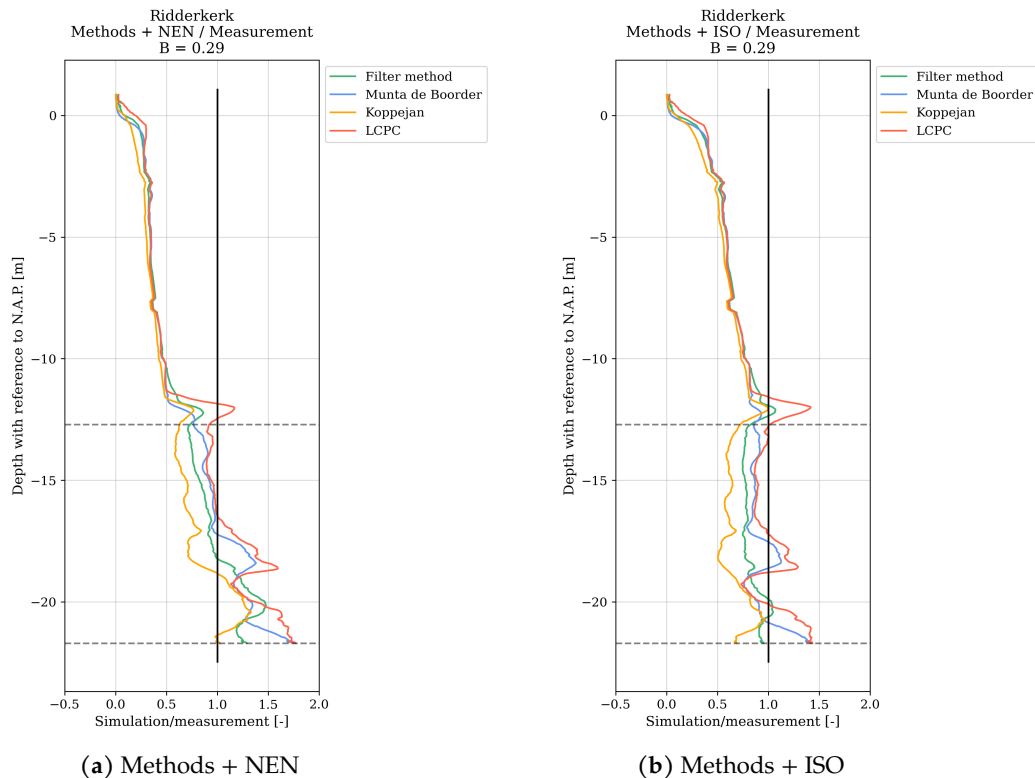
Figure 7.5: Ratio between simulations with either NEN or ISO shaft prediction method and measurements for Ridderkerk

Here again the first half of the profile is ignored in the calculations for the RMSE and COV, see Figure 7.5. Here it can be seen that the simulations with ISO (Figure 7.5b) follow the shape better since these lines straighten out at this part. In the simulation with NEN the lines keep increasing and with that overestimating the force needed.

In the bar chart this can clearly be seen from the values of COV, see Figure 7.6. Here the COV values for the simulations with ISO are significantly lower than those of the simulations with NEN. Here the best fit is very close between Filter method + ISO and Munta de Boorder + ISO, with the former scoring just a little lower. Interesting is that there is a bigger difference between Munta de Boorder + ISO and LCPC + ISO (6 and 8) than expected from the visual analysis where these two seemed quite similar.
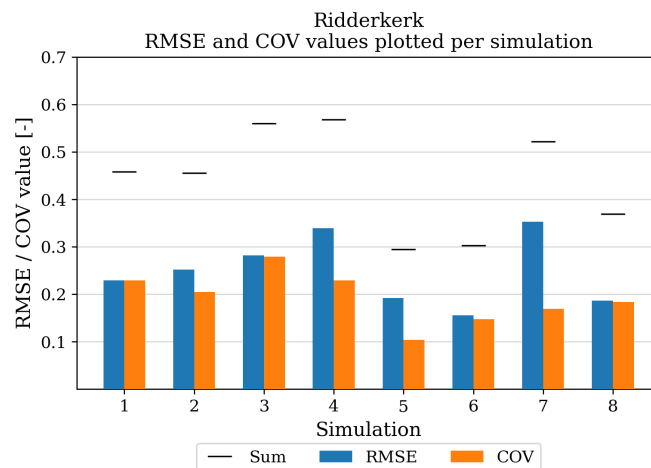
Figure 7.6: Bar chart with the RMSE and COV values and their sum plotted per simulation for Ridderkerk

Naaldwijk

(**a**) Methods + NEN   (**b**) Methods + ISO
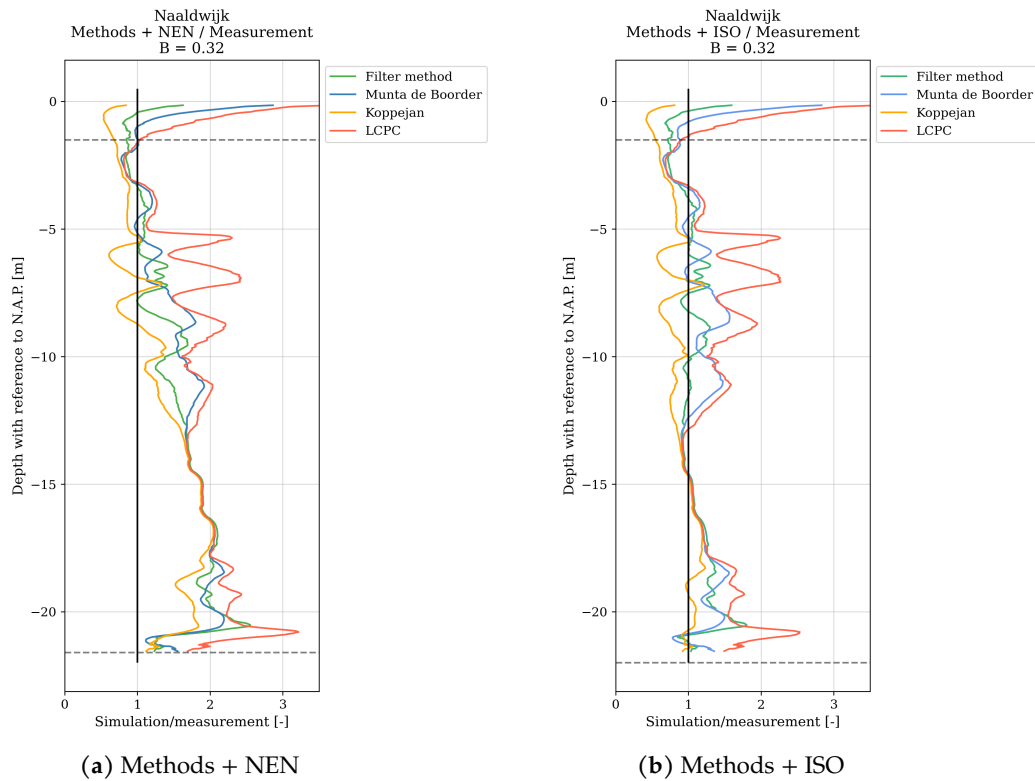
Figure 7.7: Ratio between simulations with either NEN or ISO shaft prediction method and measurements for Naaldwijk

From what was already found in the visual analysis, the simulations with NEN aren't a good fit for this profile, with sometimes overestimating the force by a factor of 2, see Figure 7.7a.

This also can be seen from the high values in RMSE in the bar chart in Figure 7.8. All the simulations with NEN are a better fit for this profile than the simulations with ISO, with Filter method and ISO being the best fit. This was also expected from the visual analysis.
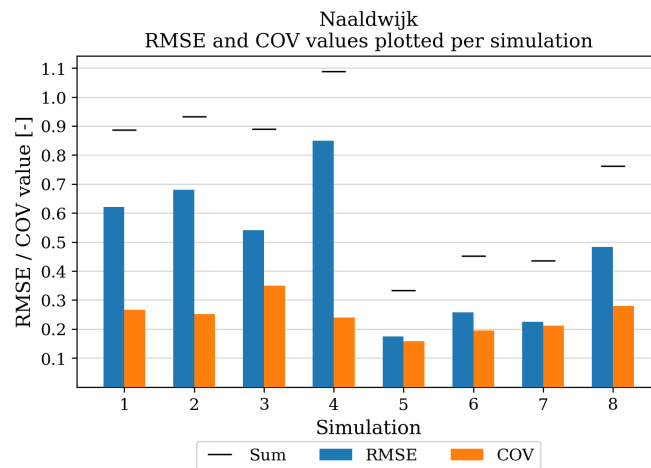
Figure 7.8: Bar chart with the RMSE and COV values and their sum plotted per simulation for Naaldwijk

Harlingen

(**a**) Methods + NEN   (**b**) Methods + ISO
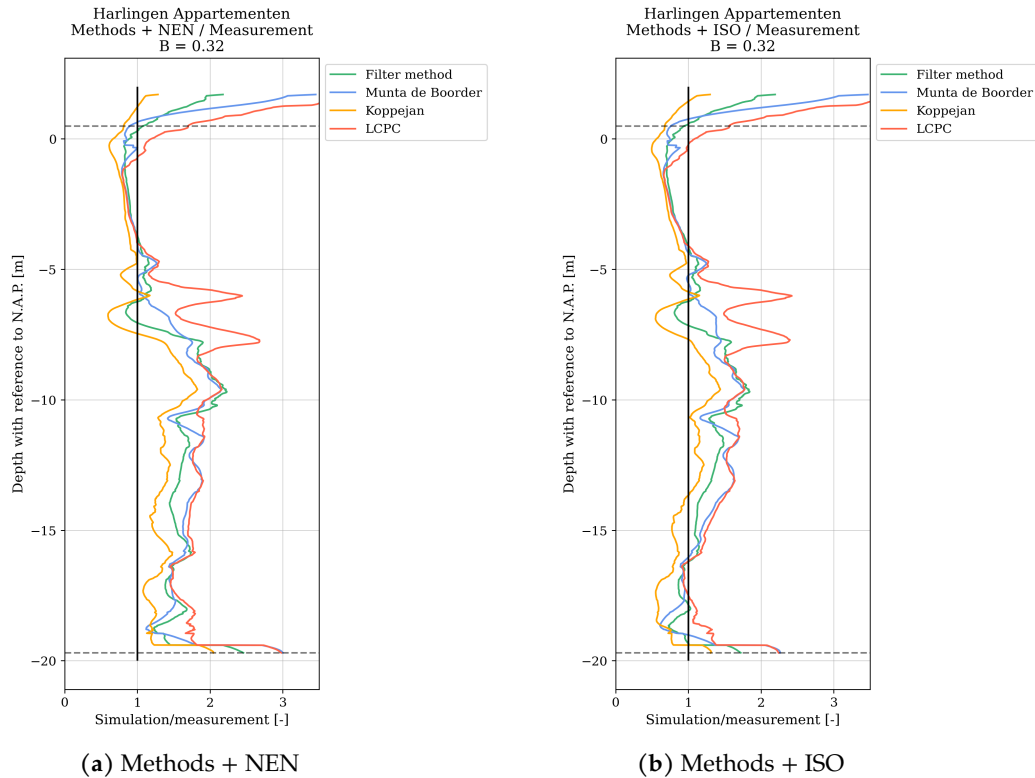
Figure 7.9: Ratio between simulations with either NEN or ISO shaft prediction method and measurements for Harlingen

In Figure 7.9 the ratio lines over depth are plotted for Harlingen. From these plots the simulations with ISO (Figure 7.9b) are expected to have a mean value closer to 1 and the simulations with NEN (Figure 7.9a) look like they might have a lower COV.

From the bar chart in Figure 7.10 the biggest differences are in the RMSE and the COV values are actually all very close to each other. The lowest RMSE value is found at 7 which is Koppejan + ISO, followed by Filter method + ISO. Something to note is that the values of COV are much higher for this project than others, which means that these simulations all vary quite a bit compared to their mean. In the visual analysis there wasn't one simulation that was overall better than the others, which was probably due to the big differences between the measurements and simulations, accounting for the big standard deviations.
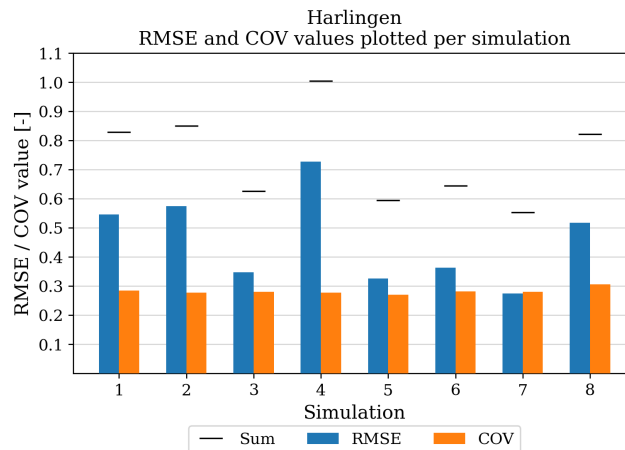
Figure 7.10: Bar chart with the RMSE and COV values and their sum plotted per simulation for Harlingen

Hoogeveen

(**a**) Methods + NEN   (**b**) Methods + ISO
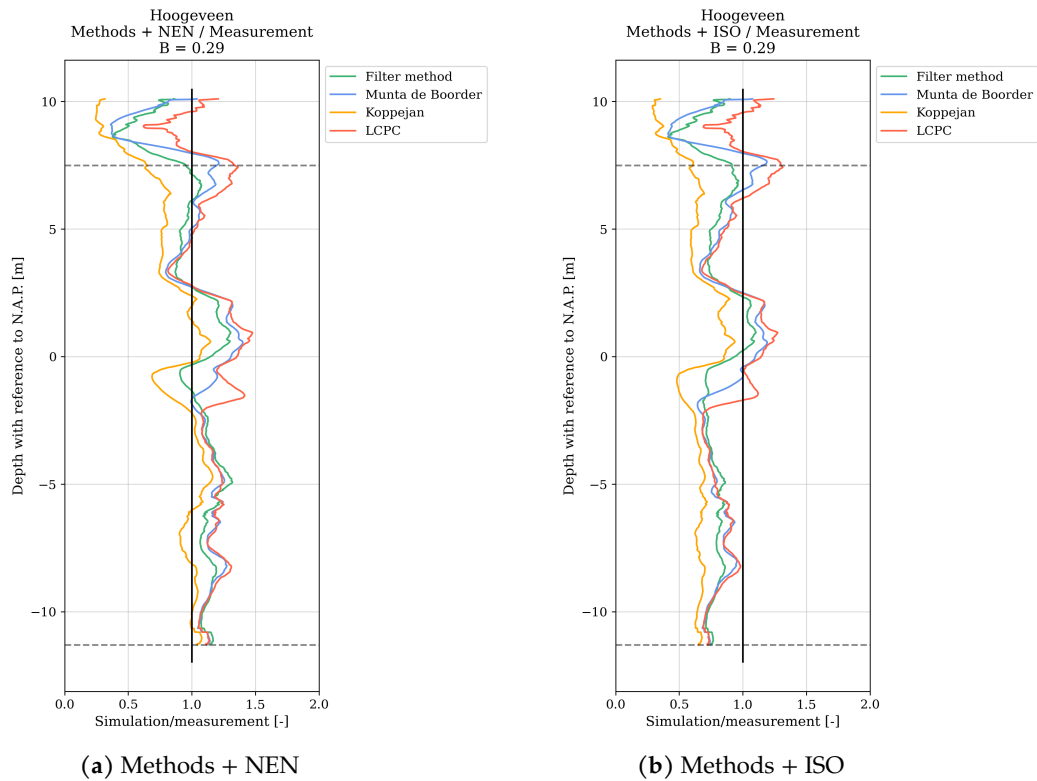
Figure 7.11: Ratio between simulations with either NEN or ISO shaft prediction method and measurements for Hoogeveen

From Figures 7.11a and 7.11b it looks like the simulations with NEN are a better fit, because the simulations with ISO underestimate the force over almost the enitre length of the profile.

In the bar chart in Figure 7.12 this is also confirmed, since the overall COV and RMSE values for the first three simulations (LCPC is excluded here) are lower than the rest. The best fit is found with the Filter method and NEN.
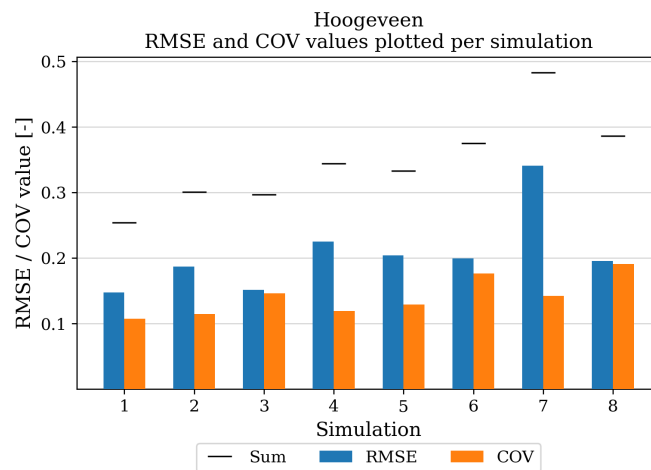
Figure 7.12: Bar chart with the RMSE and COV values and their sum plotted per simulation for Hoogeveen

Nijmegen

(a) Methods + NEN   (b) Methods + ISO
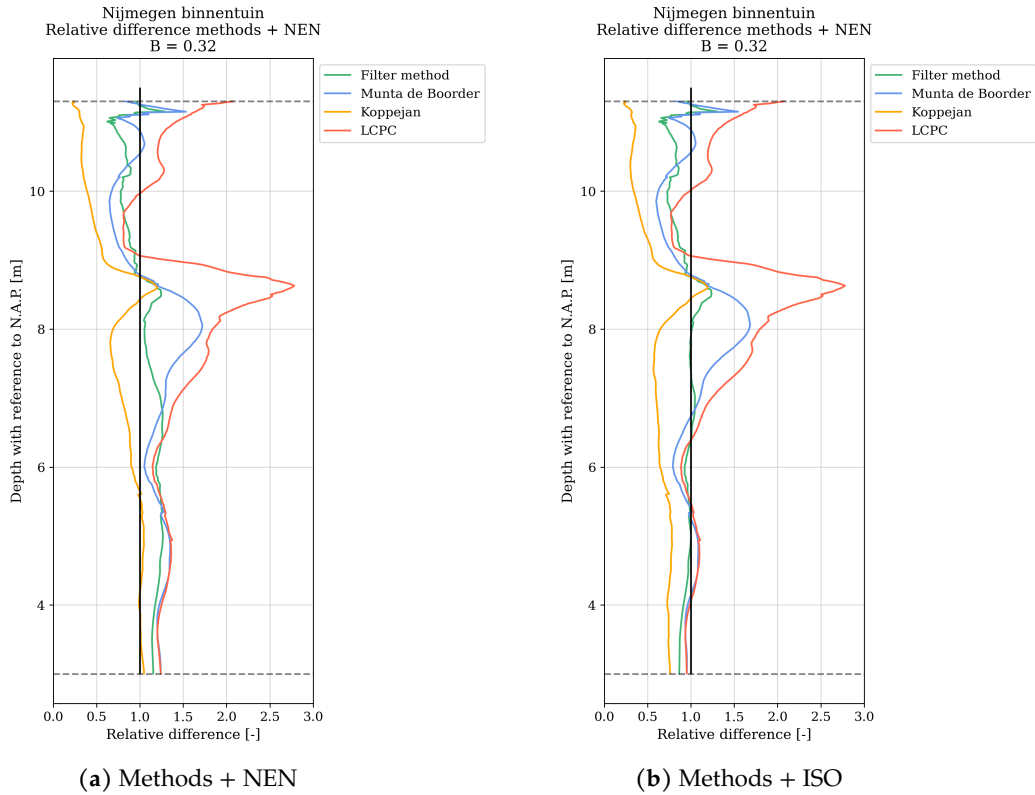
Figure 7.13: Ratio between simulations with either NEN or ISO shaft prediction method and measurements for Nijmegen

In Figure 7.13 the ratio lines over depth are plotted for Nijmegen. The biggest error in these figures is found at just above 8 meters. At this point there is a transition to a strong embedded layer. It was already found in the visual analysis that Munta de Boorder and LCPC overestimated this peak, which is also found in both these figures. The simulations with NEN seem to go just a bit above the measurement lines, which the simulations with ISO do not do.

In the bar chart a significant pattern is shown, see Figure 7.12. This pattern shows that the base capacity prediction methods in this profile have a higher impact than the shaft prediction methods, which was the other way around in previous projects. The Filter method is clearly the best fit with ISO, but closely followed by Filter method + NEN.
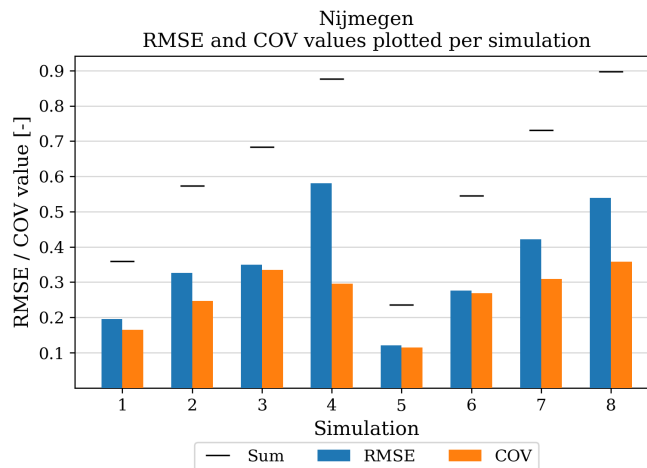
Figure 7.14: Bar chart with the RMSE and COV values and their sum plotted per simulation for Nijmegen

7.3   Conclusion of analysis

In Table 7.3 an overview is given of the best two combinations of methods according to the RMSE and COV values. Filter method + ISO is found to be the best fit for 3 of the 7 projects and the second best fit for 2 of the projects. Filter method + NEN is found to be the best fit for 2 of the seven projects and the second best fit for 1 of the projects. This shows that the filter method overall seems to work the best as base capacity method and ISO seems to be the overall best for shaft capacity method.

Table 7.3: Overview of projects and first and second best fit of method combinations

Project	Methods with best fit	Methods with second best fit
Gorinchem	LCPC + ISO	Munta + ISO
Rotterdam	Filter + NEN	Filter + ISO
Ridderkerk	Filter + ISO	Munta + ISO
Naaldwijk	Filter + ISO	Koppejan + ISO
Harlingen	Koppejan + ISO	Filter + ISO
Hoogeveen	Filter + NEN	Koppejan + NEN
Nijmegen	Filter + ISO	Filter + NEN

This can also be seen in Figure 7.15. Here a bar chart is shown, but this time the values inside this bar chart are a sum of all the outcomes from all the projects. This gives a view of overall how well these methods work. Here it is seen that number 5, the Filter method + ISO, scores the lowest, which means this method has overall a relatively low error compared to the measurements. Remarkably, the second best combination of methods is Munta de Boorder with ISO, which only showed up once in Table 7.3. This means that Munta de Boorder didn't score exceedingly in one project, but it scored very consistently over all the projects compared to the other combinations. After the first two combinations Filter method and Munta de Boorder with added NEN shaft capacity take the third and fourth place. This shows overall that these two base capicity methods are more consistent than Koppejan and LCPC, which did show up more in Table 7.3.
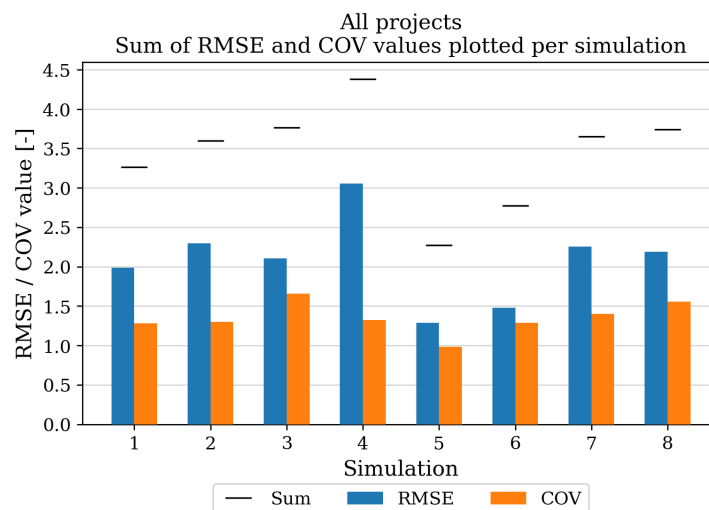
Figure 7.15: Bar chart with the total sum of RMSE and COV values of all projects and their sum plotted per simulation

Location dependency

This leads to the question: 'Are the capacity methods location dependent?'. Or it is rather a question of if certain methods are better at predicting certain soil profile aspects than others.

To get a better understanding of this a new set of bar plots were made with the existing outcomes, but in a different configuration. Here all the outcomes are grouped per combination of methods, thus showing the outcome of one simulation for all the different projects in one plot.
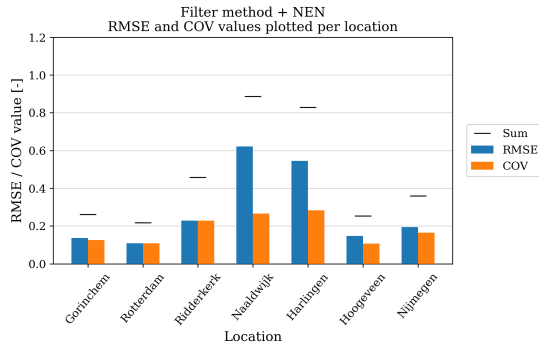
Figure 7.16: Filter method + NEN for all projects
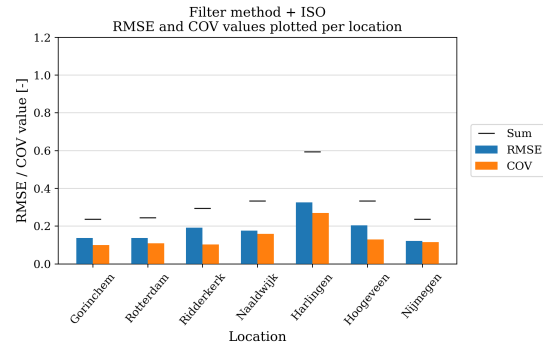
Figure 7.17: Filter method + ISO for all projects

In Figures 7.16 and 7.17 the bar plots for the filter methods with NEN and ISO are shown. Here it is seen that the Filter method together with NEN has a varying outcome dependent on the location (i.e. the subsurface profile). This would mean this combination is location dependent. The filter method together with ISO gets a very constant outcome over the different projects, so this combination is probably location independent.

In Figures 7.18 and 7.19 the bar plots for the Munta de Boorder methods are shown in combination with NEN and ISO. Here the same patterns as above can be seen. The combination together with NEN has more varying values, while the combination with ISO seems to be more constant. Here the combination of Munta de Boorder with NEN is thought to be location dependent and the combaintion of Munta de Boorder with ISO is thought to be independent.
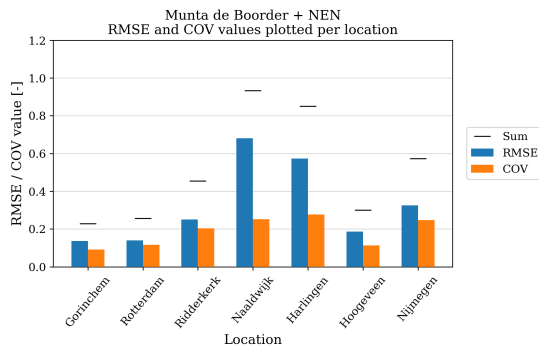
Figure 7.18: Munta de Boorder + NEN for all projects
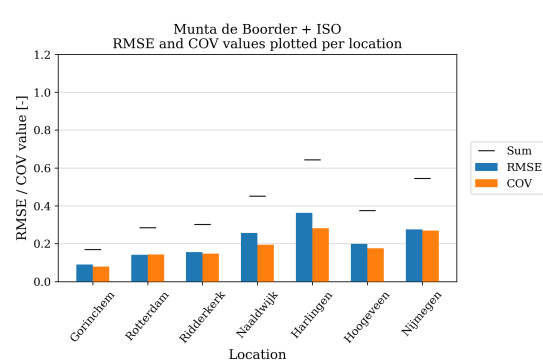
Figure 7.19: Munta de Boorder + ISO for all projects

The bar plots for Koppejan with NEN and ISO are shown in Figures 7.20 and 7.21. Again here the combination with NEN seems to vary more and is thus thought to be location dependent. Here the combination with ISO again seems to be more constant and thus location independent. However, something to note is that the values at which they are constant is quite high, compared to Munta de Boorder + ISO or Filter method + ISO. This means that even thought this combination seems location independent, it does not garner the most accurate results.

The last bar plots show the LCPC method with NEN and ISO. It is very clear from these plots that neither combination is location independent, because of how much the values vary.

When a combination of shaft and base capacity is used it is important that these are location independent. These will have a constant performance over different subsurface profiles and are therefore more reliable. In this case it turned out that all the combinations together with NEN were location dependent as well as both the combinations with LCPC. However, the Filter method, Munta de Boorder and Koppejan together with ISO were found to be location independent.
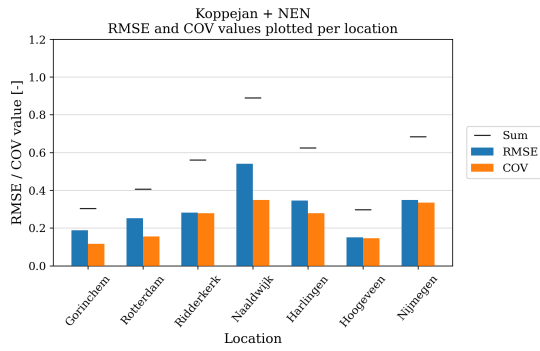
Figure 7.20: Koppejan + NEN for all projects
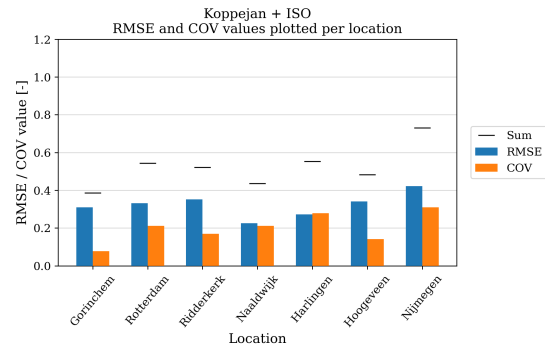
Figure 7.21: Koppejan + ISO for all projects
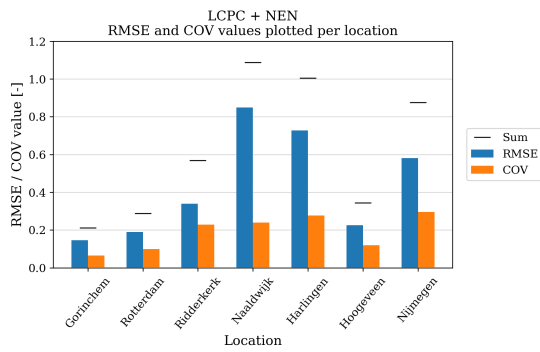
Figure 7.22: LCPC + NEN for all projects
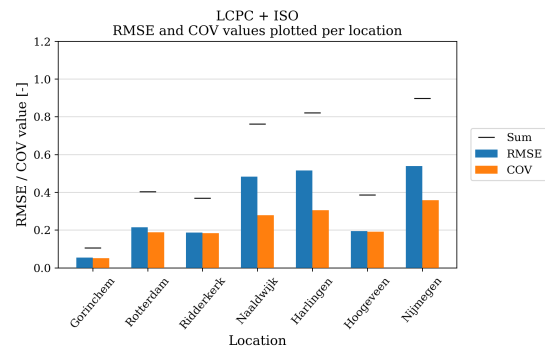
Figure 7.23: LCPC + ISO for all projects

Part III

Discussion and Conclusion

8

Discussion

This research was executed to gain a better understanding of the existing capacity prediction methods for base capacity and shaft capacity and see if these methods could be used to predict the installation force needed to push piles into the ground. This was done by comparing the different combinations of methods to registrations of pile installations, where the force was recorded over depth.

In chapter 9 the research questions of this thesis will be answered and recommendations will be given on further research regarding this topic and this data. Here the different shortcomings of this research will be mentioned and how these might influence the results of this thesis.

- Certain piles or CPTs used in the analyses were eliminated due to differences between these and the other used piles of CPTs. This was done to get the best possible comparison between the force registration and capacity prediction methods without soil variability or installation errors getting in the way. This does mean that the results of this thesis are valid for an optimal chosen set of piles and CPTs per project.

- The CPTs used in this thesis didn't always have the sleeve friction measured. This is normally used to calculate the friction ratio of the soil profile, and from there a distinction can be made between sand and clay in the shaft capacity methods. Because these weren't always available, a certain value was used for cone resistance as a boundary between what was considered clay and what was considered sand. This might have caused discrepancies between what was identified as clay or sand and what actually was clay or sand, and with that getting discrepancies in the shaft capacity calculations.

- There are multiple projects analyzed which have similar subsurface profiles and lie very close together geographically. This could have skewed the outcome of the results to a certain combination of methods getting the best fit, but this could have also caused another combination of methods to seem worse than it actually is because of the prevalence of this subsurface profile.

- The rate effects which could have influenced the tip resistance of the foundation piles have not been taken into account in this research.

- In the statistical analysis an average was taken of the measurements and simulations over depth per project. This might have influenced the values of fit found in the statistical analysis. Harlingen could be an example of this, this profile had a lot of variance in the sand layer at 14 meters depth, which was probably averaged out in the statistical analysis. However, because very similar measurements and CPTs were chosen, it is thought that this influence will be very small.

- In the statistical analysis the coefficient of variation is taken from the ratio lines. This means that lines that are straight but overestimate the force are favored above lines that are straight but underestimate the force, even though it might be preferred to have a method that slightly underestimates the needed force and with that the bearing capacity.

9

Conclusion

9.1 Answers to research questions

The research as presented in this report focused on finding an optimal combination of existing base and shaft capacity methods to predict the total force as registered by Drukpaal. This was done by doing a data analysis of multiple projects of the company of Drukpaal. The aim was to answer the following main research question:

What combination of capacity prediction methods for shaft and tip resistance works best to estimate the total force over depth as measured by Drukpaal?

To answer this main research question sub questions were formulated. First these sub-questions will be answered after which the main question will be answered together with a general conclusion from this research.

What is the best statistical method to compare the simulations to the measurements?

To be able to compare the simulations to the measurements a statistical analysis was performed. This was done on the normalized simulations where the simulations were divided by the measurements. This created a ratio line that should be as close to 1 as possible. There were two aspects on which these ratio lines should be tested.

Firstly the ratio lines should fit the shape of the measurement ratio line, which is a vertical straight line. The mean should be as close to 1 as possible and the standard deviation should be as close to zero as possible. To evaluate this the coefficient of variation is taken which should be as low as possible.

However, the coefficient of variation could be small, but the line might be too far away from the measurement ratio line. So secondly, the Root Mean Squared Error was computed for these ratio line, which gives the error between the measurement and the simulation. Here the outliers are weighed more heavily, still favoring lines that are relatively straight.

These two methods together were used to find how good the fit was of all the different simulation combinations, by comparing the sum of these values.

Are the combinations of capacity prediction methods independent on location (i.e. the subsurface profile)?

By using the same outcomes for RMSE and COV that were used to find the best fit per project the location dependency was tested. By reconfiguring these outcomes per combination of methods this could easily be seen from whether the values for a certain combination of methods were constant for the different projects (subsurface profiles). Here it was found that all combinations with the NEN as shaft capacity method were location dependent, meaning they worked better for certain projects than others. Also both the combinations with LCPC as base capacity method were found to be location dependent, with a high degree of variance in the outcome values. This base capacity method is therefore not reliable to work with.

Three combinations were found to be location independent: Filter method + ISO, Munta de Boorder + ISO and Koppejan + ISO. Filter method with ISO was the most constant with the lowest values followed

by Munta de Boorder. Koppejan with ISO didn't have a low constant score, the scores were quite high. Meaning that even though Koppejan with ISO will score relatively constant over different projects it does not get an accurate result compared to Filter method with ISO.

Answer to main research question

The best combination of capacity prediction methods was found to be the Filter method for base capacity and the ISO method for shaft capacity. This method worked for most of the projects very well and overall had the best score of the COV and RMSE combined.

9.2   Recommendations

For further research the following recommendations are made:

- A further analysis could be done to see if there is a correlation between the ratio values over depth and the installation speed. This should be done per simulation, but if there is a correlation, certain errors between the measurements and simulation could be accounted for by the difference in installation speed.

- More projects with different soil profiles should be investigated to see if the conclusion from this thesis holds, since in this thesis multiple similar profiles are discussed.

- A more in depth analysis of the shaft prediction methods could be done, to see how these differ when applied. Here also the boundary value of tip resistance between clay or sand can be further looked into.

- The Filter method and Munta de Boorder method have multiple constants which were left unchanged in this thesis, these could be altered to find a better fit. How these changes influence the how accurate the prediction is.

- The RMSE and COV were used in this thesis to find the goodness of the fit of the different simulations. However, these might not be the most optimal methods to test the simulations on, especially since the COV favors overestimation and will deem these to be a better fit.

References

Al-Mhaidib, A. I. (2001). Loading rate effect on piles in clay from laboratory model tests. *Journal of King Saud University-Engineering Sciences*, *13*(1), 39–54.

Al-Mhaidib, A. I. (2005). Shearing rate effect on interfacial friction between sand and steel. In *Isope international ocean and polar engineering conference* (pp. ISOPE–I).

Basile, F. (2020, 04). Pile groups with negative skin friction..

Bittar, E., Lehane, B., Boulanger, R., & Dejong, J. (2020). Cpt filter to estimate the end bearing of closed-ended driven piles in layered sands. In *4th international symposium on frontiers in offshore geotechnics* (pp. 520–528).

Bolton, M. (1987). Discussion: The strength and dilatancy of sands. *Géotechnique*, *37*(2), 219–226.

Boulanger, R., & DeJong, J. (2018). Inverse filtering procedure to correct cone penetration data for thin-layer and transition effects. *Cone Penetration Testing 2018*.

Bustamante, M., & Gianeselli, L. (1982, May). Pile bearing capacity prediction by means of static penetrometer CPT. In *Proceedings of the Second European Symposium on Penetration Testing* (pp. 493–500).

Chow, S. H., Bienen, B., & Randolph, M. (2018). Rapid penetration of piezocones in sand. In *Proc., 4th int. symp. on cone penetration testing* (pp. 213–219).

Costa D'Aguiar, S., Modaressi, A., Alberto dos Santos, J., & Lopez-Caballero, F. (2011). Piles under cyclic axial loading: study of the friction fatigue and its importance in pile behavior. *Canadian geotechnical journal*, *48*(10), 1537–1550.

de Boorder, M. (2019). *Development of a new CPT averaging technique and review of existing CPT based methods for the calculation of total pile capacity* (Unpublished master's thesis). Delft University of Technology, Delft, NL.

de Boorder, M., de Lange, D., & Gavin, K. (2022, September). An alternative CPT averaging procedure to estimate pile base capacity. In *Proceedings of the 11th International Conference on Stress Wave Theory and Design and Testing Methods for Deep Foundations.* Zenodo. Retrieved from https://doi.org/10.5281/zenodo.7142197 doi: 10.5281/zenodo.7142197

DeJong, J. T., White, D. J., & Randolph, M. F. (2006). Microscale observation and modeling of soil-structure interface behavior using particle image velocimetry. *Soils and foundations*, *46*(1), 15–28.

Dieteren, H., Katerberg, S., Meindhardt, G., & Tekofsky, T. (2018). De drukpaal - voordelen uit twee werelden. *Geotechniek*.

Digre, K. A., & Zwerneman, F. (2012). Insights into using the 22nd edition of api rp 2a recommended practice for planning, designing and constructing fixed offshore platforms-working stress design. In *Offshore technology conference* (pp. OTC–23558).

Doornbos, M. (2023). [*Picture taken of Drukpaal set-up in Pijnacker*] [Photograph].

Esposito, R. G., Velloso, R. Q., Jr, E. d. A. V., & Danziger, B. R. (2018). Multi-scale sensitivity analysis of pile installation using dem. *Computational Particle Mechanics*, *5*, 375–386.

Fellenius, B. (1999). Design of piles and pile groups considering capacity, settlement, and negative skin friction. *Background Notes for Demo Example for UniPile* (*www.unisoftltd.com*).

Freitas, A. C. d., Danziger, B. R., Pacheco, M., & Gerscovich, D. M. S. (2015). 3-d predictions of installation and group effect on driven piles in sands. *International Journal of Geotechnical Engineering*, *9*(1), 101–112.

Hunt, O., O'Hara, K., Chen, Y., & Martinez, A. (2023). Numerical and physical modeling of the effect of the cone apex angle on the penetration resistance in coarse-grained soils. *International Journal of Geomechanics*, *23*(2), 04022273.

Kraft Jr, L. M., Focht Jr, J. A., & Amerasinghe, S. F. (1981). Friction capacity of piles driven into clay. *Journal of the Geotechnical Engineering Division*, *107*(11), 1521–1541.

Lehane, B., Schneider, J., & Xu, X. (2005). The UWA-05 method for prediction of axial capacity of driven piles in sand. *Frontiers in offshore geotechnics: ISFOG*, 683–689.

Lehane, B., & White, D. (2004, 01). Friction fatigue on displacement piles in sand. *Geotechnique*, *54*, 645-658. doi: 10.1680/geot.2004.54.10.645

Lehane, B. M., Liu, Z., Bittar, E., Nadim, F., Lacasse, S., Jardine, R., ... Morgan, N. (2020). A new 'unified' cpt-based axial pile capacity design method for driven piles in sand. In *4th international symposium on frontiers in offshore geotechnics (postponed)* (pp. 462–477).

Lehane, B. M., Liu, Z., Bittar, E. J., Nadim, F., Lacasse, S., Bozorgzadeh, N., ... others (2022). Cpt-based axial capacity design method for driven piles in clay. *Journal of Geotechnical and Geoenvironmental Engineering*, *148*(9), 04022069.

Le Kouby, A., Dupla, J. C., Canou, J., & Francis, R. (2016). The effects of installation order on the response of a pile group in silica sand. *Soils and Foundations*, *56*(2), 174–188.

Mo, P.-Q., Marshall, A. M., & Yu, H.-S. (2017). Interpretation of cone penetration test data in layered soils using cavity expansion analysis. *Journal of Geotechnical and Geoenvironmental Engineering*, *143*(1), 04016084.

Normcommissie 351 006 'Geotechniek'. (2017, November). *NEN 9997-1: Geotechnical design of structures - Part 1: General rules* (Tech. Rep.). Delft: Nederlands Normalisatie-instituut.

Plantema, G. (1948). Results of a special loading test on a reinforced concrete pile, a so-called pile sounding. In *Proceedings of the 2nd international conference on soil mechanics and foundation engineering, rotterdam* (Vol. 2, p. 112).

Quinn, T. (2013). *Rate effects in fine grained soils* (Unpublished doctoral dissertation). University of Dundee.

Randolph, M. F. (2003). Science and empiricism in pile foundation design. *Géotechnique*, *53*(10), 847–875.

Robertson, P. K. (2010). Soil behaviour type from the cpt: an update. In *2nd international symposium on cone penetration testing* (Vol. 2, p. 8).

Robinson, S., & Brown, M. (2013). Rate effects at varying strain levels in fine grained soils. In *Proceedings of the 18th international conference on soil mechanics and geotechnical engineering, paris* (pp. 263–266).

Salgado, R., Mitchell, J., & Jamiolkowski, M. (1997). Cavity expansion and penetration resistance in sand. *Journal of Geotechnical and Geoenvironmental Engineering*, *123*(4), 344–354.

Salgado, R., Woo, S. I., & Kim, D. (2011). Development of load and resistance factor design for ultimate and serviceability limit states of transportation structure foundations. *Joint Transportation Research Program*.

Tehrani, F. S., Arshad, M. I., Prezzi, M., & Salgado, R. (2018). Physical modeling of cone penetration in layered sand. *ASCE Journal of Geotechnical and Geoenvironmental Engineering*, *144*(1). Retrieved from https://doi.org/10.1061/(ASCE)GT.1943-5606.000180 doi: 10.1061/(ASCE)GT.1943-5606.000180

Tovar-Valencia, R. D., Galvis-Castro, A., Salgado, R., & Prezzi, M. (2021). Effect of base geometry on the resistance of model piles in sand. *Journal of Geotechnical and Geoenvironmental Engineering*, *147*(3), 04020180.

Ullah, S. N., Stanier, S., Hu, Y., & White, D. (2017a). Foundation punch-through in clay with sand: analytical modelling. *Géotechnique*, *67*(8), 672–690.

Ullah, S. N., Stanier, S., Hu, Y., & White, D. (2017b). Foundation punch-through in clay with sand: centrifuge modelling. *Géotechnique*, *67*(10), 870–889.

van Mierlo, W., & Koppejan, A. (1952). Lengte en draagvermogen van heipalen. *Bouw*, *3*.

van Tol, A. (2003). Funderingstechnieken-ontwerpaspecten. *Delft University of Technology*.

White, D. J., & Bolton, M. D. (2005). Comparing cpt and pile base resistance in sand. *Proceedings of the Institution of Civil Engineers-Geotechnical Engineering*, *158*(1), 3–14.

Xu, X. (2007). *Investigation of the end bearing performance of displacement piles in sand* (Unpublished doctoral dissertation). University of Western Australia.

A
Pile plans

A.1 Pile plan - Gorinchem

A.2 Pile plan - Rotterdam

24.0m -N.A.P.

22.75m -N.A.P.

19.5m -N.A.P.

24.0m -N.A.P.

22.5m -N.A.P.

24.5m -N.A.P.

24.0m -N.A.P.

23.0m -N.A.P.
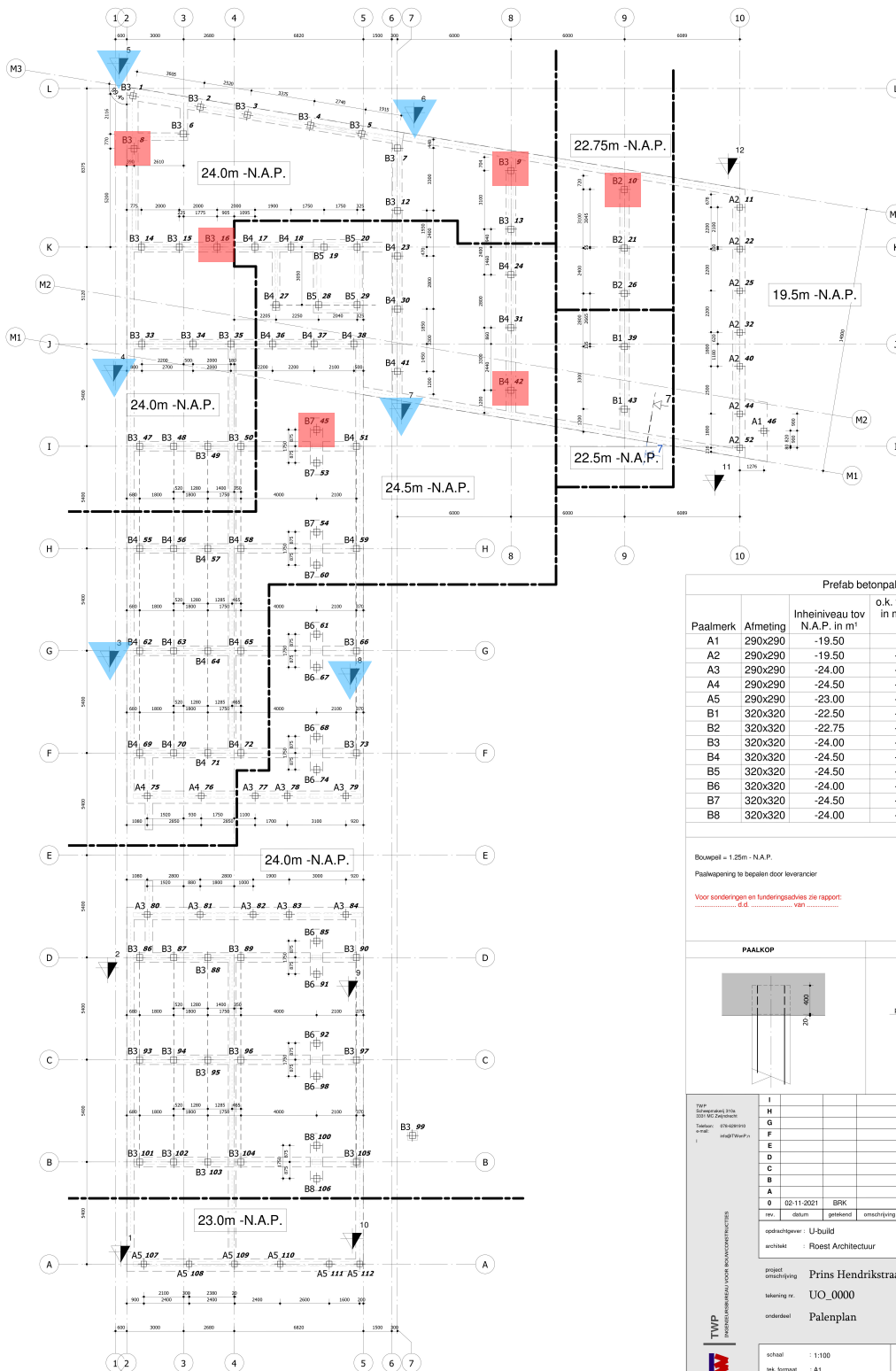
Prefab betonpalen

Paalmerk	Afmeting	Inheiniveau tov N.A.P. in m¹	o.k. fundering in mm t.o.v. Peil	Theor. paallengte in m¹	Aantal
A1	290x290	-19.50	-730	17.94	1
A2	290x290	-19.50	-1080	17.59	7
A3	290x290	-24.00	-1080	22.09	8
A4	290x290	-24.50	-1080	22.59	2
A5	290x290	-23.00	-1080	21.09	6
B1	320x320	-22.50	-1080	20.59	2
B2	320x320	-22.75	-1080	20.84	3
B3	320x320	-24.00	-1080	22.09	39
B4	320x320	-24.50	-1080	22.59	26
B5	320x320	-24.50	-1300	22.37	4
B6	320x320	-24.00	-1280	21.89	8
B7	320x320	-24.50	-1280	21.89	4
B8	320x320	-24.00	-1880	21.29	2
					112

Bouwpeil = 1.25m - N.A.P.

Inheiniveau zie plattegrond

Paalwapening te bepalen door leverancier

....m-N.A.P

Voor sonderingen en funderingsadvies zie rapport:
.... d.d. .... van ....

PAALKOP

PAALCODERING

paalmerk   paalnummer

B 48

TWP
Scheepmakerij 310a
3331 MC Zwijndrecht
Telefoon: 076-6291910
e-mail: info@TWerP.n

I		
H		
G		
F		
E		
D		
C		
B		
A		
0	02-11-2021	BRK
rev.	datum	getekend omschrijving

opdrachtgever : U-build

architekt   : Roest Architectuur

project omschrijving : Prins Hendrikstraat te Rotterdam

project nr. 18081

tekening nr. UO_0000

onderdeel Palenplan

stadium UO

schaal	: 1:100	senior adviseur :
tek. formaat	: A1	projectleider : Tjan Huang
project tekenaar : Evelyn van den Abeele		constructeur :

TWP
TWEEDE WERKBUREAU VOOR BOUWCONSTRUCTIES

A.3   Pile plan - Ridderkerk

A.4 Pile plan - Naaldwijk

A.5 Pile plan - Hoogeveen

A.6 Pile plan - Harlingen

A.7   Pile plan - Nijmegen

B

Statistical values simulations

B.1 Gorinchem

Table B.1: Statistical values of fit of simulations for Gorinchem

	1	2	3	4	5	6	7	8
RMSE	0.137	0.137	0.188	0.146	0.137	0.09	0.309	0.054
COV	0.125	0.091	0.116	0.065	0.1	0.079	0.077	0.051
Sum	0.262	0.228	0.304	0.211	0.237	0.169	0.386	0.105
Mean	1.041	1.095	0.84	1.126	0.896	0.95	0.695	0.981
STD	0.131	0.099	0.098	0.073	0.089	0.075	0.054	0.05
Area	0.788	0.773	1.031	0.815	0.668	0.399	1.965	0.289
MAE	0.122	0.12	0.16	0.127	0.104	0.062	0.305	0.045

B.2 Rotterdam

Table B.2: Statistical values of fit of simulations for Rotterdam

	1	2	3	4	5	6	7	8
RMSE	0.108	0.14	0.252	0.189	0.136	0.142	0.332	0.215
COV	0.108	0.116	0.155	0.099	0.108	0.143	0.211	0.188
Sum	0.216	0.256	0.407	0.288	0.244	0.285	0.543	0.403
Mean	0.981	1.066	0.779	1.151	0.905	0.99	0.702	1.075
STD	0.106	0.123	0.12	0.115	0.098	0.141	0.148	0.202
Area	0.556	0.854	1.654	1.271	0.876	0.814	2.284	1.079
MAE	0.074	0.114	0.221	0.169	0.117	0.109	0.305	0.144

B.3 Ridderkerk

Table B.3: Statistical values of fit of simulations for Ridderkerk

	1	2	3	4	5	6	7	8
RMSE	0.229	0.251	0.282	0.339	0.191	0.155	0.352	0.186
COV	0.229	0.204	0.279	0.229	0.103	0.147	0.169	0.183
Sum	0.458	0.455	0.561	0.568	0.294	0.302	0.521	0.369
Mean	1.012	1.109	0.848	1.199	0.83	0.927	0.666	1.017
STD	0.229	0.226	0.237	0.274	0.085	0.136	0.113	0.186
Area	1.787	1.778	2.335	2.222	1.582	1.241	3	1.345
MAE	0.199	0.198	0.259	0.247	0.176	0.138	0.334	0.149

B.4 Naaldwijk

Table B.4: Statistical values of fit of simulations for Naaldwijk

	1	2	3	4	5	6	7	8
RMSE	0.621	0.681	0.541	0.849	0.175	0.257	0.225	0.483
COV	0.266	0.252	0.349	0.239	0.158	0.195	0.211	0.279
Sum	0.887	0.933	0.890	1.088	0.333	0.452	0.436	0.762
Mean	1.479	1.557	1.296	1.739	1.05	1.131	0.871	1.313
STD	0.393	0.3939	0.452	0.417	0.166	0.221	0.184	0.367
Area	9.372	10.742	8.178	14.057	2.569	3.783	3.506	6.855
MAE	0.507	0.581	0.442	0.76	0.139	0.205	0.189	0.371

B.5 Harlingen

Table B.5: Statistical values of fit of simulations for Harlingen

	1	2	3	4	5	6	7	8
RMSE	0.545	0.573	0.346	0.727	0.325	0.362	0.273	0.516
COV	0.283	0.277	0.279	0.277	0.269	0.281	0.279	0.305
Sum	0.828	0.850	0.625	1.004	0.594	0.643	0.552	0.821
Mean	1.38	1.418	1.138	1.581	1.121	1.159	0.879	1.322
STD	0.391	0.393	0.317	0.438	0.302	0.326	0.245	0.404
Area	8.346	9.037	5.677	11.784	4.869	5.716	4.531	7.773
MAE	0.439	0.476	0.299	0.621	0.256	0.301	0.239	0.409

B.6   Hoogeveen

Table B.6: Statistical values of fit of simulations for Hoogeveen

	1	2	3	4	5	6	7	8
RMSE	0.147	0.187	0.151	0.225	0.204	0.199	0.341	0.195
COV	0.107	0.114	0.146	0.119	0.129	0.176	0.142	0.191
Sum	0.254	0.301	0.297	0.344	0.333	0.375	0.483	0.386
Mean	1.089	1.135	0.935	0.824	0.827	0.872	0.673	0.913
STD	0.117	0.129	0.136	0.139	0.107	0.153	0.095	0.174
Area	2.258	2.896	2.113	3.509	3.356	3.117	5.887	3.115
MAE	0.125	0.161	0.117	0.195	0.187	0.177	0.327	0.173

B.7   Nijmegen

Table B.7: Statistical values of fit of simulations for Nijmegen

	1	2	3	4	5	6	7	8
RMSE	0.195	0.326	0.349	0.581	0.121	0.276	0.422	0.529
COV	0.164	0.247	0.334	0.295	0.115	0.269	0.309	0.358
Sum	0.254	0.301	0.297	0.344	0.333	0.375	0.483	0.386
Mean	1.089	1.135	0.935	1.176	0.827	0.872	0.673	0.913
STD	0.117	0.129	0.136	0.139	0.107	0.153	0.095	0.174
Area	2.258	2.896	2.113	3.509	3.356	3.177	5.887	3.115
MAE	0.125	0.161	0.117	0.195	0.187	0.177	0.327	0.173